FIRE-RES

Innovative technologies & socio-ecological-economic solutions for fire resilient territories in Europe

D1.5 ADAPTED LONG-TERM CLIMATE CHANGE PROJECTIONS AND SEASONAL FORECASTS

www.fire-res.eu

fire-res@ctfc.cat

Project Acronym: FIRE-RES

Project name: Innovative technologies and socio-ecological-economic solutions for fire resilient territories in Europe

Call ID: H2020-LC-GD-1-1-2020 (Preventing and fighting extreme wildfires with the integration and demonstration of innovative means)

Work Package: WP1

Task Number: T1.2

Lead beneficiary: Forest Science and Technology Centre of Catalonia (CTFC)

Contributing beneficiaries: Forest Science and Technology Centre of Catalonia (CTFC) & National Observatory of Athens (NOA).

This document was produced under the terms and conditions of Grant Agreement No. 101037419 of the European Commission. It does not necessarily reflect the view of the European Union and in no way anticipates the Commission's future policy in this area.

Publication

Publication date: 30/11/2023

Authors: Aymen Moghli, CTFC; Anna Karali, NOA; Konstantinos V. Varotsos, NOA; Christos Giannakopoulos, NOA; Lluís Brotons, CTFC; Andrea Duane, CTFC.

Abstract: The current global change is increasing the occurrence of extraordinary wildfires that overwhelm the suppression capacities, provoking substantial damages, and often resulting in human fatalities and threatening ecosystem integrity. Generating reliable and robust climate projections decisive for extreme wildfire events occurrence in Europe at different scales is of high priority to offer the specific conditions under which wildfires will develop to policymakers and stakeholders, so actions aimed to decrease extreme fire risk, enhance the safety and preparedness of citizens and firefighters are built according to future new conditions. In addition to essential variables such as air temperature and precipitation, this report aims to generate spatial projections and analyze indices such as the Fire Weather Index (FWI) and the continuous atmospheric instability (C-Haines index), both at the pan-European scale and at the living lab scale (in 5 biomes representative FIRE-RES living labs) to allow a better understanding of the future changes in the occurrence of extreme wildfire events. We mobilized climate projections from the Coupled Model Intercomparison Project Phase 6 (CMIP6) to evaluate new-future (2041-2060) and far-future (2081-2100) weather conditions under three socio-economic pathway scenarios (SSP1-2.6, SSP2-4.5 and SSP5-8.5). Besides, we also evaluated the accuracy of high-resolution FWI seasonal forecasts on historical records of three Mediterranean Living Labs of the FIRE-RES project. The main temporal and spatial results of both the future projections and seasonal forecasts are discussed, and the generated spatial data is available under the ZENODO repository of the FIRE-RES project.

Keywords: atmospheric variables, climate change, Continuous Haines Index, Fire Weather Index, pyrocumulonimbus, statistical downscaling, seasonal forecasts

Quote as: Moghli, A., Karali, A., Varotsos, K.V., Giannakopoulos, C., Brotons, L., Duane, A. (2023). Adapted long-term climate change projections and seasonal forecasts. Deliverable D1.5 FIRE-RES project. 90 pages. DOI: 10.5281/zenodo.10211205

DOI: 10.5281/zenodo.10211205

Dissemination level

[X] PU- Public: must be available on the website

[ ] CO- Confidential: Only for members of the Consortium and the Commission Services

[ ] CI – Classified: As referred into Commission Decision 2001/844/EC

Document history

Edition	Date	Status	Author
Version 1	16/10/2023	Draft	Aymen Moghli, CTFC; Anna Karali, NOA; Konstantinos V. Varotsos, NOA; Christos Giannakopoulos, NOA; Lluís Brotons, CTFC; Andrea Duane, CTFC.
Version 2	02/11/2023	Revision	Edgar Nebot i Hernandez, CFRS, Laia Estivill, CFRS, Guglielmo Borghini, Spire
Version 3	24/11/2023	Final Version	Aymen Moghli, CTFC; Anna Karali, NOA; Konstantinos V. Varotsos, NOA; Christos Giannakopoulos, NOA; Lluís Brotons, CTFC; Andrea Duane, CTFC.

Contents

List of figures

between the future periods and the reference one. Black dots indicate robust changes at the grid point scale.

Figure 8. Average annual RR1 for all periods and scenarios examined. In each plot M indicates the average value calculated over all grid points in each zone whereas D is the relative change between the future periods and the reference one. Black dots indicate robust changes at the grid point scale.

Figure 9. Total annual RR for all periods and scenarios examined. In each plot M indicates the average value calculated over all grid points in each zone whereas D is the relative change between the future periods and the reference one. Black dots indicate robust changes at the grid point scale.

Figure 10. Total JJA RR for all periods and scenarios examined. In each plot M indicates the average value calculated over all grid points in each zone whereas D is the relative change between the future periods and the reference one. Black dots indicate robust changes at the grid point scale.

Figure 11. JJA average FWI values for all periods and scenarios examined. In each plot M indicates the average value calculated over all grid points in each zone whereas D is the relative change between the future periods and the reference one. Black dots indicate robust changes at the grid point scale.

Figure 12. Mean changes in the summer enhanced Fire Weather index (Jun-July-August) between the near future (2020-2041) and the historical period (1995-2014) under the SSP1-2.6, SSP2-4.5 and SSP5-8.5 respectively.

Figure 13. Mean changes in the summer enhanced Fire Weather index (Jun-July-August) between the far future (2081-2041) and the historical period (1995-2014) under the SSP1-2.6, SSP2-4.5, and SSP5-8.5 respectively.

Figure 14. Average JJA TX changes between the 2041-2060 future period and the reference one (1995-2104) for the three SSP scenarios examined. In each plot M indicates the absolute change between the future period and the reference one averaged over all gid points. Black dots indicate robust changes at the grid point scale.

Figure 15. Average JJA TX changes between the 2081-2100 future period and the reference one (1995-2104) for the three SSP scenarios examined. In each plot M indicates the absolute change between the future period and the reference one averaged over all gid points. Black dots indicate robust changes at the grid point scale.

Figure 16. Average JJA TN changes between the 2041-2060 future period and the reference one (1995-2104) for the three SSP scenarios examined. In each plot M indicates the absolute change between the future period and the reference one averaged over all gid points. Black dots indicate robust changes at the grid point scale.

Figure 17. Average JJA TN changes between the 2081-2100 future period and the reference one (1995-2104) for the three SSP scenarios examined. In each plot M indicates the absolute change between the future period and the reference one averaged over all gid points. Black dots indicate robust changes at the grid point scale.

List of tables

1. Introduction

Extreme wildfire events (EWEs) have been challenging firefighting capabilities during the last two decades, causing substantial damage to ecosystems and society. These events are often associated with intense coupling of fire behavior and atmospheric conditions, leading to extreme fire characteristics (Di Virgilio et al. 2019; Ndalila et al. 2020; Castellnou et al. 2022; Tedim et al., 2018). Climate change is increasing the occurrence of severe weather conditions globally (Jolly et al. 2015; Abatzoglou and Williams 2016; Di Virgilio et al. 2019) resulting in unprecedented fire events (Duane et al. 2021). The prediction of extreme wildfire events is essential for the safety and preparedness of citizens and firefighters, as well as to design management plans. Thus, it is crucial to provide reliable and robust projections of the potential evolution of landscapes and wildfires in Europe under a changing climate.

Climate variability and extreme events have been studied extensively over the years, typically by examining daily climatic variables such as temperature or precipitation that exceed certain physically based thresholds (Easterling et al. 2000). Although these thresholds have provided valuable insights into local conditions, much of them often lack global applicability (Nicholls and Murray 1999). Hence, the approach to study extremes has evolved, with greater emphasis given on using relative thresholds that capture the extreme aspects of meteorological data distributions. To facilitate a global understanding of how extreme events are changing, there is now international coordination in selecting a subset of indices from a wide range of possibilities. This coordination allows researchers from various regions to harmoniously integrate their findings into a cohesive global perspective. A suite of indices known as the ETCCDI indices (Frich et al. 2002) based on the European Climate Assessment (ECA) indices was identified to assess trends over the second half of the 20th century (Klein Tank et al. 2002). The main aim of selecting these indices was to encompass a diverse range of climate conditions. ETCCDI adopted the majority of the ECA indices but made adjustments to those that posed some limitations when applied to diverse geographical regions. In total, they defined 27 indices. Indices such as monthly or yearly maxima and minima of daily temperatures, the maxima of daily

precipitation, dryness, and wetness, summer period and other indices calculated as the number of days exceeding a specific threshold (fixed values or relative to reference period). These indices are useful to assess extreme events such as wildfires in Europe.

In addition, some more sophisticated indices have been proposed to assess fire danger in Europe (e.g., San-Miguel-Ayanz et al. 2012; Dacamara et al. 2014; Pinto et al. 2018; Meier et al. 2023). These methods are usually based on the Fire Weather Index (FWI, Wagner et al. 1974; Van Wagner 1987). Since 2007, the FWI has been adopted at the EU level by the European Forest Fire Information System (EFFIS), a component of the Copernicus Emergency Management Service (CEMS), to assess fire danger level in a harmonized way throughout Europe after several tests on its validity and robustness for the European domain (San-Miguel-Ayanz et al. 2012).

Nonetheless, while fire weather is most often understood as a surface phenomenon (e.g., through surface temperature, wind speed, and relative humidity), atmospheric processes such as atmospheric instability can also drive extreme fire development (Castellnou et al. 2022). During convective fires (Duane et al., 2015, Costa et al., 2011, Lecina-Diaz et al., 2014), atmospheric instability plays a key role in which the interaction of the fire plume with atmospheric air can lead to pyrocumulonimbus (PyroCb) development. PyroCb (officially known as *cumulonimbus flammagenitus* clouds) are a type of cloud formed because of the condensation of the water vapor present in the plume of a wildfire. When a PyroCb is formed, it can result in extreme fire intensity and unpredictable fire behavior.

Widely used indices such as the FWI exhibited some constraints that can affect the precision of fire risk assessments because they are based on surface meteorological information and fuel moisture, lacking the atmospheric instability conditions crucial for the development of very large and extreme wildfires (Fernandes et al., 2016). To measure fire-prone atmospheric instability conditions, the Haines Index (Haines 1988) was proposed and used firstly over some regions such as the United States of America, New Zealand (Simpson et al 2014), the Mediterranean basin (Tatli and Turkes 2014) and Australia (Mccaw et al 2007). Yet, the original formula of the Haines Index presented some

limitations which were addressed by proposing the Continuous Haines Index (CHI, Mills, and McCaw 2010). Interestingly, Pinto et al. (2020) proposed a new way of incorporating atmospheric instability in widely used weather indices: by adding the C-Haines index to the FWI, they obtained the FWIe, which modulates FWI information with the instability of upper atmospheric layers.

Seasonal forecasting is an important aspect of climate science that provides valuable insights into long-term weather patterns and trends, predicting weather conditions and anomalies on seasonal timescale typically spanning a few months to a year (Luo et al. 2011). Seasonal forecasting relies on a combination of historical climate data, coupled with the understanding of large-scale climate phenomena (e.g., El Niño event), and the application of sophisticated computer models. These models, often based on coupled ocean-atmosphere circulation models, allow the simulation of the complex interactions between the atmosphere and ocean that play a key role in determining seasonal weather patterns (Collins et al. 2018). Seasonal forecasting can be applied in various sectors, including agriculture, water resource management, and disaster preparedness (Doblas-Reyes et al. 2013). Therefore, forecasting the seasonal weather conditions that can lead to increased fire risk is of great importance in enhancing proactive fire prevention efforts. Foreseeing adverse fire-prone conditions before each fire season can help policymakers and civil protection agencies in design appropriate strategies for managing fuels in fire prone areas. Additionally, it enables the efficient allocation of firefighting resources to minimize the damaging impacts of wildfires (Turco et al. 2019).

2. Deliverable aim

In this report, we aim at generating new climate projections, at different scales, decisive for the occurrence of extreme wildfire events in Europe, as well as seasonal forecast determinants for wildfire activity. We do so by using the state-of-the-art global climate model projections to calculate the variations in the mean climate and extremes through a range of absolute and threshold indices based on essential climate variables (daily

maximum (TX), minimum temperatures (TN), and daily precipitation (RR)), in the atmospheric instability through the Continuous Haines Index (CHI), the surface Fire Weather Index (FWI), and the enhanced Fire Weather Index (FWIe). The deliverable has the triple goal of 1) informing about likely evolutions of fire weather danger in Europe at the medium and long scale, and 2) providing useful climate projections at higher resolution statistically downscaled projections (~9km) to six Living Labs (i.e., representing different bioregions in Europe) of the FIRE-RES consortium, and 3) provide a sound tool of high-resolution probabilistic fire danger seasonal forecasts validation for selected Living Labs of the FIRE-RES project located in the Mediterranean region.

3. Data

In order to provide climate change projections at different spatial scales (Pan-European and Living lab levels), we mobilized monthly and daily data climate data (depending on the availability of data for each evaluated index). The time window spans three periods of 20 years: the historical period (1995-2014), the near future (2041-2060), and the far future (2081-2100).

3.1. Global Climate Models (GCMs)

To generate climate projections linked to EWEs occurrence at the Pan-European scale, we mobilized data from the Coupled Model Intercomparison Project Phase 6 (CMIP6), available at the Copernicus Climate Data Store https://cds.climate.copernicus.eu. The Climate Data Store (CDS) provides information about the past, present, and future climate, on the global, continental, and regional scale. It contains a variety of data types including satellite observations, in-situ measurements, climate model projections, and seasonal forecasts. The CMIP6 is the latest project by the World Climate Research Programme's Working Group on Coupled Modelling. It started in the late 90s as a comparison of a handful of early global coupled climate models making experiments using atmospheric models coupled to a dynamic ocean, land surface, and thermodynamic sea ice (Meehl et al., 1997). The global models produced by the CMIP6

feature a vertical coverage between 1 to 1000hPa pressure levels. CMIP6 incorporates new scenarios based on a matrix that uses the shared socioeconomic pathways (SSP, O'Neill et al. 2015).

Data were mobilized under 5 climatic models (CMCC-ESM2 (Italy); CNRM-CM6-1-HR (France); CNRM-ESM2-1 (France); EC-Earth3-Veg-LR (Europe); HadGEM3-GC31-LL (UK; used only in the calculation CHI and FWIe)). These climate models were selected according to the data availability at different scales (i.e., different atmospheric levels and near future level) and due to their good performance in capturing a range of large-scale processes thar are important for the European climate representation (Palmer et al. 2023).

Projections were made using three shared socioeconomic pathways scenarios: SSP1-2.6; SSP2-4.5; SSP5-8.5. The differences between these SSPs lie in their socioeconomic and climate mitigation characteristics. SSP1-2.6 represents a sustainable and low-emission pathway, SSP2-4.5 represents a moderate-emission pathway, and SSP5-8.5 represents a high-emission and fossil-fuel-dependent pathway. These scenarios are used to explore a range of potential futures and their implications for climate change and adaptation and mitigation strategies (O'Neill et al. 2015).

3.2. ERA5-Land

In addition, as reference observational dataset for the bias correction in the downscaling of climate data to the Living Lab scale, the state-of-the-art global reanalysis dataset ERA5-Land (Muñoz-Sabater, 2019) available in Copernicus CDS was used. The dataset provides a total of 50 variables describing the water and energy cycles over land, globally, hourly, and at a spatial resolution of 9 km from 1950 to present (Muñoz-Sabater et al., 2021).

3.3. Seasonal forecasts

To perform the seasonal forecasting, the fifth generation ECMWF seasonal forecasting system (SEAS5) (Johnson et al., 2019) version 5.1 available in the C3S Climate

Data Store (CDS) was used. SEAS5 has been operational since November 2017, replacing System 4. The system includes updated versions of the atmospheric (IFS) and ocean (NEMO) models with the addition of the interactive sea-ice model LIM2 (Johnson et al., 2019). The set of re-forecasts (hindcasts) available in the CDS starts on the 1st of every month for the years 1981-2016 and contains 25 ensemble members. The data from these re-forecasts are used to verify the forecasting system and calibrate real-time forecast products. Real-time forecasts (from 2017 onwards) consist of a 51-member ensemble initialized every month and integrated for 7 months. Both re-forecast and forecast data are available at a global 1x1 degree grid.

4. European Scale

4.1. Methods

4.1.1. Region and projection

The analysis has been performed for the whole European domain (exception are of the outermost islands neither overseas European regions, as Guadalupe, Martinique, Guyane, Reunion and Mayotte (France), and Jan Mayen and Svalbard (Norway)). We used the WGS84 datum with latitude / longitude coordinates.

4.1.2. Variables

4.1.2.1. Essential Climate Variables

Essential climate variables (such as temperature and precipitation) are included in the projections at the European scale. Table 1 includes the definition of all the variables and indices examined.

Table 1. List of variables and indices examined.

Index	Abbreviation	Definition
-	TX	Average daily maximum temperature (ºC)
-	TN	Average daily minimum temperature (ºC)
-	RR	Total precipitation amount (mm)
Summer days	SU	Number of days with TX>25oC
Very hot days	SU35	Number of days with TX>35oC
Tropical nights	TR	Number of days with TN>20oC
Number of wet days	RR1	Number of days with RR>1mm

Index	Abbreviation	Definition
Monthly maximum 1-day precipitation	Rx1day	Maximum daily precipitation (mm)
Fire Weather Index	FWI	Values of fire weather danger start at 0 and are open ended
Continuous Haines Index	C-Haines	Values between 0 and 13 of atmospheric instability
Enhanced Fire Weather Index	FWIe	Values between 0 and 100 of weather fire danger together with instability

4.1.2.2. Fire Weather Index (FWI)

FWI is a daily meteorologically based system used worldwide to estimate fire danger in a generalized fuel type (mature pine forest) (van Wagner 1987). It consists of six components each measuring a different aspect of fire danger (Figure 1). Three components (Fine Fuel Moisture Code (FFMC), Duff Moisture Code (DMC), and Drought Code (DC)) represent the fuel moisture codes, which are numeric ratings of the moisture content of the forest floor and other dead organic matter. Their values rise as the moisture content decreases. There is one fuel moisture code for each of the three layers of fuel: litter and other fine fuel, loosely compacted organic layers of moderate depth; and deep, compact organic layers. The two intermediate subcomponents, Initial Spread Index (ISI) and Build-Up Index (BUI), are fire behavior indices. The ISI is a numerical rating of the expected fire rate of spread which combines the effect of wind and FFMC. The BUI is a numerical rating of the total amount of fuel available for combustion that combines the DMC and the DC. The resulting index is the Fire Weather Index (FWI), which combines ISI and BUI, and can be used as a general index of fire danger (Wotton 2009). The meteorological data required to calculate FWI are noon values of 2m air temperature and relative humidity, 10m wind speed, and 24h accumulated precipitation. According to the European Forest Fire Information System (EFFIS), FWI can be classified for the European domain into six levels of fire danger as follows: Very low danger: FWI ≤5.2; Low danger: 5.2 <FWI ≤11.2. Moderate danger: 11.2 <FWI ≤21.3. High danger: 21.3 <FWI ≤ 38.0. Very high danger: 38.0 <FWI ≤50. Extreme danger: FWI ≥50

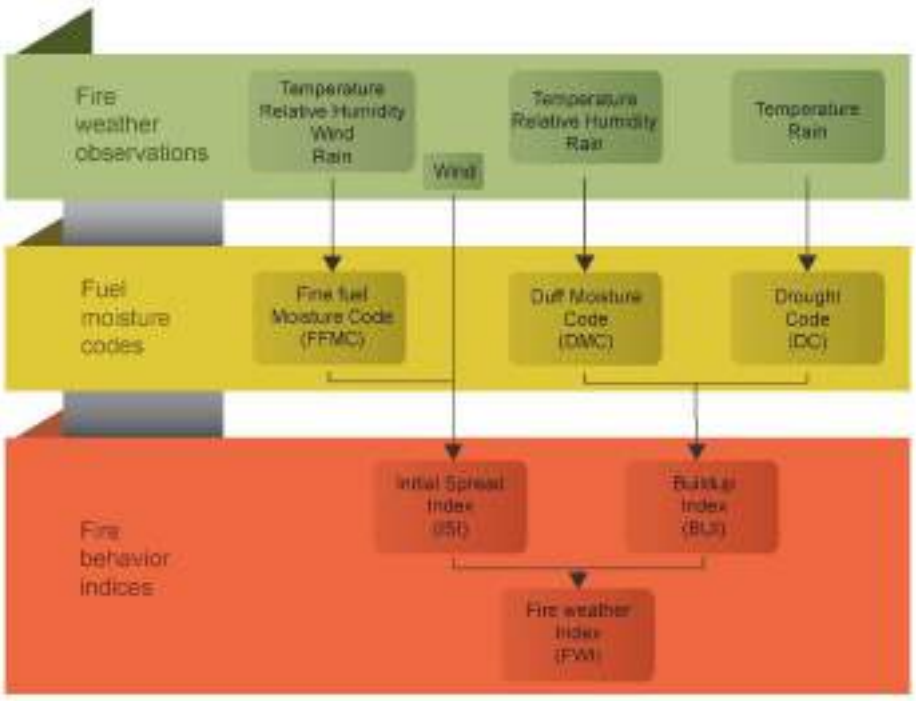

Figure 1: Structure of the Fire Weather Index (FWI) System (Van Wagner 1987).

4.1.2.3. Continuous Haines Index

The Continuous Haines Index (CHI) is a measure of vertical stability and dryness, linked to the fire-convections phenomena (Mills, and McCaw 2010). CHI is composed of two terms: (1) an instability term (*CA*) representing the difference in temperature at two different atmospheric levels (850 and 700 hPa) and (2) a moisture term (*CB*) representing the difference between temperature and dew point at the lower atmospheric level. CHI ranges between 0 and 13 where high values of CHI (≥5) means a higher instability promoting strong convection, and therefore, the potential for fire to become large and exhibiting unpredictable behavior. This is because the upward movement of the air can generate strong convection columns above the fire with strong indraft winds at ground level. Moreover, when the pyro-cloud loses its buoyancy and collapses, it generates downdrafts and spotting, leading to unpredictable and rapid fire spread (Figure 2). CHI is calculated as follows (Ndalila et al. 2020):

$$CA = (T850 - T700) /2-2, \quad (1)$$

$$CB = \min (T850 - DP850,30) /3-1, \quad (2)$$

If CB > 5, then CB = 5+ (CB - 5) / 2

CHI=CA+CB, (3)

where the T700 and T850 are the temperatures at 700 and 850 hPa, and DP850 is the dew point temperature at 850 hPa calculated using the relative humidity at the same atmospheric level using the package "*weathermetrics*" R package. The min (T850 – DP850, 30) term in equation (2) means that an upper threshold of 30 ºC is established to the difference between the temperature and dewpoint at 850 hPa. CHI is therefore calculated by using equation (3) for each grid pixel.

Figure 2. Pyrocumulonimbus at the Santa Coloma de Queralt Fire, 2021, Catalonia, Spain. Credits: Gerard Reyes.

4.1.2.4. *Enhanced Fire Weather Index (FWIe)*

The enhanced fire weather index (FWIe), incorporates, in addition to the common conventional FWI, the atmospheric instability in the form of the CHI. FWIe has similar fire risk levels classification to the FWI, however it shows higher values than FWI (Figure 3) in the case of high atmospheric instability and it presents lower values than FWI in the case of stable atmospheres (Pinto et al. 2020).

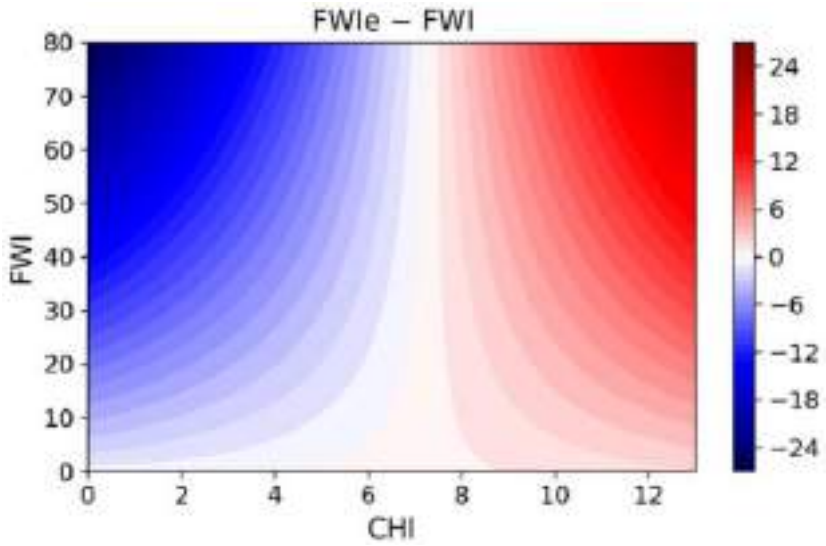

Figure 3: The difference between FWIe and FWI for successive values of the FWI and CHI (Pinto et al. 2020)*. The figure shows that FWIe takes higher values than FWI (red colors) in case of higher levels of atmospheric instability (between 8 and 12 CHI).*

4.1.3. Analysis

For the essential Climate Variables mobilized, an annual and seasonal basis are examined to investigate variations in the mean climate and extremes across the European domain. For each of the indices, the difference between the future and the reference period is considered robust following the study of Varotsos et al. (2021). In particular in each (land) grid point across the European domain, the change is considered robust when the changes in at least three out of five models are statistically significant and of the same sign. The first criterion is tested using bootstrap 95th percentile confidence intervals. If only one of the requirements is met, the change at the particular

grid point is considered insignificant. The results in this report are shown for TX, TN and RR while the results for the rest of the indices will be available in ncdf format files.

For the FWI, CHI and FWIe we calculated the monthly means (of the 5 climate models) over the three-study period (reference, near future and far future) under the three climate scenarios (ssp1-2.6, ssp2-4.5, and ssp5-8.5). As the period between June and August is the most fire active period (summer period), we calculated also the mean of summer period for the three indices over the three study periods and under the three climate scenarios. We calculated the projected changes as follows:

$$\textit{Projected Change} = \text{index}_{[T,\,S]} - \text{index}_{[R]}$$

Where:

Index: is one of the three studied indices (CHI, FWI, FWIe)

R: reference period (1995-2014)

T: study period (near future and far future)

S: climate scenarios (SPP1-2.6, SSP2-4.5, and SSP5-8.5)

Moreover, in order to evaluate which country is expected to experience higher increases over the summer season in the potential conditions leading to EWE occurrence, we conducted an analysis wherein we computed the average, maximum, minimum, and mode of changes in the FWIe for each European country.

4.2. Results

4.2.1. Temperature

In Figures 4-7 the results for the average annual and JJA TX and TN are shown for the three periods examined and under all SSP scenarios. In terms of annual TX, Figure 4 indicates that, according to the SSP5-8.5 future climate scenario, warming is clearly higher over the period 2081-2100, reaching around 5.5°C with respect to 1995-2014. Lower increases are shown for the same period under SPP1-2.6 and SSP2-4.5, of roughly 1.5°C and 2.5°C, respectively. As far as the 2041-2060 period is concerned, the highest increases are projected under SSP5-8.5 reaching about 1.6°C, while for the rest of the scenarios the

increases do not exceed about 1.3°C. It should be noted that in most of the scenarios considered, the greatest warming is projected for the northern European regions, followed by the Mediterranean. Similar spatially averaged magnitude of warming is shown for the JJA TX for all future periods and under all SSP scenarios (Figure 5) with the highest increases however found in the Mediterranean region. Higher increases than TX are found for TN (Figure 6 and 7). In particular, the highest increase reaches about 7°C under SSP5-8.5 for the distant future period while under SSP2-4.5 and SSP1-2.6 the warming is about 2.8°C and about 1.5°C, respectively. For the near future period (2031-2060) the highest increases are found under SSP5-8.5 reaching about 1.8°C with the other two scenarios indicating increases of about 0.3°C lower. Regarding the JJA TN, for the distant future the increase reaches about 6°C under SSP5-8.5 followed by an increase of about 2.5oC and about 1.5oC under SSP2-4.5 and SSP1-2.6, respectively. For the near future the projected increases reach about 1.6oC, 1.2oC and 1.1oC under SSP5-8.5. SSP2-4.5 and SSP1-2.6, respectively.

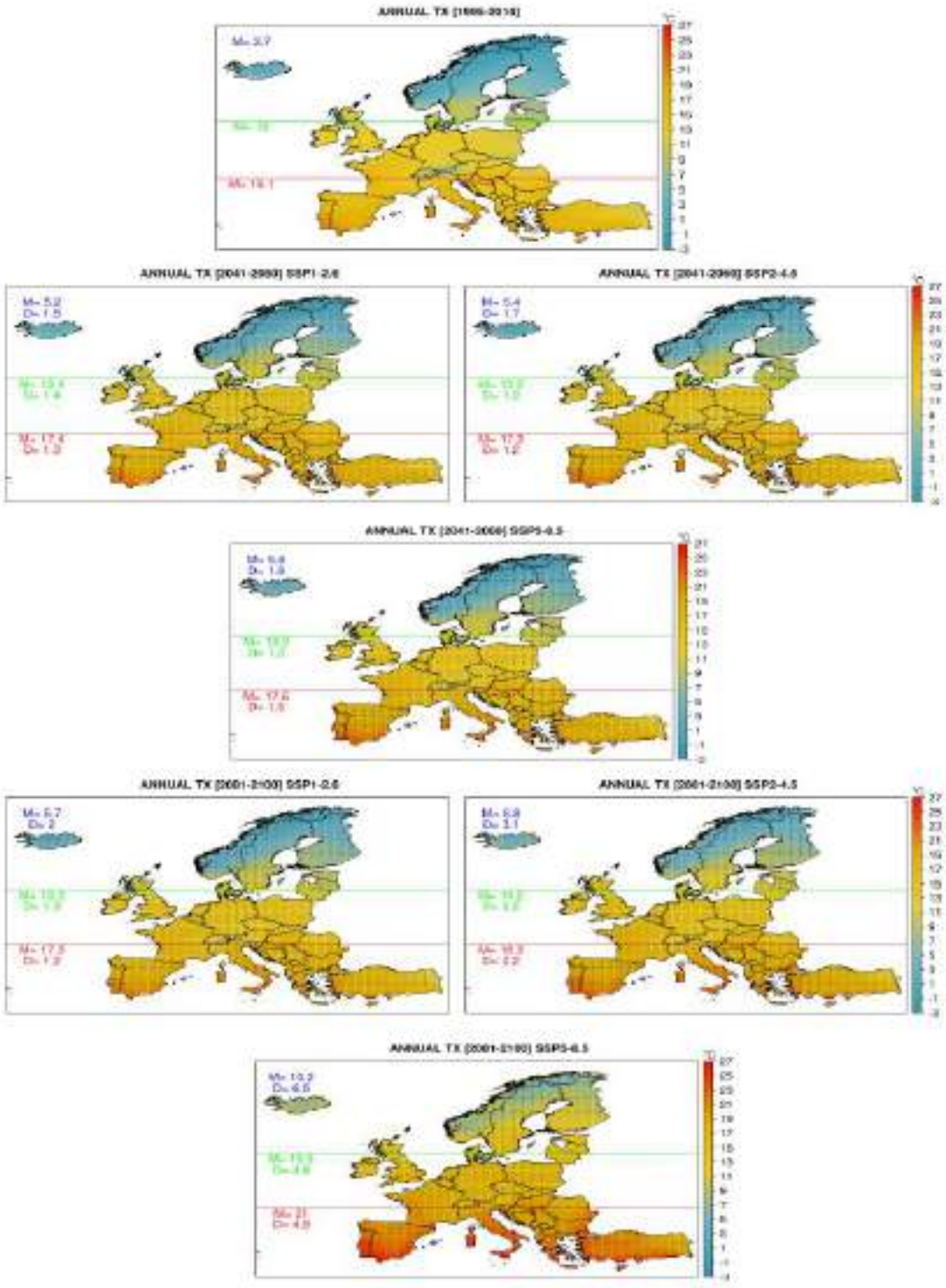

Figure 4. Average annual TX for all periods and scenarios examined. In each plot M indicates the average value calculated over all grid points in each zone whereas D is the absolute change between the future periods and the reference one. Black dots indicate robust changes at the grid point scale.

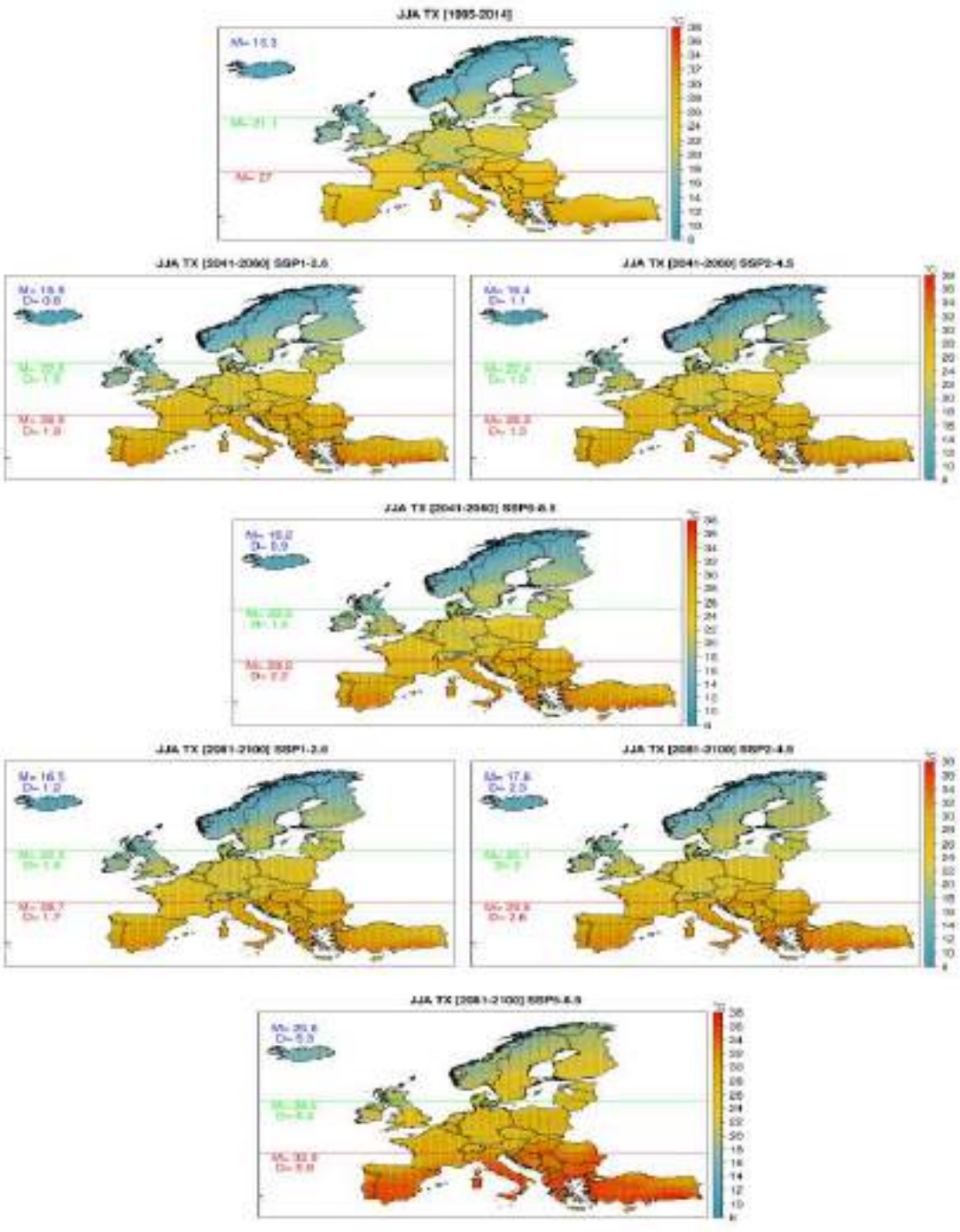

Figure 5. Average JJA TX for all periods and scenarios examined. In each plot M indicates the average value calculated over all grid points in each zone whereas D is the absolute change between the future periods and the reference one. Black dots indicate robust changes at the grid point scale.

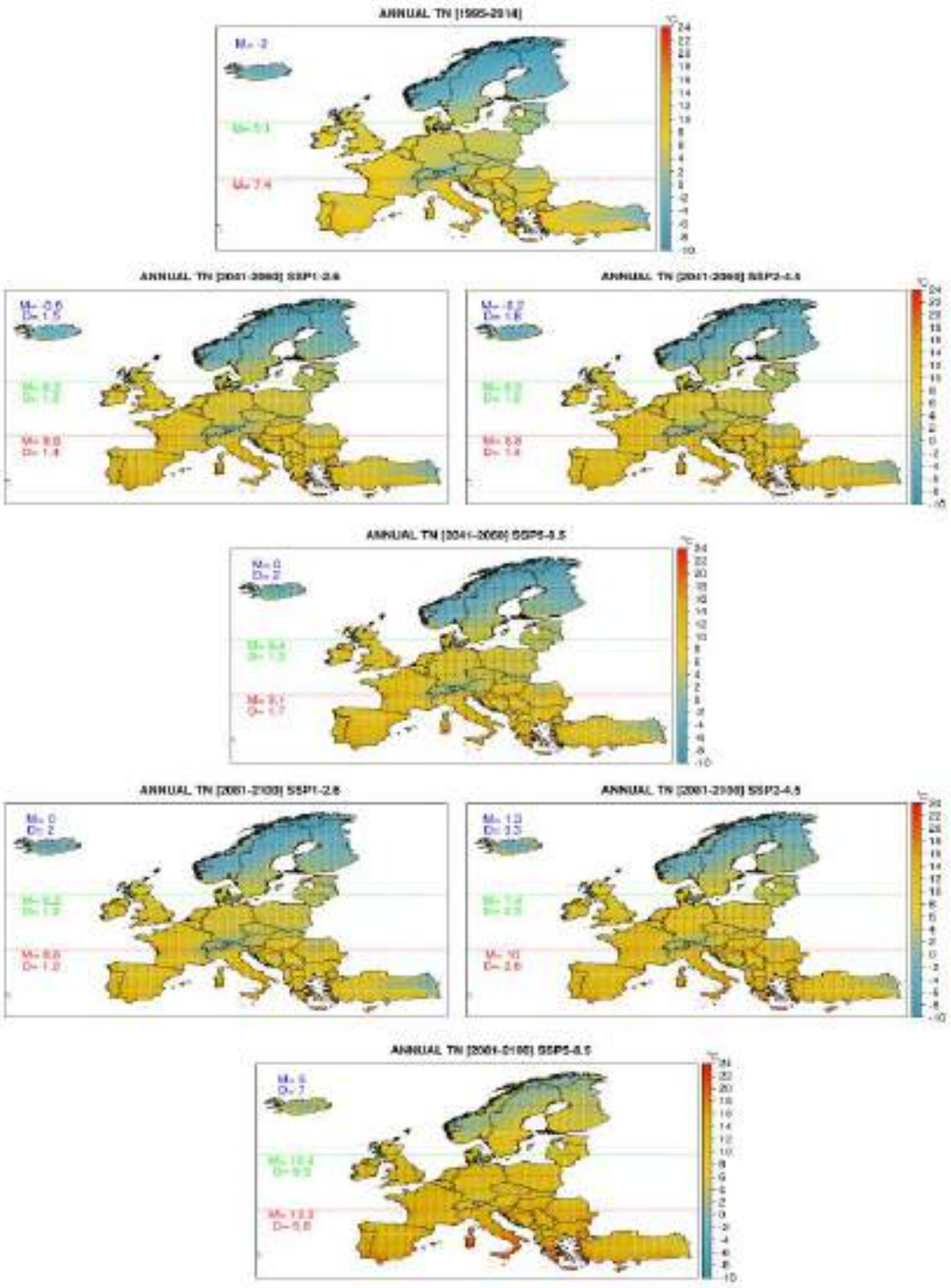

Figure 6. Average annual TN for all periods and scenarios examined. In each plot M indicates the average value calculated over all grid points in each zone whereas D is the absolute change between the future periods and the reference one. Black dots indicate robust changes at the grid point scale.

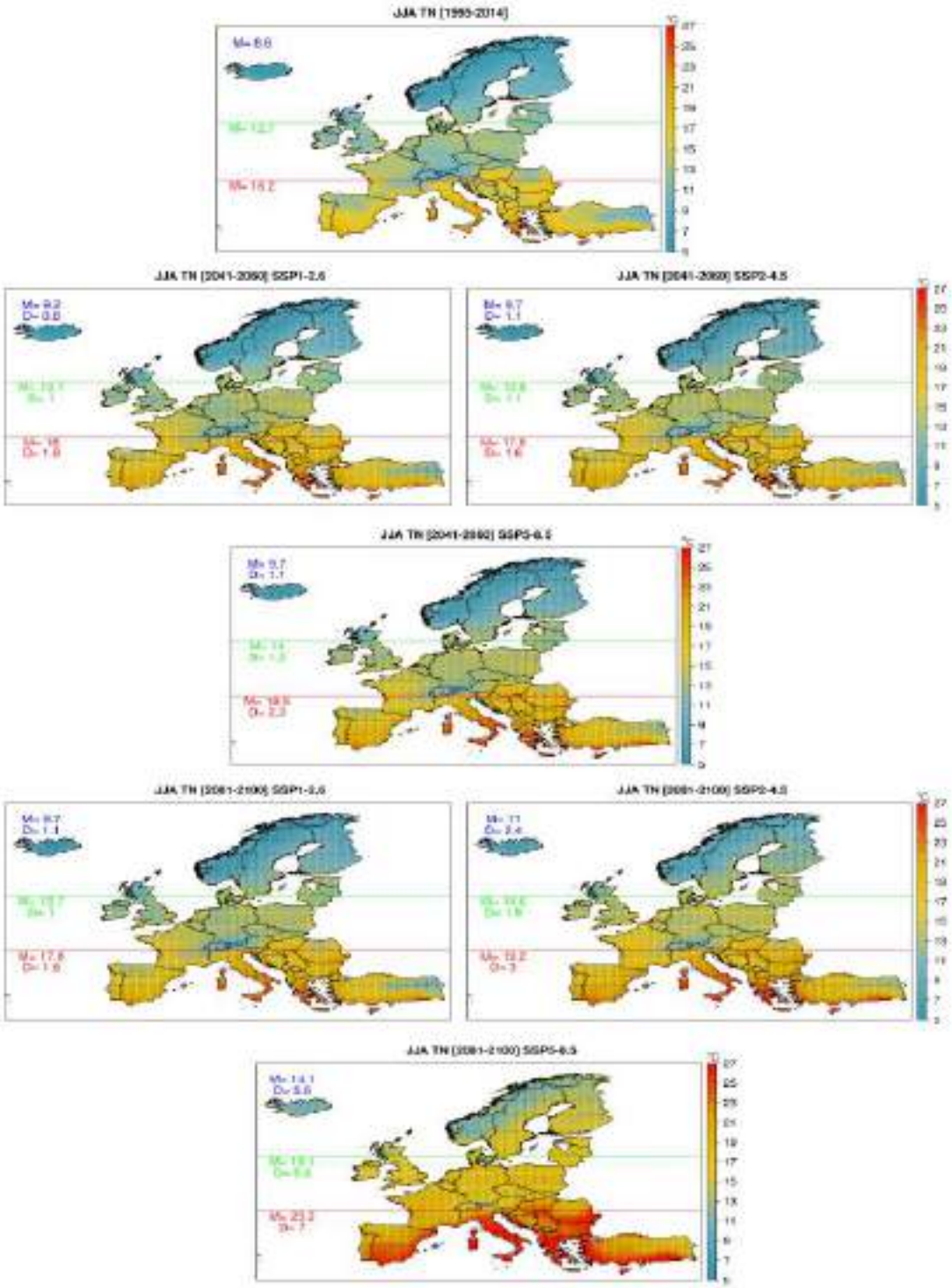

Figure 7. Average JJA TN for all periods and scenarios examined. In each plot M indicates the average value calculated over all grid points in each zone whereas D is the absolute change between the future periods and the reference one. Black dots indicate robust changes at the grid point scale.

4.2.2. Precipitation

In contrast to temperatures, precipitation spatial changes in Europe are more variable regarding the signal of climate change as well as the robustness of the results. In Figure 8 the results for the average annual number of wet days (RR1) are shown. From the Figure it is evident that the number of wet days declines in the Mediterranean by about 8-10% for the near future period under all scenarios examined while for the distant future the decline is higher reaching about -23% under SSP5-8.5 and about -10% for both the SSP2-4.5 and the SSP1-2.6. Regarding Central Europe the decline ranges from -5% to -1% while for the northern European area increases are projected ranging from 1% to 9% depending on the period and the scenario examined. Regarding the total annual precipitation (RR) amount (Figure 9), decreases are projected for the Mediterranean under both future periods and under all scenarios. The decreases range from -41% to -9% for the distant future under SSP5-8.5 and the near future under SSP2-4.5, respectively. For the Central Europe and for the majority of the simulations, increases are projected in the range from 4% to 9% while in only two simulation declines of about -1% are shown. For the northern areas an increase in the total annual RR is projected under both future periods and under all scenarios. The highest increases are found by the end of the century and under the SSP5-8.5 reaching about 28%. Overall, the highest precipitation decreases in the Mediterranean are projected for the summer (JJA) period (Figure 10). In particular the highest deceases are simulated by the end of the century under SSP5-8.5 reaching about -40% while the lowest ones are simulated for the near future under SSP2-4.5, about -10%. For the Central European the highest deceases are simulated by the end of the century under SSP5-8.5 reaching about -17%, while for the Northern areas, increases are simulated under all experiments with the highest increase simulated for the same period and scenario reaching about 18%.

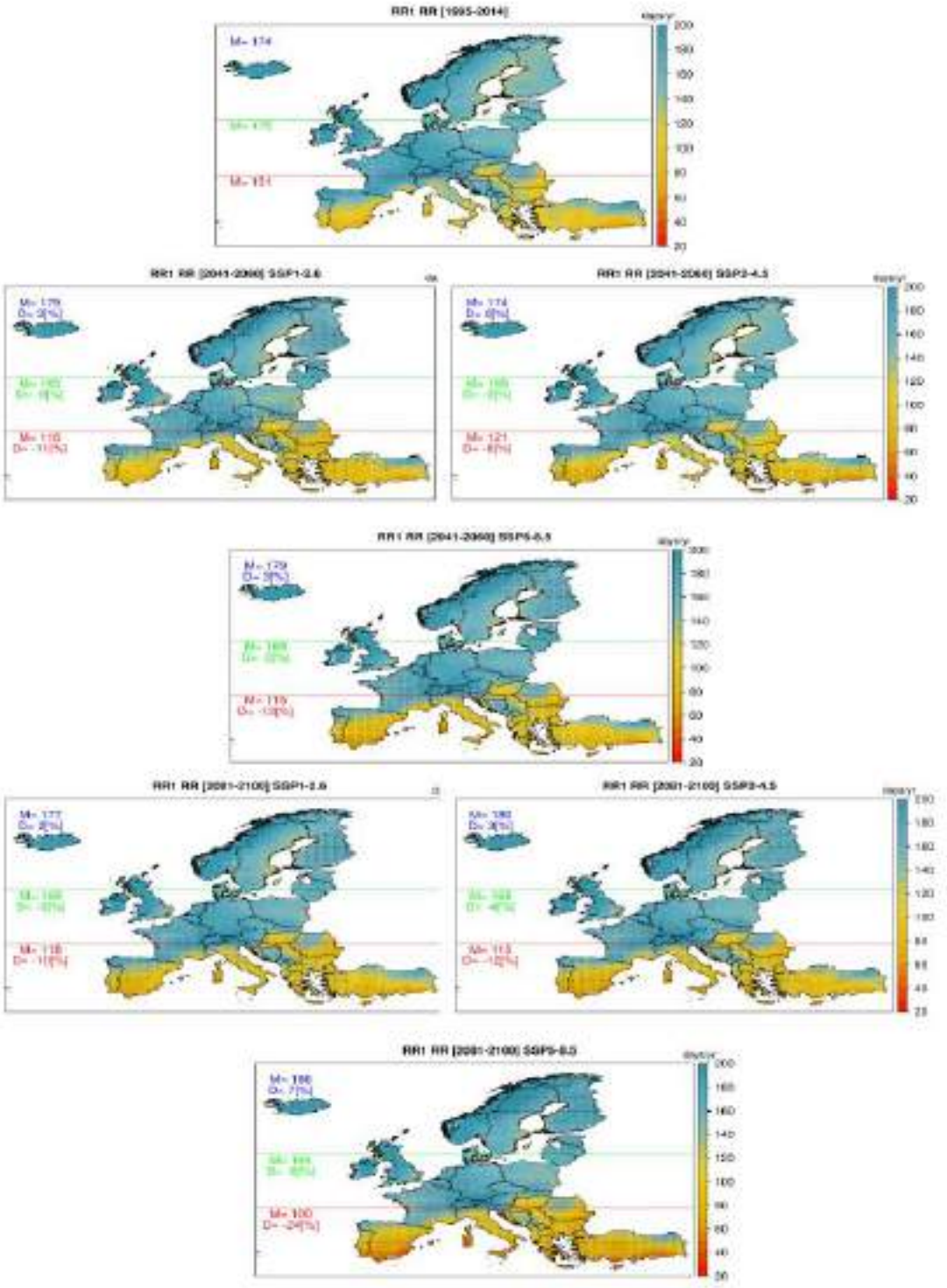

Figure 8. Average annual RR1 for all periods and scenarios examined. In each plot M indicates the average value calculated over all grid points in each zone whereas D is the relative change between the future periods and the reference one. Black dots indicate robust changes at the grid point scale.

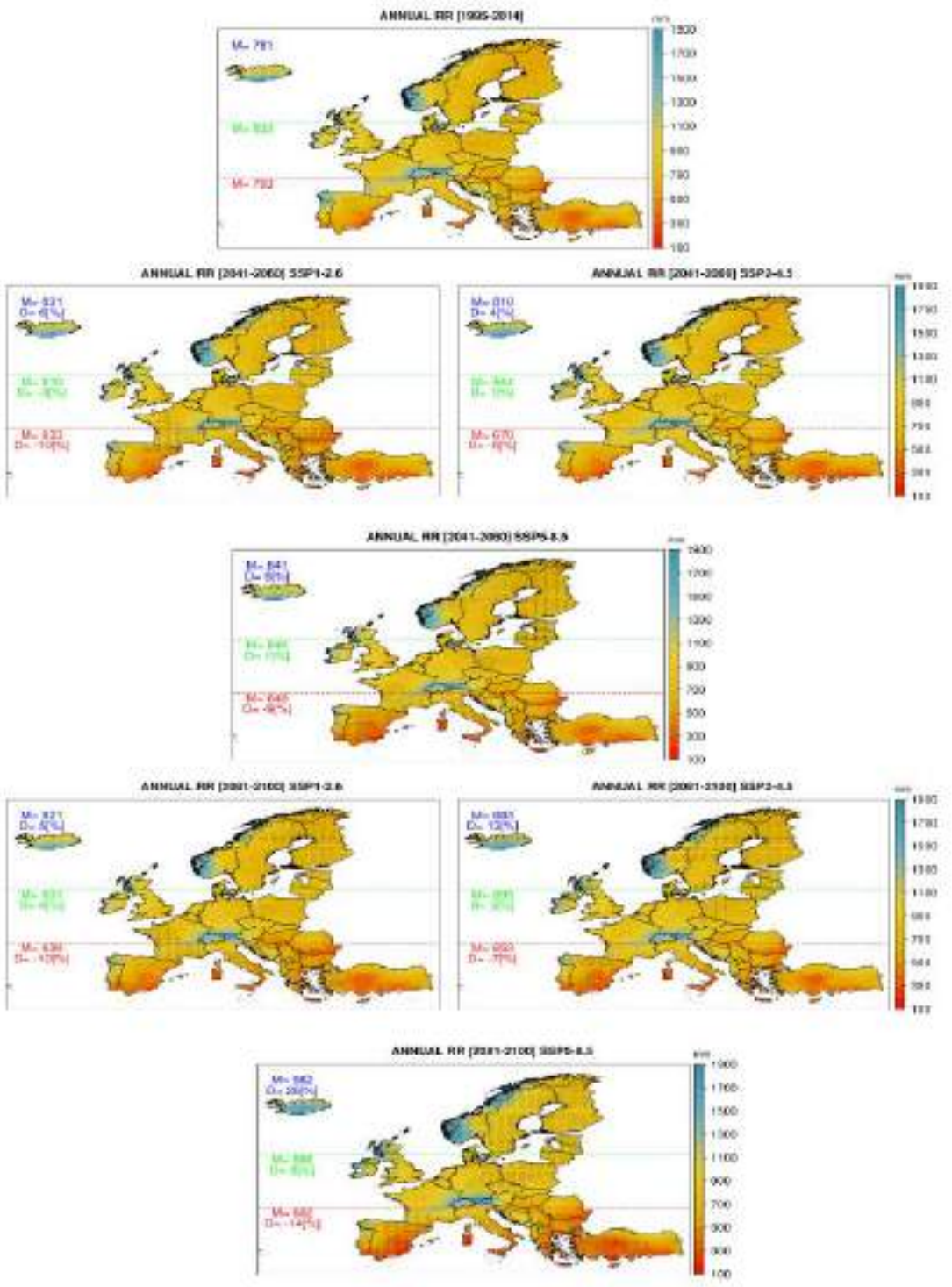

Figure 9. Total annual RR for all periods and scenarios examined. In each plot M indicates the average value calculated over all grid points in each zone whereas D is the relative change between the future periods and the reference one. Black dots indicate robust changes at the grid point scale.

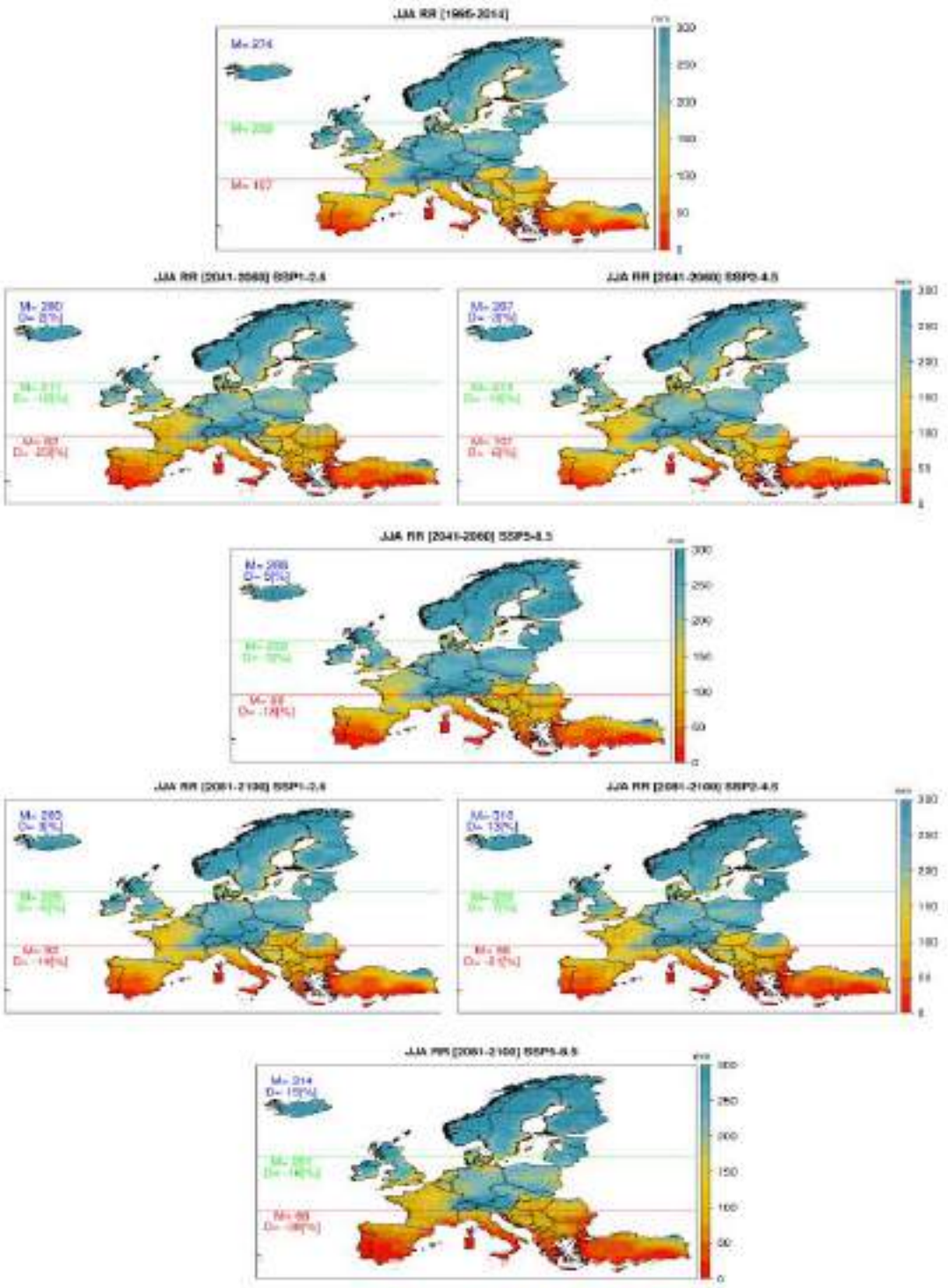

Figure 10. Total JJA RR for all periods and scenarios examined. In each plot M indicates the average value calculated over all grid points in each zone whereas D is the relative change between the future periods and the reference one. Black dots indicate robust changes at the grid point scale.

4.2.3. FWI, CHI and FWIe

4.2.3.1 Observed conditions

Over the historical period (1995-2014), JJA FWI results (Figure 11) show an increase for all future periods and under all examined scenarios. The Mediterranean is expected to have the most significant alterations, with FWI average class changes ranging from moderate during the reference period to high for the future periods. Furthermore, in Spain and Greece, fire danger increases even more with FWI levels under very high and extreme situations. The FWI levels in central and northern Europe are anticipated to be in the lowest class with low fire danger conditions, while rises are projected in most future scenarios.

The continuous Haines index showed high values (CHI>5) starting from April to October especially within southern Europe (Mediterranean countries such as Portugal, Spain, Italy, Greece, and Turkey, Figure S1). The highest values were observed during the summer period, between June and August. The lowest values were observed however in northern countries of Europe (e.g., United Kingdom). These regions showed low values of CHI (>5) during the 12 months with non-significant increases during the summer period.

The enhanced fire weather index showed high values that exceeded 21.3 corresponding to a high risk of large fire (Figure S10). These high values were observed in the Southern regions (i.e., Mediterranean basin), between May and October (Figure S10). In these regions, extreme risk of wildfires (FWIe ≥ 50) was observed during July and August, except in Southeast Turkey where extreme wildfire risk was extended between May and September. This is because of the coincident higher values of FWI and CHI over the same period (1995-2014).

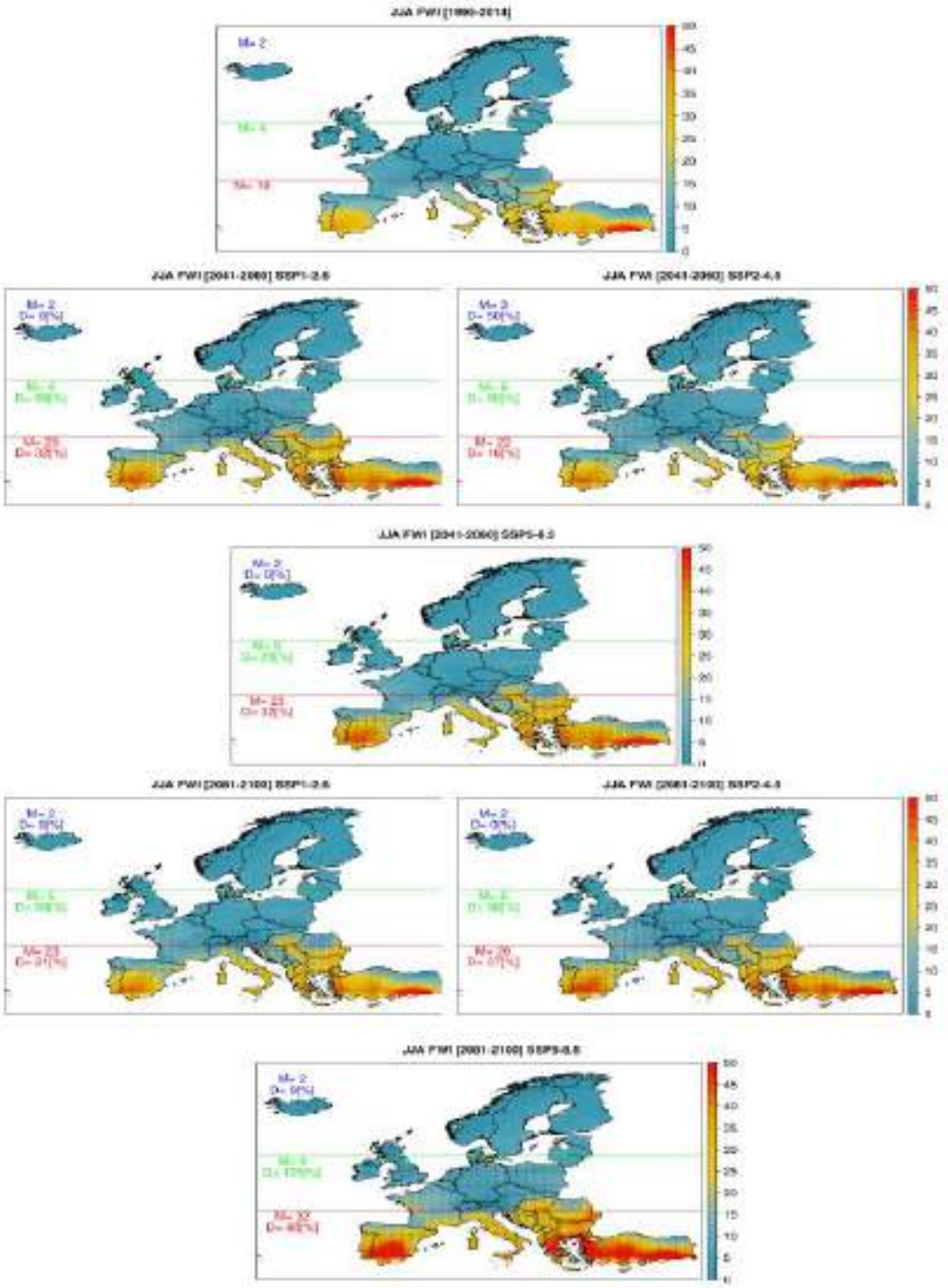

Figure 11. JJA average FWI values for all periods and scenarios examined. In each plot M indicates the average value calculated over all grid points in each zone whereas D is the relative change between the future periods and the reference one. Black dots indicate robust changes at the grid point scale.

4.2.3.2. Climate projections of indices linked to the occurrence of EWE in Europe

The potential conditions that lead to the EWE occurrence in Europe are expected to increase over the next decades. The JJA enhanced fire weather index results showed high increases (up to +27), especially in the southern regions such as Spain, Portugal, Greece Turkey, and some regions in the Balkans peninsula (Figure 11). These increases were observed under all SSP climate models with the higher values observed under the ssp5-8.5 climate model over the far future period (2081-2100). Moreover, the increases over the far future are expected to extend northward to reach central and northern European countries. Indeed, high increases in the enhanced FWI were observed within central Europe in countries such as France and Austria and northwestern countries such as Belgium and Germany. Regarding the CHI projections, we observed slightly higher atmospheric instability than the historical period covering the same regions but lasted until November within some regions such as southeaster of Spain and Turkey (Figures S2-S9).

The climate projections of the FWIe showed almost similar spatial distribution patterns of the conditions linked to the EWE occurrence. However, the fire risk was much higher than the reference period (1995-2014) and covered a larger period of the year (Figures 12-13, S12-16). Moderate fire risk (FWIe ≥11.2) was observed in April and November within some regions in the southeast of Spain and Turkey under all SSP scenarios over the two future periods. The high risk of EWE occurrence (FWIe ≥21.3) was observed between May and October in the Southern and Southern east of Europe (e.g., the Iberian Peninsula, Greece and Balkans; Tables 2 and 3). Similarly, to the observed period, the projected conditions linked to extreme risk of EWE occurrence (FWIe ≥50) was observed, yet with higher values and more extent, between June and September over the two future study periods and under all SSP climate scenarios. Similarly, to the reference periods, these results were the consequence of the coincidence of high atmospheric instability and near-surface fire risks expected in the future (Figures 11,12-13 and S1-S16).

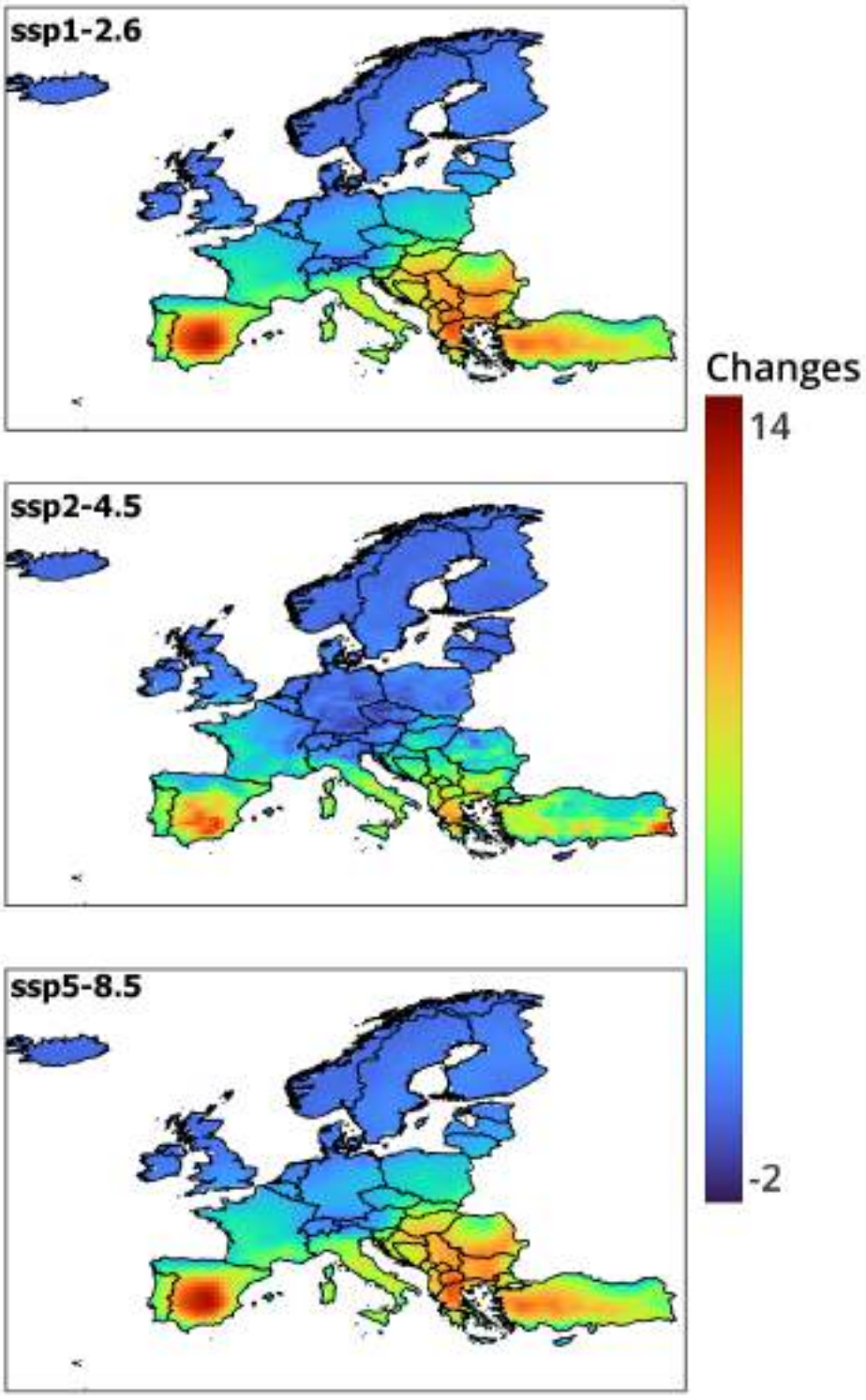

Figure 12. Mean changes in the summer enhanced Fire Weather index (Jun-July-August) between the near future (2020-2041) and the historical period (1995-2014) under the SSP1-2.6, SSP2-4.5 and SSP5-8.5 respectively.

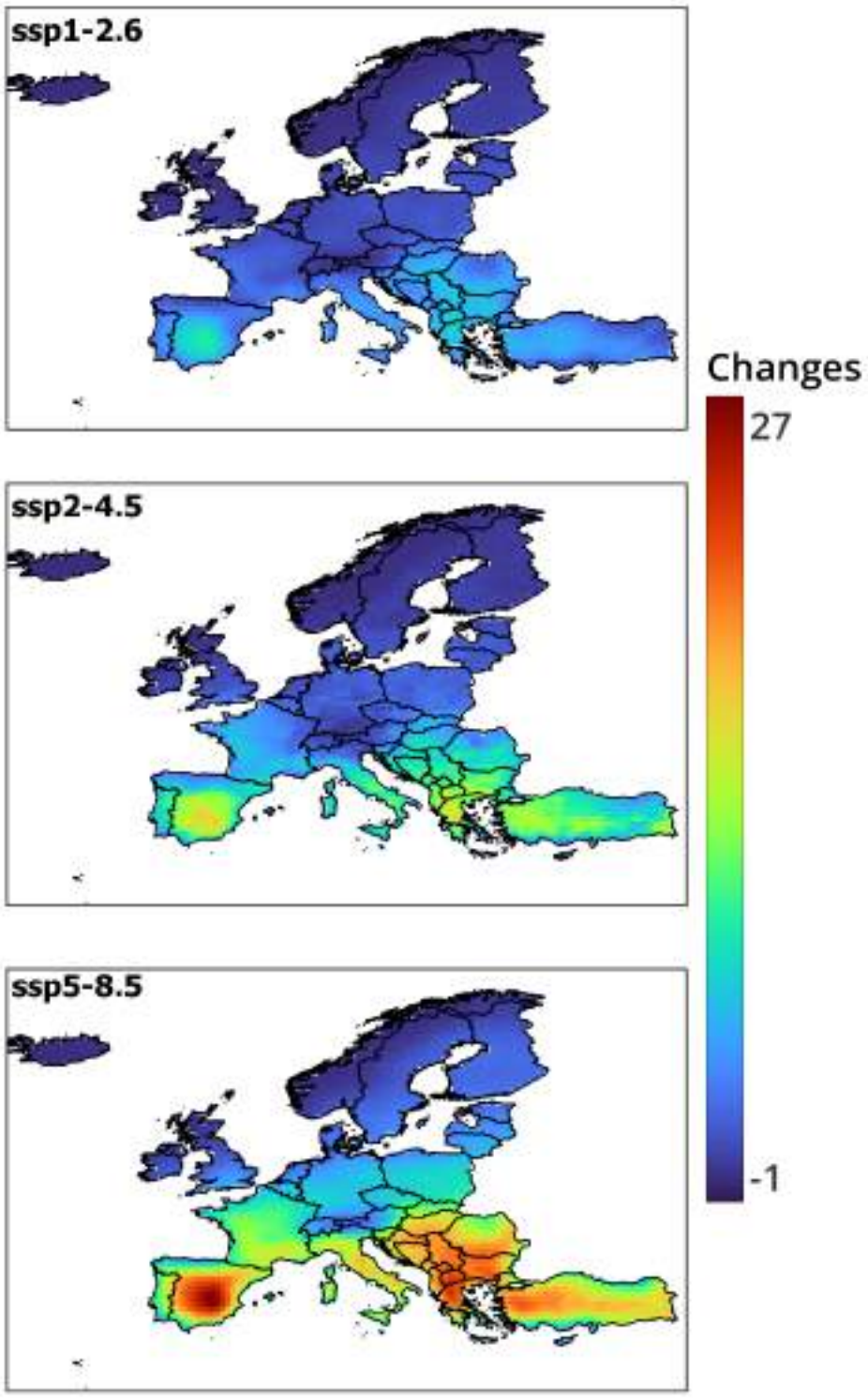

Figure 13. Mean changes in the summer enhanced Fire Weather index (Jun-July-August) between the far future (2081-2041) and the historical period (1995-2014) under the SSP1-2.6, SSP2-4.5, and SSP5-8.5 respectively

Table 2. Descriptive statistics of the changes in summer FWIe according to the European countries over the near future period (2041-2060) under the ssp1-2.6, ssp2-4.5 and ssp8.5 climate scenario respectively.

	SSP1-2.6			SSP2-4.5			SSP5-8.5		
	mean	min	max	mean	min	max	mean	min	max
Greece	6.57	2.60	8.60	6.52	1.80	10.50	8.09	3.20	11.00
Netherlands	0.68	0.40	1.00	0.27	-0.20	0.50	0.68	0.30	1.30
Albania	6.81	5.90	7.90	6.48	4.70	8.10	8.35	7.00	9.90
Finland	0.07	-0.40	0.30	0.19	-0.30	0.70	0.57	0.00	0.90
Liechtenstein	0.70	0.70	0.70	0.10	0.10	0.10	0.60	0.60	0.60
Belgium	1.23	1.00	1.50	0.75	0.00	1.20	1.52	1.10	1.80
Bosnia and Herzegovina	5.64	4.90	6.50	4.17	2.80	5.90	7.27	6.50	8.30
Bulgaria	6.57	3.30	7.70	5.52	2.70	9.00	8.86	4.90	9.80
Germany	1.09	0.60	1.70	0.03	-1.10	1.10	1.38	0.30	2.30
Czechia	2.00	1.30	3.60	0.03	-1.40	1.50	2.64	1.70	4.70
Lithuania	0.37	0.10	0.80	0.27	-0.30	1.00	1.76	0.90	2.80
Latvia	0.05	-0.20	0.30	0.05	-0.40	0.50	1.22	0.80	1.80
Türkiye	4.18	1.00	7.10	5.04	1.40	12.70	6.91	2.60	10.40
Luxembourg	1.09	1.00	1.30	0.64	-0.20	1.00	1.79	1.70	1.90
France	2.75	1.10	4.60	2.15	-0.20	5.90	3.09	1.20	5.30
Hungary	5.38	3.50	6.50	2.29	0.10	3.90	7.45	5.60	8.90
United Kingdom	0.33	-0.20	1.10	0.66	-0.20	2.20	0.54	-0.10	1.40
Kosovo	6.85	6.60	7.20	5.45	4.70	6.10	9.15	8.60	9.60
Croatia	5.28	3.70	6.90	2.82	1.00	4.60	7.11	5.30	8.90
Slovenia	3.01	1.80	4.10	1.40	0.10	2.50	4.38	2.70	5.80
Denmark	0.45	0.20	0.60	0.68	0.20	1.10	0.38	0.20	0.60
Sweden	0.23	-0.10	0.70	0.22	-0.30	0.80	0.42	0.00	0.90
North Macedonia	7.86	7.10	8.20	6.49	5.10	7.60	10.06	8.90	10.60
Montenegro	5.88	5.10	6.20	5.58	4.00	6.10	7.57	6.70	8.00

	SSP1-2.6			SSP2-4.5			SSP5-8.5		
	mean	min	max	mean	min	max	mean	min	max
Ireland	0.11	-0.10	0.40	0.49	0.00	1.00	0.34	0.10	0.70
Estonia	-0.03	-0.10	0.20	0.05	-0.20	0.20	0.73	0.50	1.20
Switzerland	1.02	0.70	1.60	0.48	-0.30	1.10	1.03	0.60	1.70
Portugal	5.14	2.90	7.50	5.18	3.40	6.80	6.08	3.80	8.50
Malta	2.30	2.30	2.30	2.00	2.00	2.00	3.00	3.00	3.00
Slovakia	3.64	2.70	4.90	1.73	0.40	2.50	5.17	4.00	6.80
Italy	4.38	0.70	6.60	3.49	-1.00	7.10	5.04	0.60	7.50
Serbia	6.94	6.20	7.50	4.37	2.30	6.60	8.97	8.00	9.80
Cyprus	1.33	1.20	1.50	-0.93	-1.40	-0.30	1.67	1.40	1.90
Austria	1.75	0.60	4.30	0.33	-0.90	1.80	2.44	0.50	5.80
Iceland	0.00	-0.10	0.10	0.01	-0.10	0.10	0.02	-0.10	0.10
Romania	5.05	2.60	7.40	2.93	-0.10	5.30	7.37	4.30	10.00
Poland	1.47	0.40	2.80	0.55	-0.60	2.80	2.66	0.80	4.70
Spain	6.46	1.50	11.30	5.98	1.10	12.00	7.56	1.60	13.20
Norway	0.06	-0.10	0.50	0.09	-0.30	0.40	0.11	-0.10	0.50

Table 3. Descriptive statistics of the changes in summer FWIe according to the European countries over the far future period (2081-2100) under the ssp1-2.6, ssp2-4.5 and ssp8.5 climate scenario respectively.

	SSP1-2.6			SSP2-4.5			SSP5-8.5		
	mean	min	max	mean	min	max	mean	min	max
Greece	5.46	2.60	7.30	11.02	3.30	15.90	17.12	5.90	23.60
Netherlands	0.61	0.30	1.00	1.50	1.00	2.00	3.59	2.10	6.00
Albania	5.72	4.90	6.60	11.72	9.00	14.30	18.92	15.50	22.00
Finland	0.64	0.00	1.10	0.65	0.10	1.20	2.13	0.20	3.10
Liechtenstein	0.30	0.30	0.30	0.80	0.80	0.80	3.00	3.00	3.00
Belgium	1.12	0.90	1.30	2.55	1.90	3.30	6.09	4.30	7.40
Bosnia and Herzegovina	4.30	3.70	5.00	8.65	7.40	10.70	17.39	15.50	18.90
Bulgaria	5.52	2.60	6.50	10.28	5.70	14.30	19.14	10.30	21.50
Germany	1.21	0.30	1.70	1.68	0.10	3.00	5.55	2.30	7.80
Czechia	1.45	0.90	2.50	2.44	1.00	4.60	7.11	5.10	10.50
Lithuania	1.59	1.40	1.90	1.92	1.40	2.70	5.07	3.60	6.40
Latvia	1.49	0.90	1.80	1.89	1.30	2.40	4.15	2.70	5.20
Türkiye	3.65	0.80	5.80	9.10	2.70	14.30	15.07	5.10	21.50
Luxembourg	1.22	1.10	1.60	2.50	1.60	2.80	7.32	6.70	8.00
France	2.04	0.90	4.00	4.69	1.10	8.10	10.34	4.40	16.10
Hungary	5.05	3.50	6.30	6.27	3.40	8.30	16.20	12.80	18.90
United Kingdom	0.28	-0.10	0.90	1.14	-0.20	3.30	2.00	-0.10	5.20
Kosovo	6.00	5.60	6.40	10.32	9.40	11.10	20.60	19.90	21.40
Croatia	4.67	3.50	6.00	6.94	3.90	8.70	16.59	11.60	19.60
Slovenia	2.44	1.10	3.70	4.15	1.80	6.20	11.24	7.70	14.70
Denmark	1.14	0.80	1.40	1.86	1.40	2.40	2.64	1.90	3.40
Sweden	0.57	0.00	1.40	0.62	0.10	1.80	1.63	0.10	3.80
North Macedonia	6.70	6.00	7.00	12.33	10.60	13.80	21.82	20.20	23.00
Montenegro	4.67	4.50	4.80	10.13	8.00	10.90	17.52	15.10	18.60
Ireland	0.22	0.00	0.60	0.70	0.10	1.30	1.19	0.30	2.30

	SSP1-2.6			SSP2-4.5			SSP5-8.5		
	mean	min	max	mean	min	max	mean	min	max
Estonia	1.27	0.80	1.70	1.35	0.90	1.80	3.06	2.10	4.20
Switzerland	0.64	0.30	1.00	1.51	0.70	2.40	4.64	3.00	6.40
Portugal	3.88	2.40	5.50	7.88	4.60	10.80	12.05	6.20	17.40
Malta	2.00	2.00	2.00	3.50	3.50	3.50	5.60	5.60	5.60
Slovakia	3.09	2.30	4.30	5.13	3.70	6.50	11.38	9.10	14.70
Italy	3.32	0.40	5.10	6.11	0.80	11.30	12.42	2.70	18.10
Serbia	6.00	4.90	6.60	9.05	6.80	11.50	19.67	18.50	21.50
Cyprus	1.00	0.90	1.10	-0.47	-0.90	0.10	2.83	2.60	3.10
Austria	1.29	0.20	3.60	2.20	0.80	4.90	6.36	2.20	13.10
Iceland	0.05	0.00	0.20	0.05	-0.10	0.10	0.10	-0.10	0.30
Romania	4.30	2.10	6.40	6.67	2.60	10.00	15.94	10.10	20.90
Poland	1.58	1.10	2.80	2.50	1.50	5.70	6.83	3.30	10.40
Spain	4.57	0.50	8.90	9.71	3.00	16.80	16.47	4.90	27.00
Norway	0.14	0.00	0.70	0.22	-0.20	1.00	0.47	0.00	2.10

5.Living Lab scale

5.1. Methods

5.1.1. Region and resolution

Apart from analysis on the European scale, higher resolution statistically downscaled climate projections (~9km) have been produced using ERA5-Land as the reference dataset for the following Living Labs (LL), all of them representative of the different bioregions in Europe: 1) Peloponnese (GR), 2) Catalonia (ES), 3) Aquitanie (FR), 4) Portugal, 5) Lower Saxony and North Rhine Westphalia (DE) and 6) Netherlands.

5.1.2. Variables

We provide the downscaling of the variables detailed in Table 4.

Table 4. List of variables and indices examined at the Living Lab level.

Index	Abbreviation	Definition
-	TX	Average daily maximum temperature (°C)
-	TN	Average daily minimum temperature (°C)
-	RR	Total precipitation amount (mm)
Fire Weather Index	FWI	Values of fire weather danger start at 0 and are open ended

5.1.3. Downscaling

For the statistical downscaling of both climate change projections and the seasonal forecasts the methodology of Varotsos et al. (2023) has been followed. In particular, the GCM/seasonal forecast daily data are remapped on the ERA5-Land grid using bilinear interpolation and consequently the models' output is bias adjusted using ERA5-Land as the reference dataset. Bias adjustment is performed using the empirical quantile method (EQM). EQM works by constructing a transfer function calibrated over the reference period to map quantiles from the empirical cumulative distribution function of the model output onto the corresponding observed distribution (Iturbide et al. 2019; Casanueva et al. 2020).

5.2. Results

5.2.1. Temperature and precipitation results

In Figures 14-17 the results of the average changes between the two future periods and the reference one under the three SSP scenarios examined are shown for the summer (JJA) TX and TN. From Figures 14 and 15 it is evident that, the highest JJA TX increases are projected for the LL of Peloponnese for both the 2041-2060 and 2081-2100 periods under SSP5-8.5 reaching about 3.7°C and 7.1°C, respectively. For the rest of the LLs the increases do not exceed 2.6°C and 6.1°C under the same scenario for the 2041-2060 and 2081-2100 periods, respectively. Intermediate increases are shown under the

SPP2-4.5 while the lowest increases are shown under SPP1-2.6. Similar spatial distribution, with lower absolute increases, is projected for the JJA TN (Figures 16-17). In particular the highest JJA TN increases are projected for the LL of Peloponnese under SSP5-8.5 (about 2.5°C and 4.7°C for the 2041-2060 and 2081-2100 periods), followed by Catalonia (about 1.6°C and 4°C for the same periods, respectively) and Aquitaine (about 1.6°C and 4°C for the same periods, respectively) with the lowest increases found for Portugal and the three areas of the northern LL. The lowest increases for all LLs are found under SPP1-2.6 while intermediate increases are found under SSP2-4.5.

In contrast to temperature results, the changes in JJA precipitation are less robust in the majority of the LLs examined and for the period 2041-2060 under all scenarios (Figure 18). For instance, although increases in summer precipitation are projected for the Peloponnese LL, they are not statistically significant because to a lack of agreement across models on the sign of the changes. The rest of the LLs exhibit similar behavior, with the exception of Portugal, where significant declines in the range of –16% to -8% are projected depending on the scenario. Changes projected for the 2081-2100 time period are found to be robust for all LLs under the SPP5-8.5 (Figure 19). Nonetheless, the data show a considerable degree of heterogeneity, with changes ranging between -53% and -3% for Portugal and the Peloponnese, respectively.

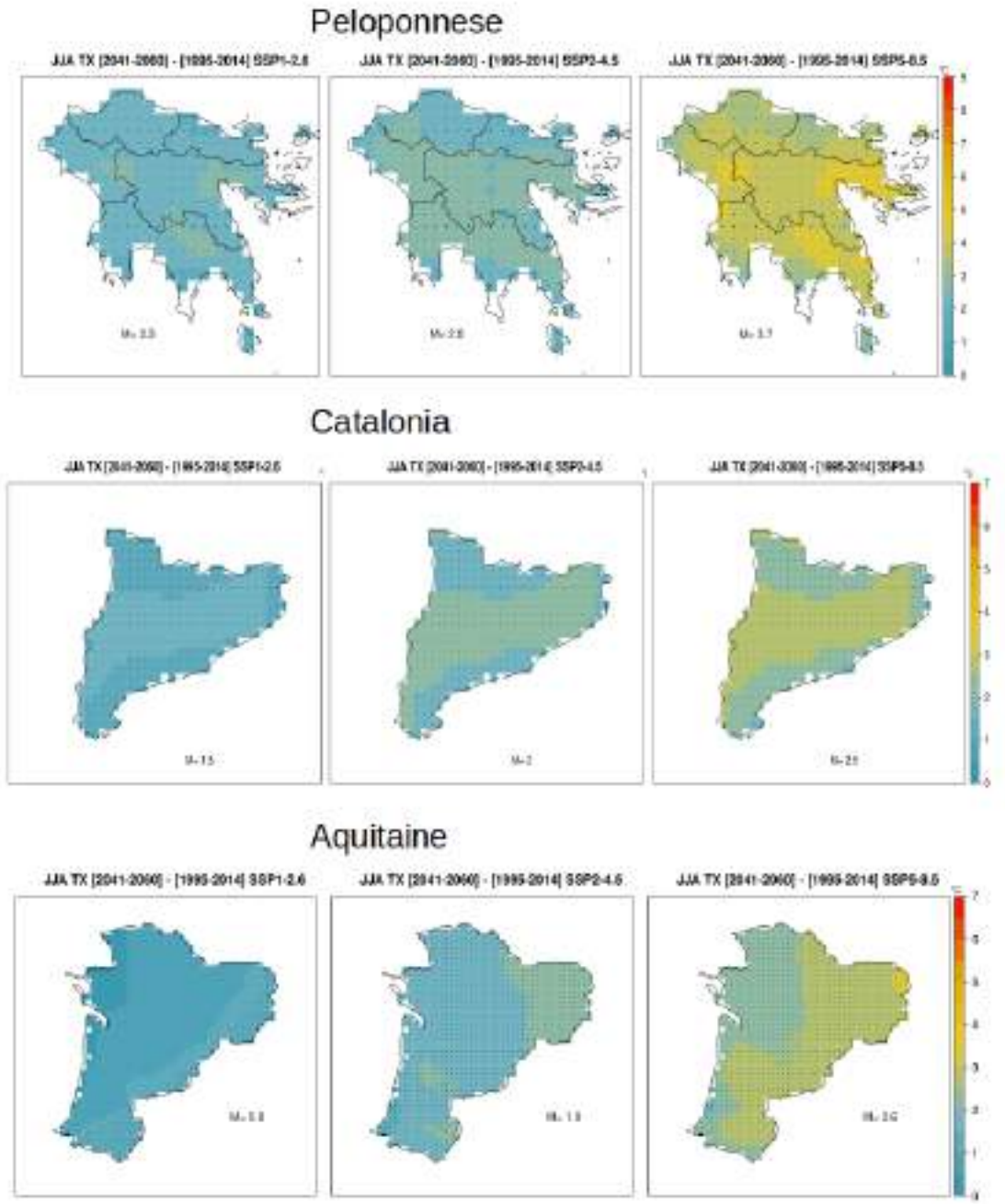

Figure 14. Average JJA TX changes between the 2041-2060 future period and the reference one (1995-2104) for the three SSP scenarios examined. In each plot M indicates the absolute change between the future period and the reference one averaged over all gid points. Black dots indicate robust changes at the grid point scale.

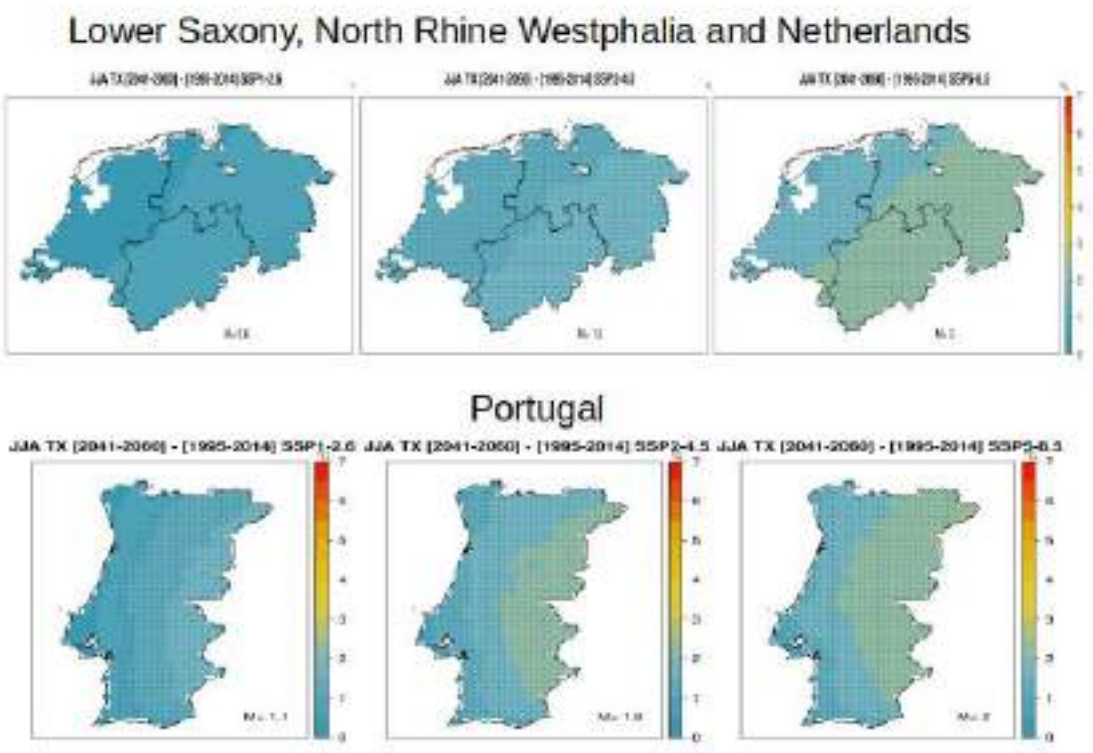

Figure 14 continued.

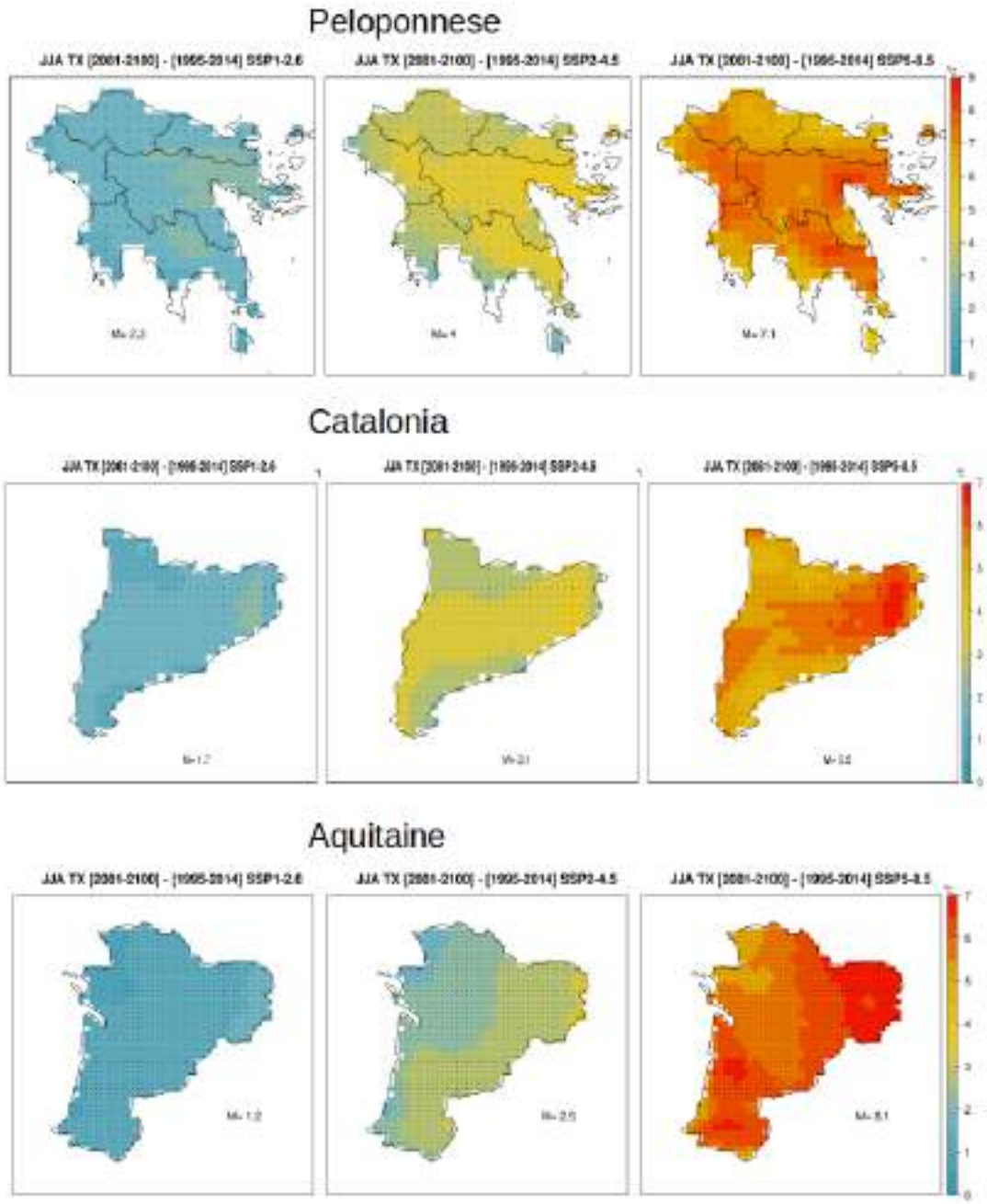

Figure 15. Average JJA TX changes between the 2081-2100 future period and the reference one (1995-2104) for the three SSP scenarios examined. In each plot M indicates the absolute change between the future period and the reference one averaged over all gid points. Black dots indicate robust changes at the grid point scale.

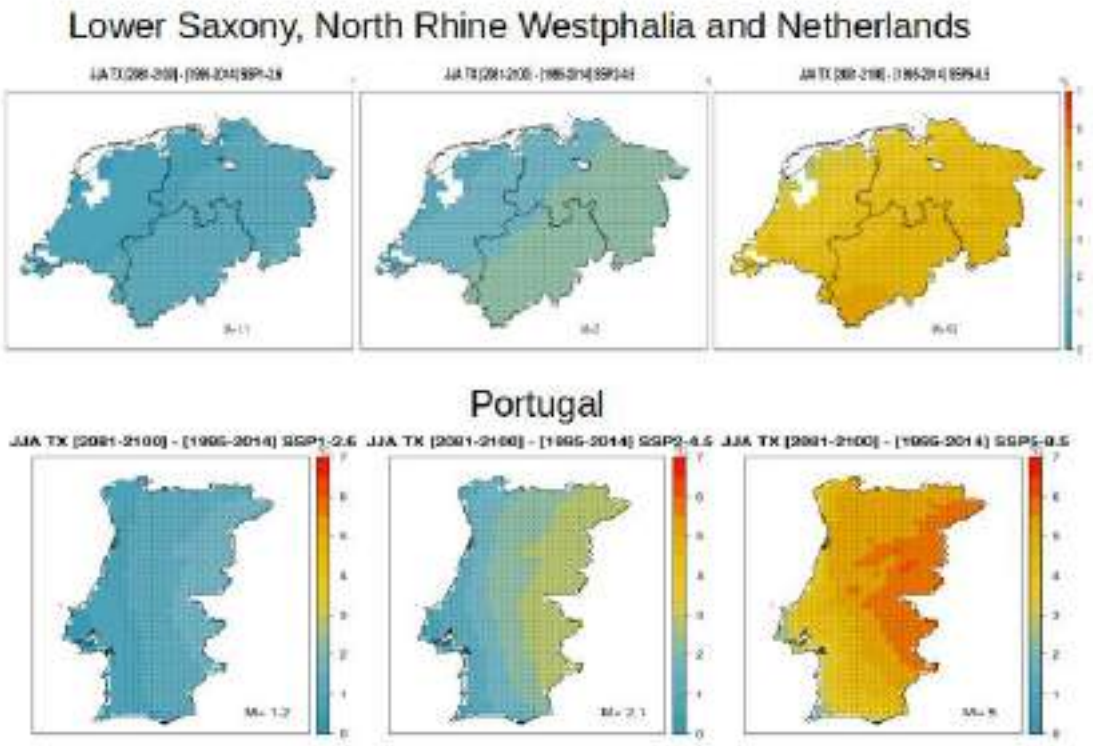

Figure 15 continued.

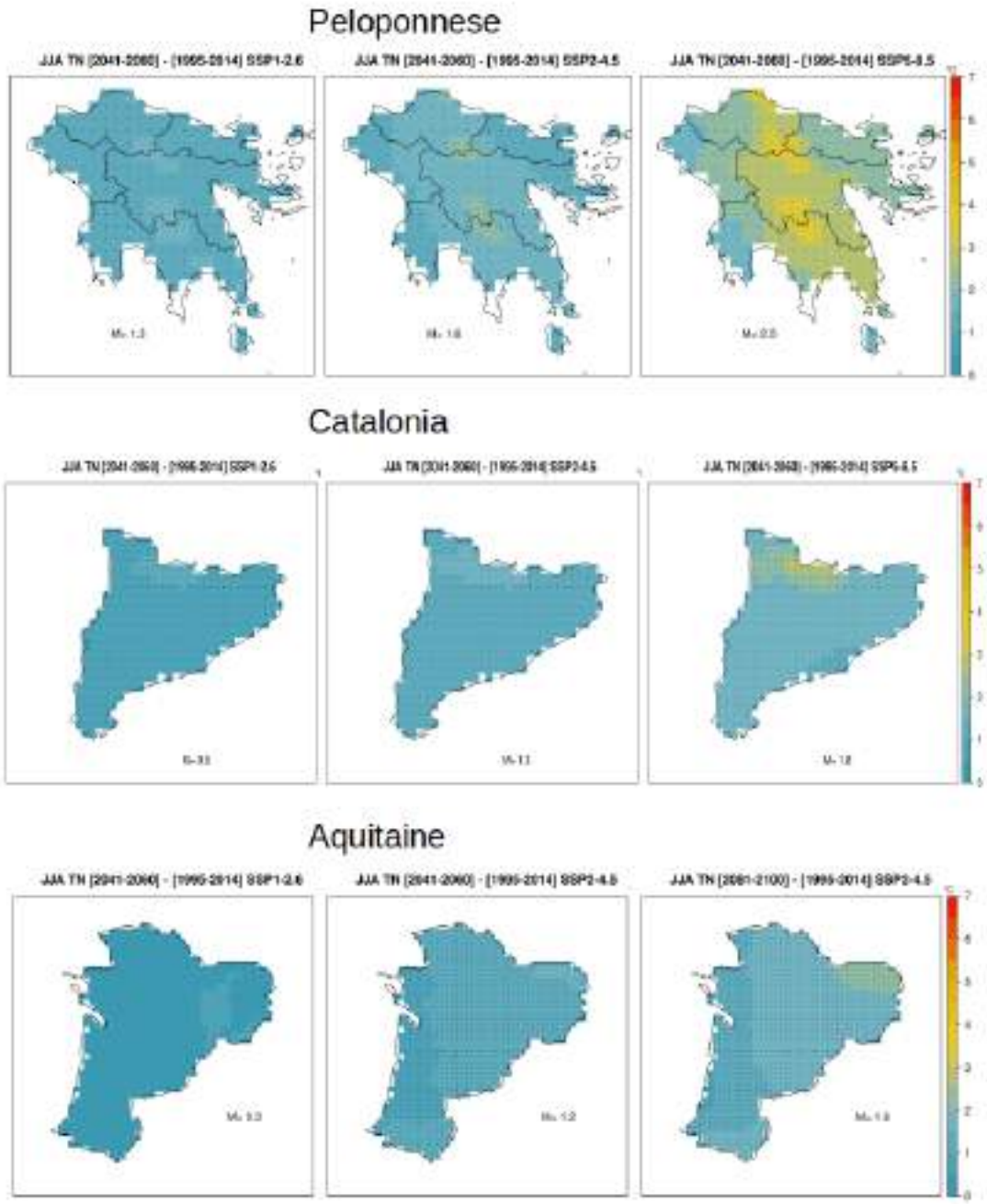

Figure 16. Average JJA TN changes between the 2041-2060 future period and the reference one (1995-2104) for the three SSP scenarios examined. In each plot M indicates the absolute change between the future period and the reference one averaged over all gid points. Black dots indicate robust changes at the grid point scale.

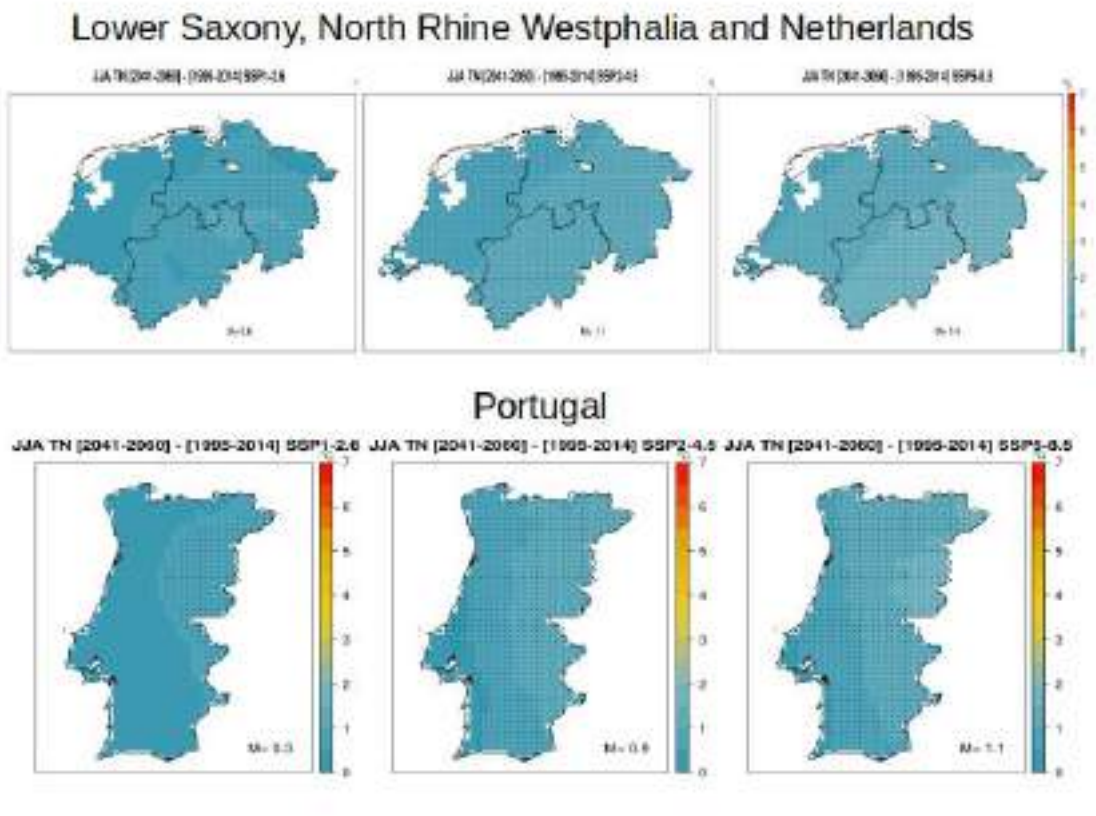

Figure 16 continued.

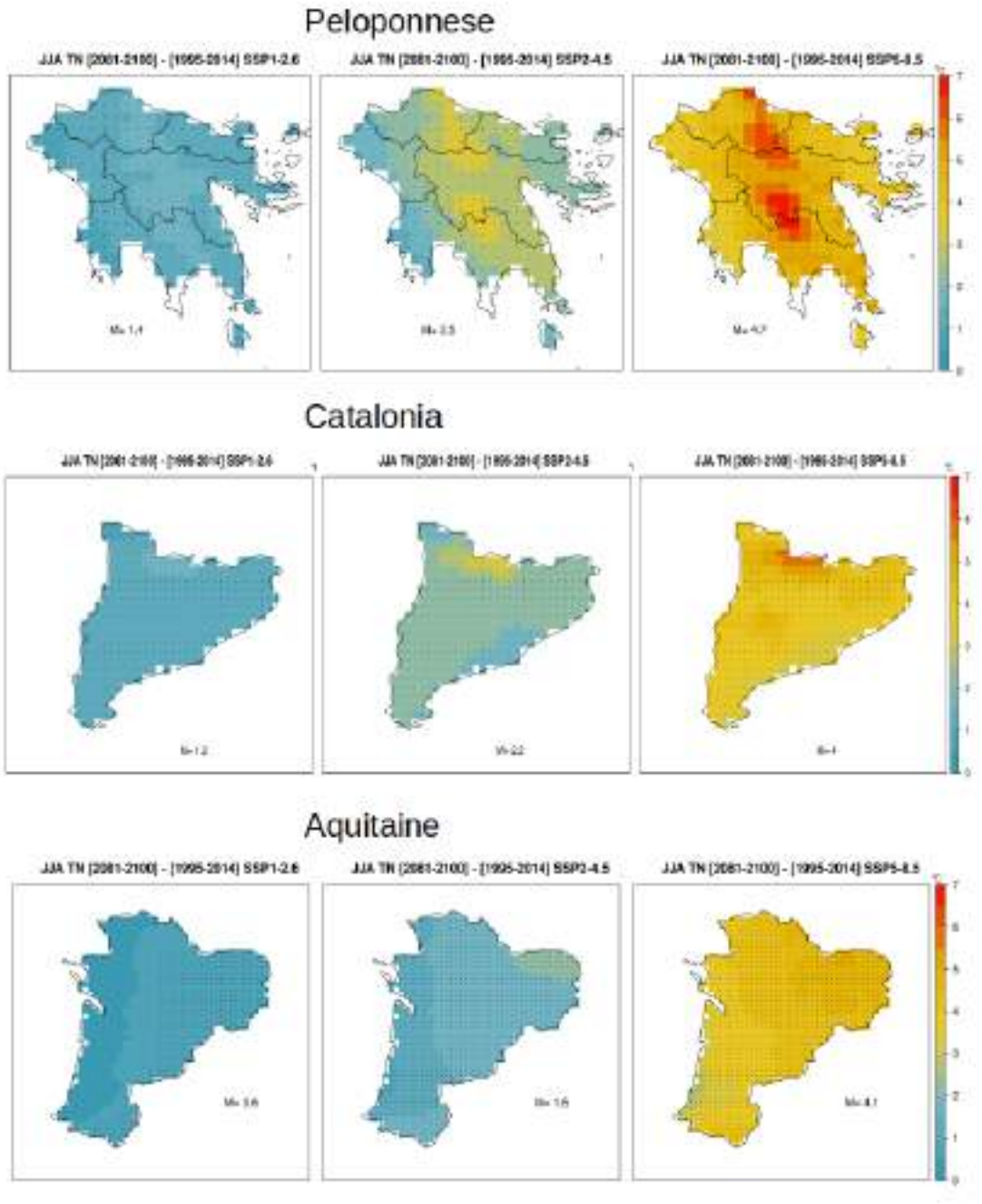

Figure 17. Average JJA TN changes between the 2081-2100 future period and the reference one (1995-2104) for the three SSP scenarios examined. In each plot M indicates the absolute change between the future period and the reference one averaged over all gid points. Black dots indicate robust changes at the grid point scale.

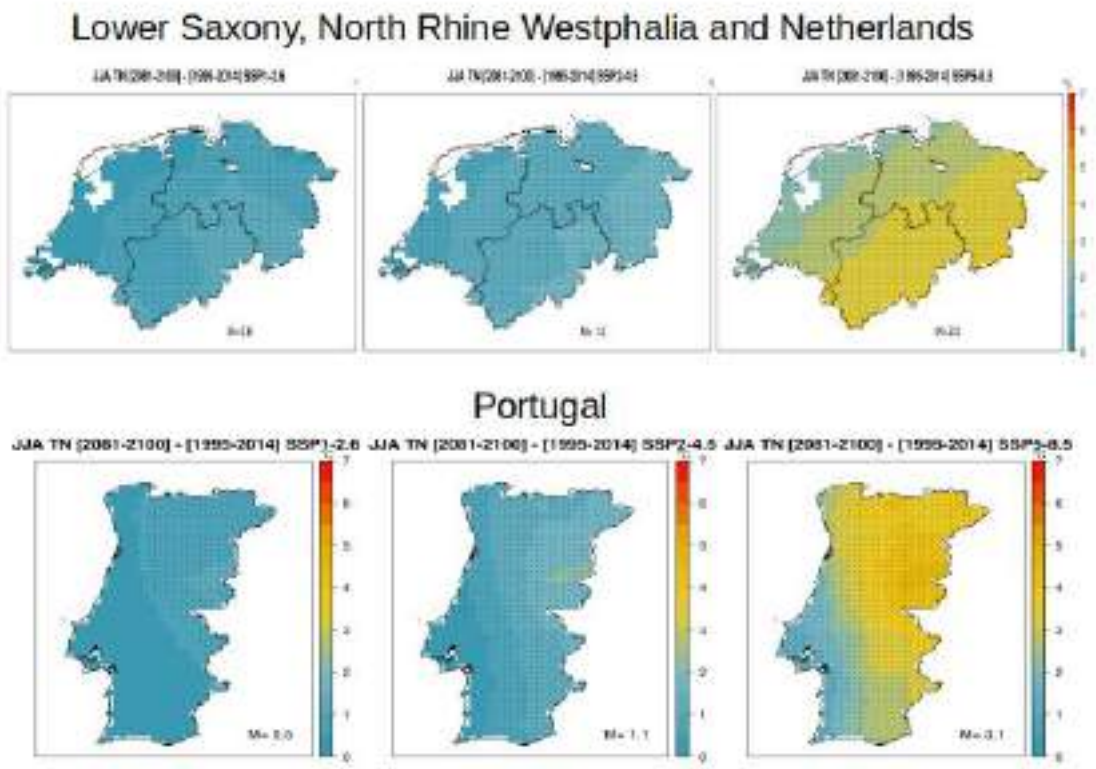

Figure 17 continued.

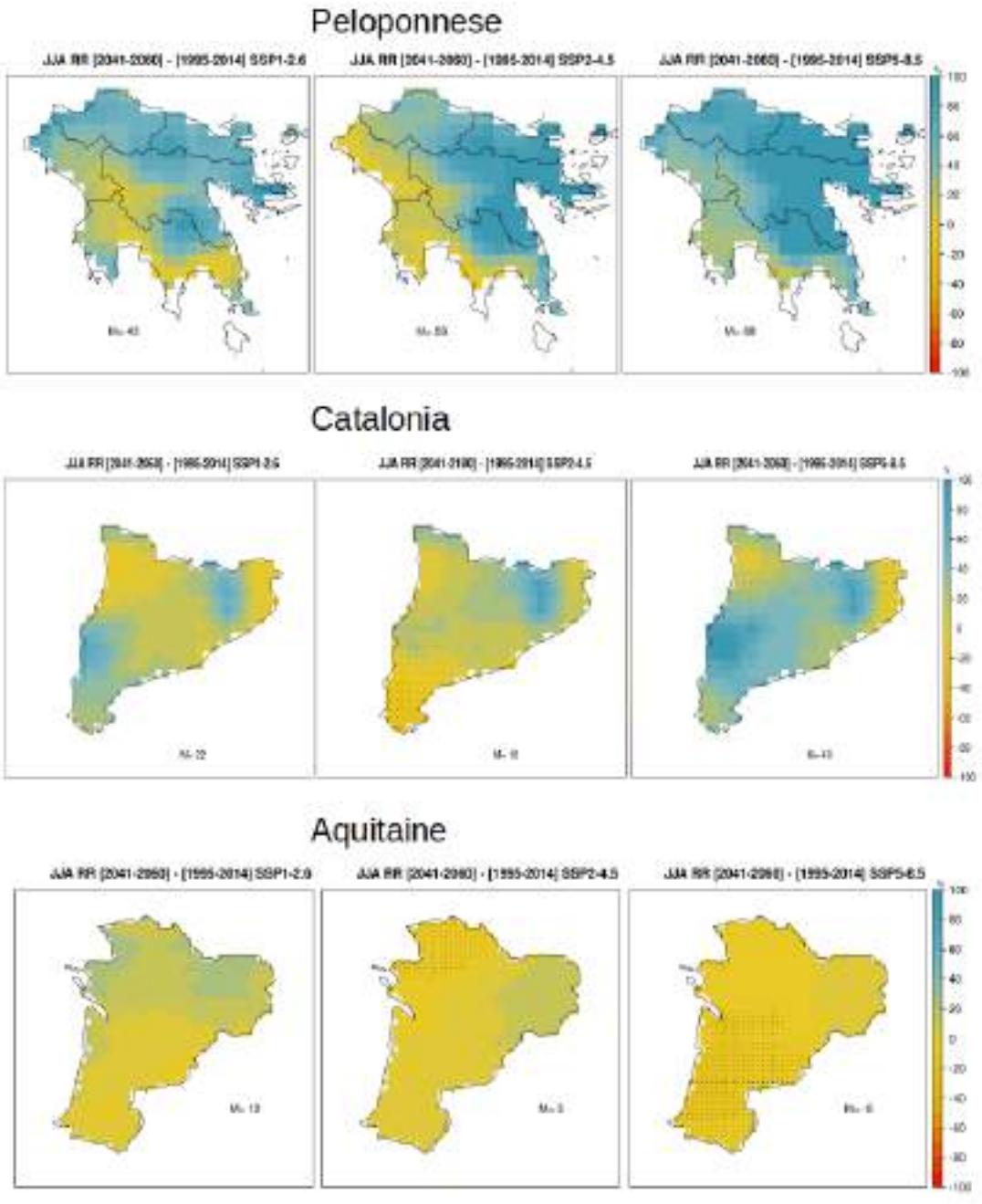

Figure 18. Total JJA RR changes between the 2041-2060 future period and the reference one (1995-2104) for the three SSP scenarios examined. In each plot M indicates the relative change between the future period and the reference one averaged over all gid points. Black dots indicate robust changes at the grid point scale.

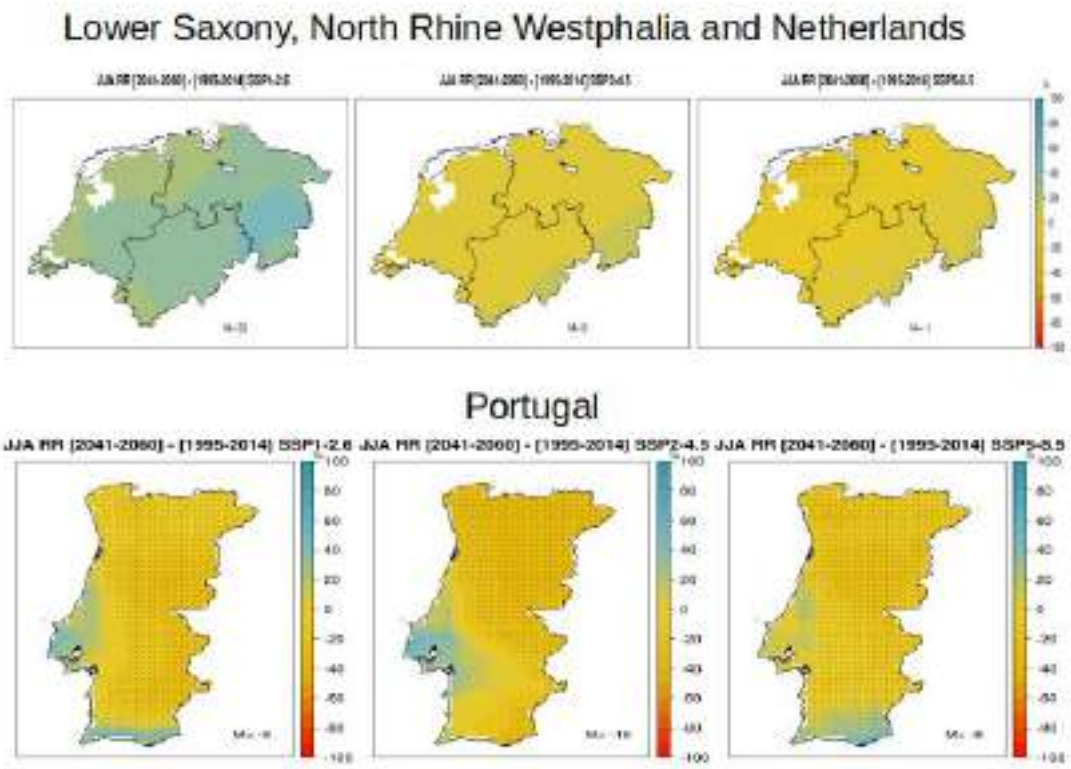

Figure 18 continued.

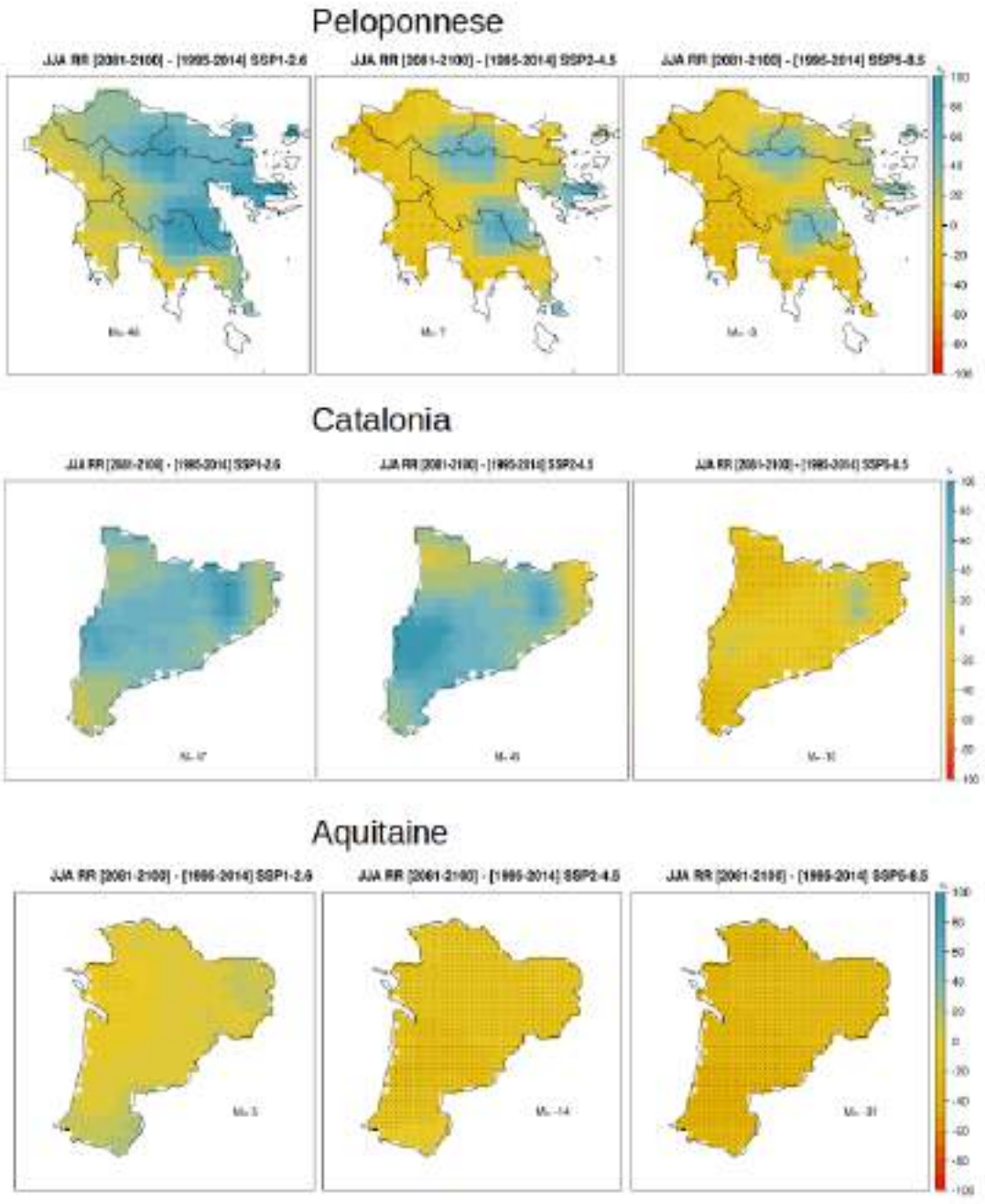

Figure 19. Total JJA RR changes between the 2081-2100 future period and the reference one (1995-2104) for the three SSP scenarios examined. In each plot M indicates the relative change between the future period and the reference one averaged over all gid points. Black dots indicate robust changes at the grid point scale.

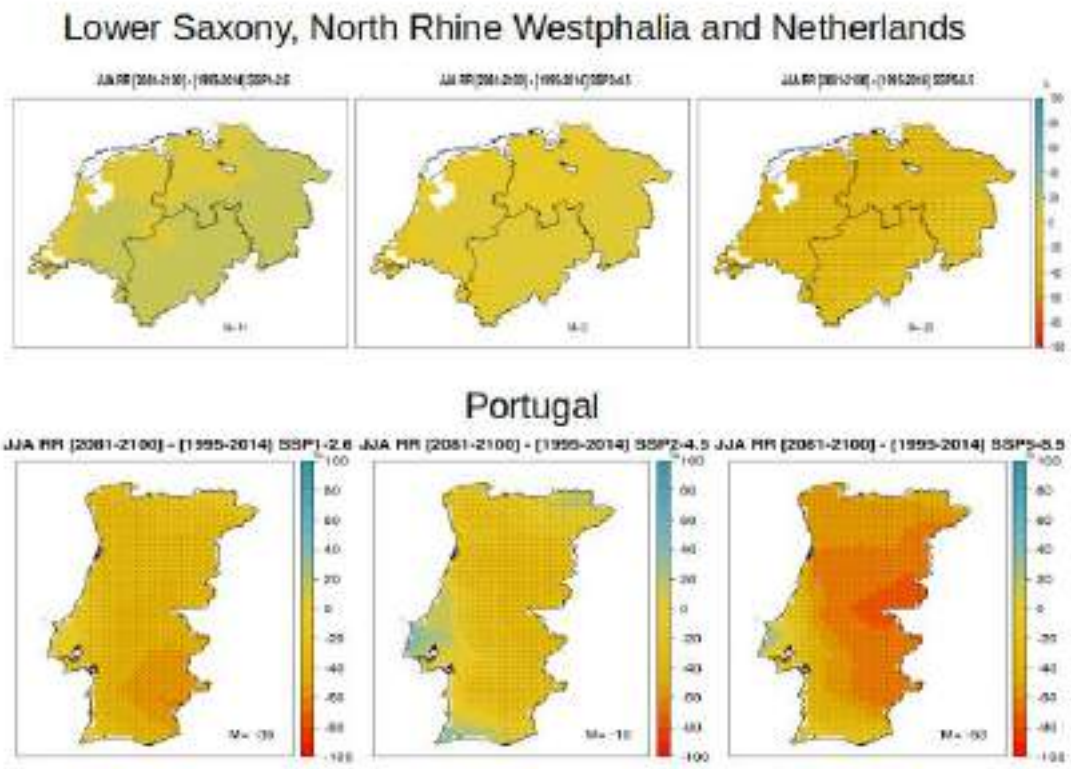

Figure 19 continued.

5.2.2. FWI results

In Figures 20-23 the 90th percentile summer FWI results are shown for all periods and all scenarios examined. More specifically, in Figure 20 the results of the specific indices are shown for the reference period. From the figure it is evident that for Peloponnese and Portugal the values of the specific index fall within the high danger FWI class (on average over all grid boxes), with higher values (indicating higher danger FWI class) simulated in the eastern regions for both LLs. For Catalonia and Aquitaine, the values fall within the moderate danger class (with higher values in the western parts of both LLs) while for the northern Europe LL the values fall within low fire danger class. Under SSP1-2.6 (Figure 21) the changes are found robust for the majority of the LLs by the end of the century (2081-2100) while robust changes are projected for the southern Europe LLs (Peloponnese, Catalonia and Portugal) for the 2041-2060 period. However, the fire danger class does

not change on average for all LLs and for both future periods. For the SSP2-4.5 Catalonia and the northern Europe LLs change fire danger class by the end of the century (2081-2100) compared to reference period, from moderate and low to high and moderate respectively. For the rest of the LLs no FWI class change (on average) is projected. Robust changes are projected for all LLs under SSP5-8.5 for both periods. Nevertheless, during the 2041-2060 period a class change in the FWI danger is projected only for Catalonia (compared to reference period) while by the end of the century in the majority of the LLs a FWI class change to worsening conditions is projected.

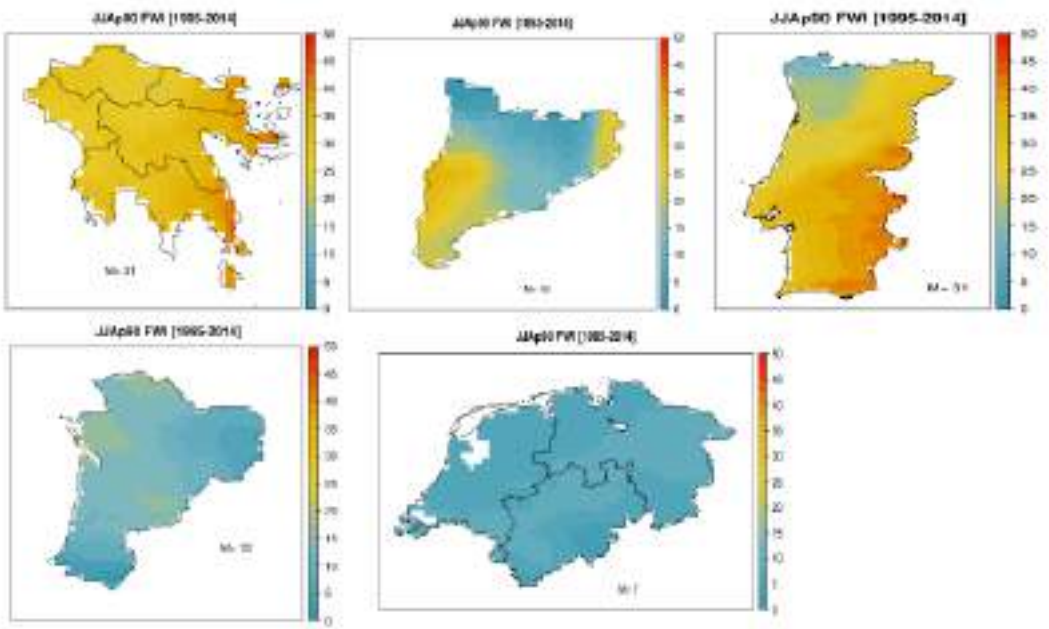

Figure 20. 90th percentile JJA FWI for reference period, 1995-2014. In each plot M indicates the value of the index averaged over all gid points.

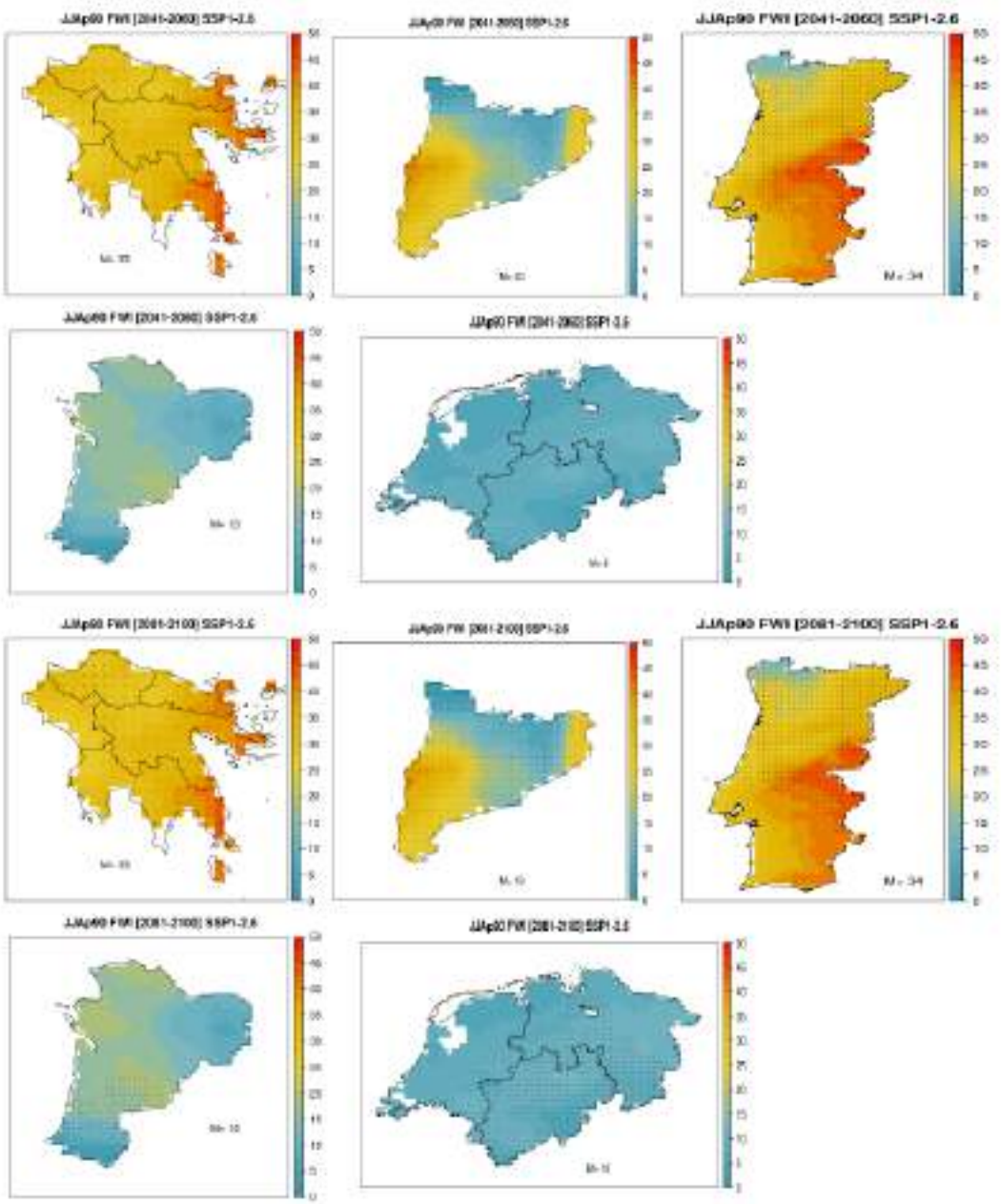

Figure 21. 90th percentile JJA FWI under SSP1-2.6 for 2041-2060 (top) and 2081-2100 (bottom) periods. In each plot M indicates the value of the index averaged over all gid points.

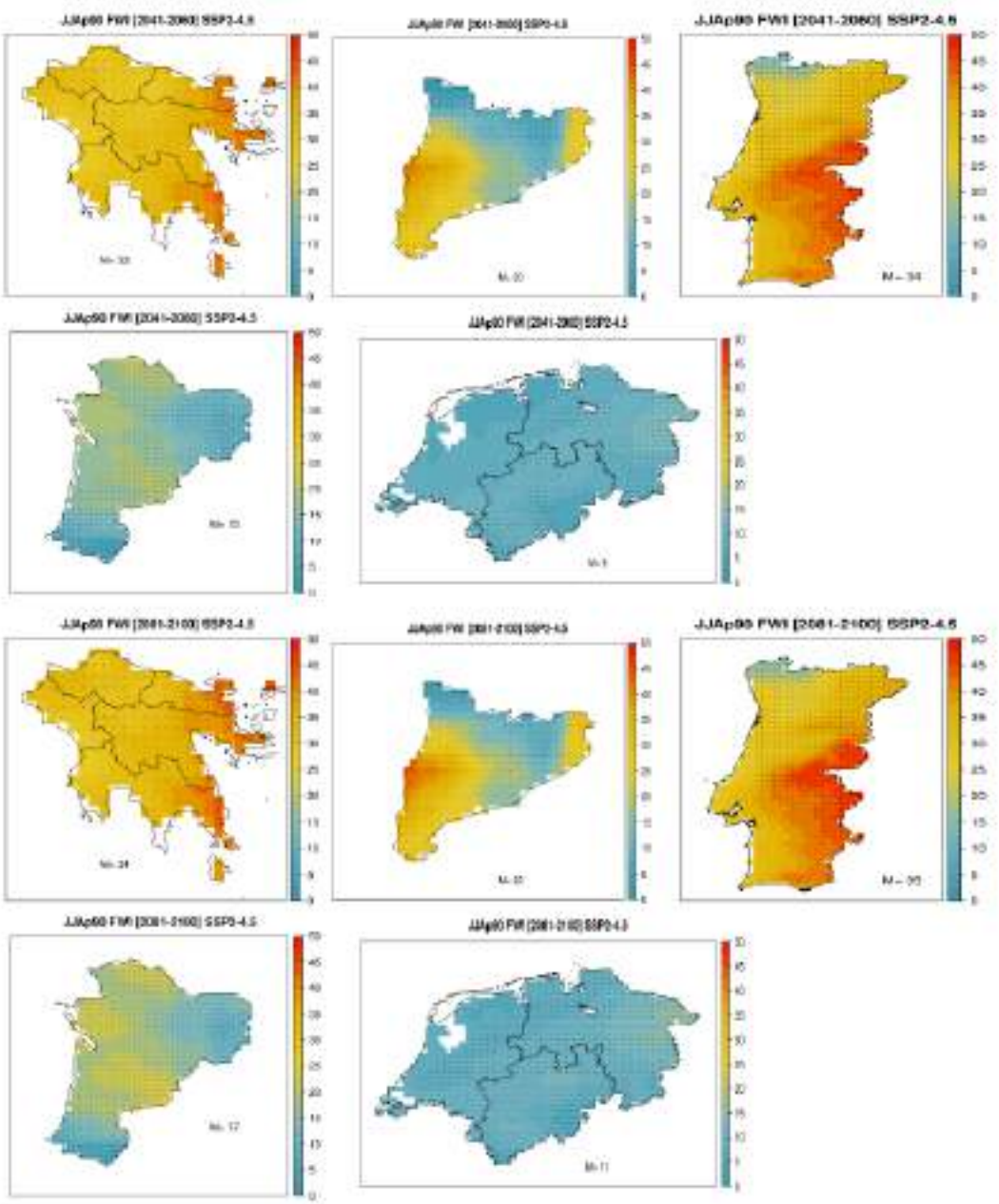

Figure 22. 90th percentile JJA FWI under SSP2-4.5 for 2041-2060 (top) and 2081-2100 (bottom) periods. In each plot M indicates the value of the index averaged over all gid points.

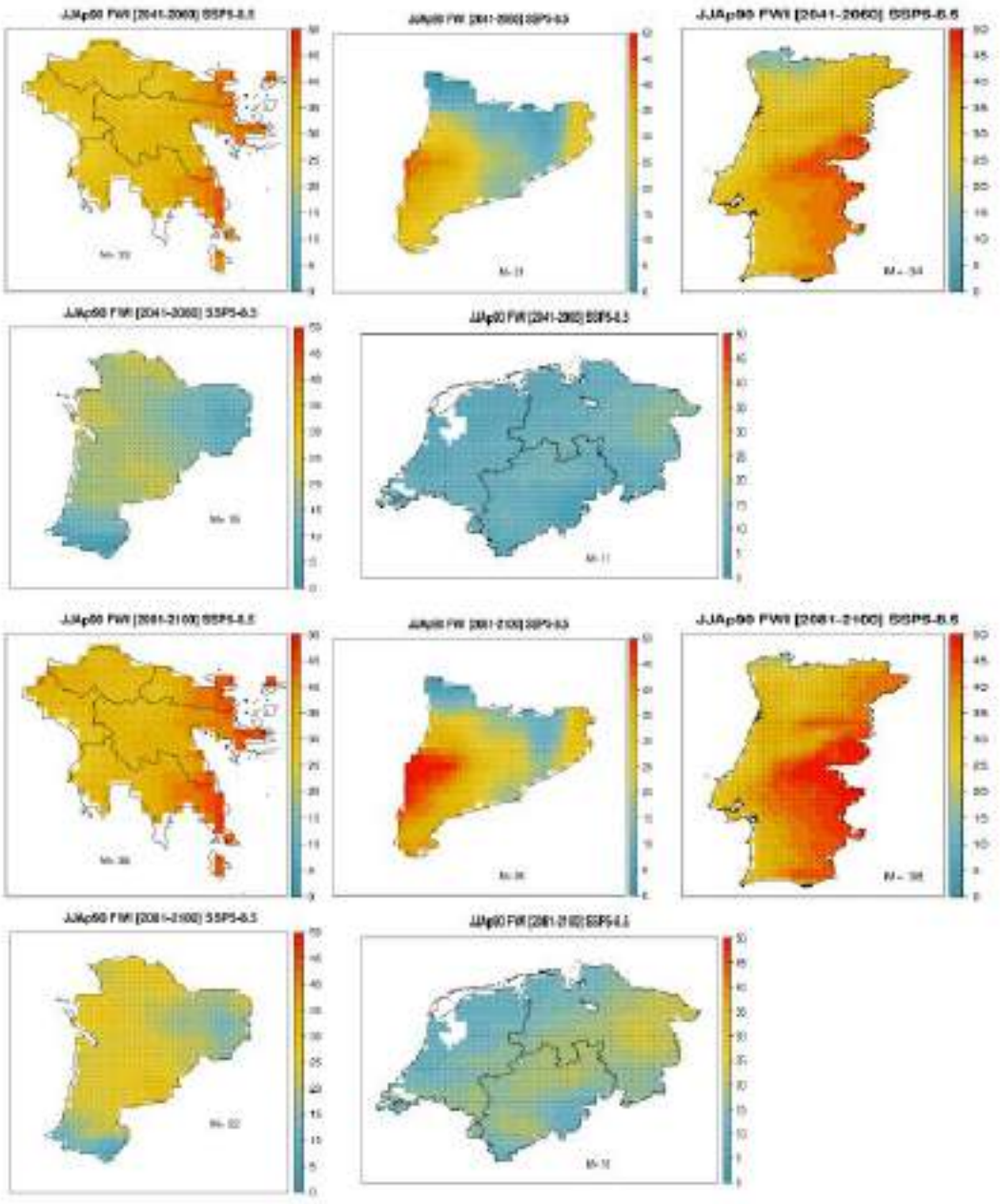

Figure 23. 90th percentile JJA FWI under SSP5-8.5 for 2041-2060 (top) and 2081-2100 (bottom) periods. In each plot M indicates the value of the index averaged over all gid points.

6. High resolution probabilistic fire danger seasonal forecasts

We show the development and validation of high-resolution probabilistic fire danger (FWI) forecasts for some of the FIRE-RES Living Labs. The methodology described in Karali et al. (2023) was implemented for the forecast calculation and the tercile-based probabilistic approach used in forecast verification.

6.1. Methods

6.1.1. Regions

We have developed the seasonal forecasts for the Mediterranean FIRE-RES Living Labs of Catalonia, Sardinia and Peloponnese.

6.1.2. FWI calculation

For the daily FWI calculations, the SEAS5 and ERA5-Land instantaneous outputs at 12 UTC for 2-m air temperature, northward and eastward 10-m wind components, 2-m dewpoint temperature, and daily accumulated precipitation were used. The 12 UTC was used as a proxy for local noon values required as input to FWI as proposed by several previous studies for the Mediterranean region (e.g., Bedia et al. 2018; Herrera et al. 2013). Seasonal forecasts initialized in May were used and a fire season ranging from June to September (JJAS) was considered for the analysis (1-month lead time forecasts). To initiate the calculations of FWI, default initial values of FFMC, DMC, and DC were used. This means that a spin-up period was required to minimize the effects of errors in the initial conditions. Therefore, the FWI time series for May was first calculated for the index to stabilize and was then removed from the analysis.

6.1.3. Statistical downscaling of seasonal forecasts

To statistically downscale FWI a two-step approach was used following the methodology of Varotsos et al. (2023). FWI was bias corrected after its calculation from the regridded fields of temperature, relative humidity, wind speed and precipitation to avoid unrealistic

FWI trends that could occur by calculating FWI from the bias corrected meteorological variables (Bedia et al. 2018). For more information, please refer to Section 3.

6.1.4. Forecast verification

We used the probabilistic Relative Operating Characteristic (ROC) skill score, measuring forecast discrimination, together with the reliability diagrams, to assess the potential skill and usefulness of fire danger seasonal forecasts after spatial disaggregation and bias adjustment.

6.1.4.1. ROC skill score (ROCSS)

ROC skill measures the frequency of occasions when the system correctly distinguished between events occurring and not occurring (Jolliffe and Stephenson, 2003). ROC Skill Score (ROCSS) ranges from -1 (perfectly bad discrimination) to 1 (perfectly good discrimination). A value of zero indicates no skill compared to a random prediction or the climatological value.

6.1.4.2. Reliability diagrams

Reliability diagrams are diagnostic tools measuring how closely the forecast probabilities of a specific event (i.e., a particular tercile category) correspond to the observed frequency of that event (Weisheimer and Palmer 2014). Based on the slope of the reliability line and the uncertainty associated with it, six easy-to-interpret categories can be defined: perfect, still very useful, marginally useful+, marginally useful, not useful, and dangerously useless (Manzanas et al. 2018). The marginally useful+ category differentiated those cases for which the reliability line lies within the skill region.

6.2. Results

In this section measures of historical predictive skill for the examined living labs will be presented, in order to provide an indication of the trustworthiness of the forecasts in these regions. For brevity, only 4 out of the 7 components of the Fire Weather Index System will be displayed, namely the Fire Weather Index (FWI), Initial Spread Index (ISI), the Fine Fuel Moisture Code (FFMC) and the Drought Code (DC).

The quality of the downscaled fire danger hindcasts is initially assessed via the ROCSS. In addition, tercile plots for the FWI (and its subcomponents) are presented to complement the spatial analysis provided by the ROCSS maps, presenting the performance of the seasonal forecast along the hindcast period. Finally, in order to complete the analysis, forecast reliability, which is crucial in determining the advantages of using seasonal forecast data, is presented. It should be noted that concerning FWI (and its subcomponents), both in the tercile maps/plots and the reliability diagrams, only the results of the upper tercile category (above normal conditions) are discussed, as high FWI (and its subcomponents) values are related to increased fire danger conditions and, hence, to increased wildfire activity.

6.2.1. Catalonia

In Figure 24, the spatial distribution of the ROCSS for the upper tercile category of the FWI and its subcomponents for JJAS fire season, are presented. As can be seen, ISI exhibits medium discrimination skill for an extended part of the domain. Sporadically distributed low skill is found for FFMC and FWI, while no skill is found for DC. In particular, statistically significant ROCSSs ranging between 0.4 and 0.6 are found for ISI, while lower scores of up to 0.4 are attained for FFMC and FWI. Figure 25 depicts the tercile plots of FWI and its subcomponents averaged over Catalonia. According to the spatially averaged ROCSSs, only ISI attains a statistically significant positive value (0.47). Regarding the temporal performance on a year-by-year basis, for all examined indices, except for the ISI, the majority of the observed above normal (upper tercile) years is predicted by less than 50% of the ensemble members. Finally, concerning the reliability of the hindcasts, ISI and FFMC predictions are classified as marginally useful+, while FWI and DC fall in the not useful category (Fig. 26).

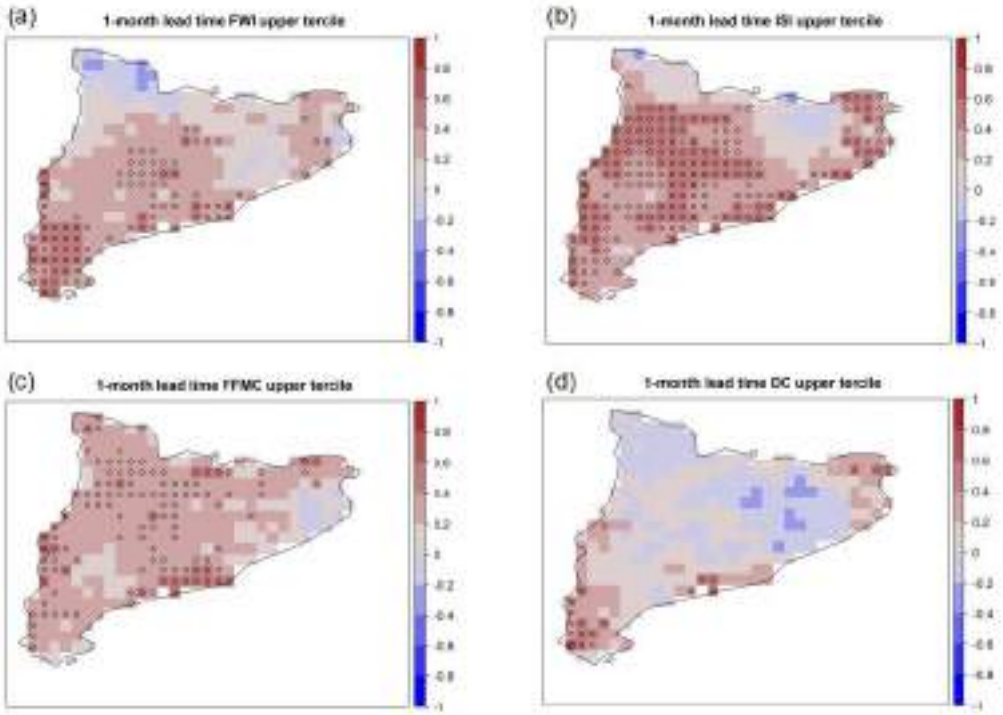

Figure 24: ROC Skill Scores (ROCSSs) of the upper tercile SEAS5 hindcasts for the LL of Catalonia of: a) FWI, b) ISI, c) FFMC and d) DC subcomponent. The grid points with significant ROCSS values are indicated by circles (α=0.05).

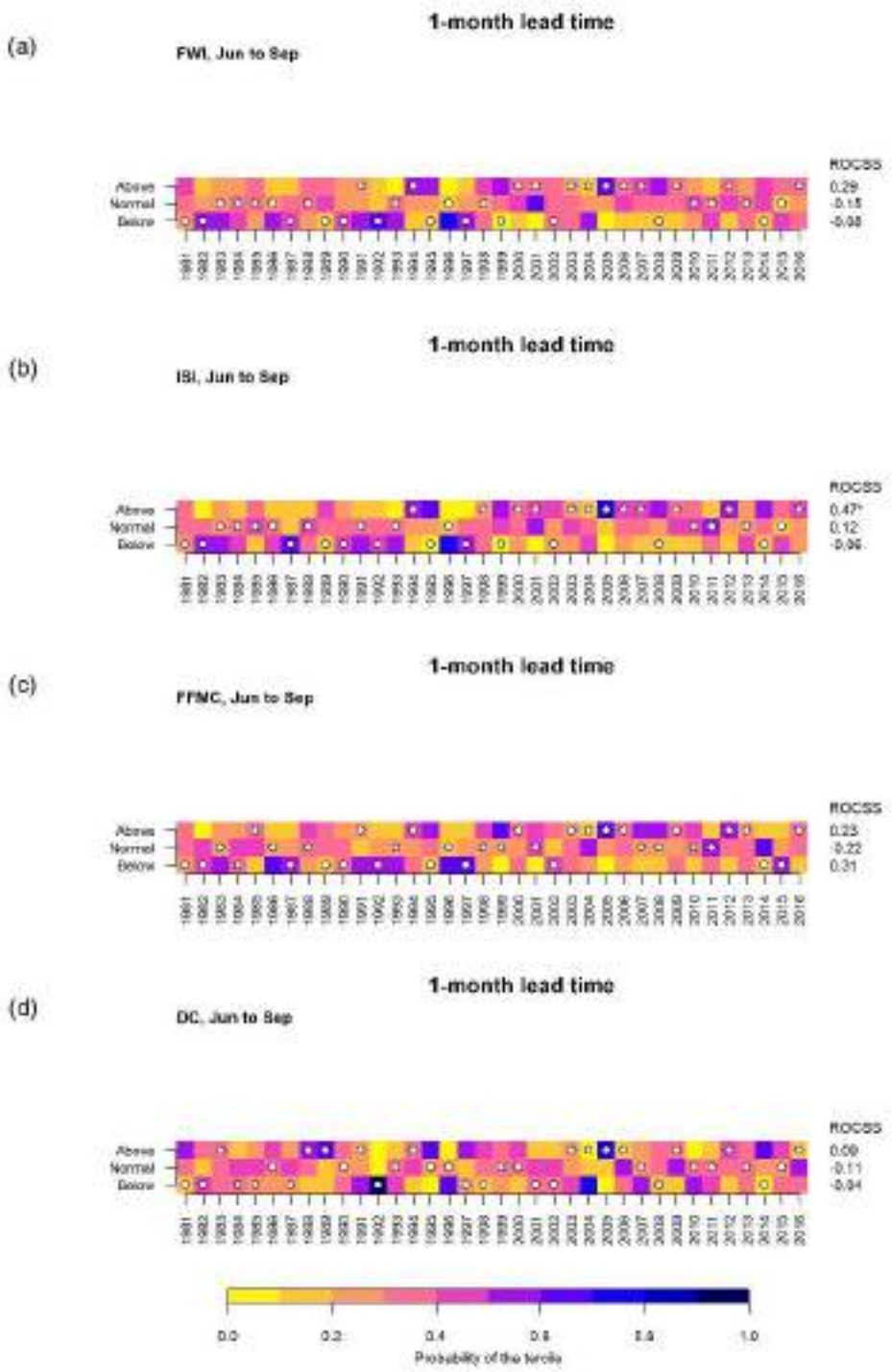

Figure 25: Tercile plots for Catalonia covering the May to September hindcast period (1981-2016) for: a) FWI, b) ISI, c) FFMC and d) DC. Forecast probabilities for the three tercile categories are codified in a yellow (0, no member forecasts in one category) to blue (1, all the members in the same category) scale. The white bullets represent the observed category according to the ERA5-Land dataset. ROCSS values obtained from the hindcast period are shown on the right side of each category and the asterisk indicates significant values (α=0.05).

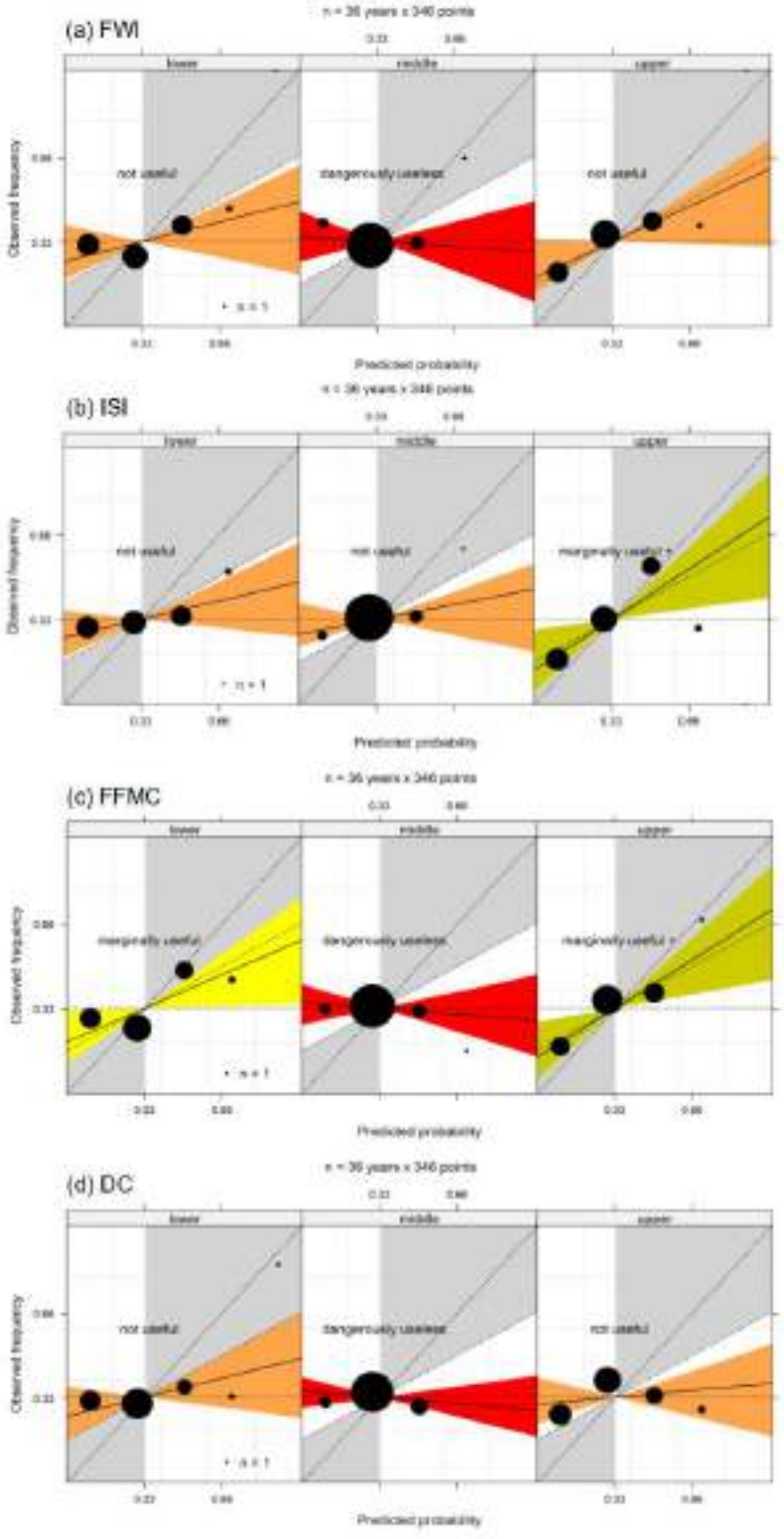

Figure 26: Reliability diagrams for each one of the FWI terciles (lower, middle, upper) for the LL of Catalonia for: a) FWI, b) ISI, c) FFMC and d) DC. The different colors correspond to the reliability categories proposed by Weisheimer and Palmer (2014) and further updated by Manzanas et al. (2018). The perfect reliability (dashed diagonal line), no resolution (horizontal dashed line) and no skill (dashed line between the no-resolution line and the diagonal) lines and the skill region (in grey) are also indicated.

6.2.2. Sardinia

ROCSS maps depict high (0.6-0.8) discrimination skill scores for the central and northern part of the domain for both ISI and FWI predictions (Fig. 27). For FFMC and to a lesser degree for DC hindcasts, sporadic areas of medium skill (0.4-0.6) are found in the same areas. According to the spatially averaged ROCSSs over Sardinia as depicted in Fig. 28, only ISI attains a statistically significant positive value (0.59). From the interannual perspective, FWI and FFMC hindcasts tend to underestimate the observed above normal years, as less than 40% of the above normal years are predicted by most of the ensemble members (by more than 60% of the members) (Fig. 28). Concerning ISI and DC hindcasts, almost 60% of the observed above normal years were predicted by 50%-80% of the members. Lastly, according to the reliability diagrams (Fig. 29), the FWI and ISI predictions are classified as marginally useful+, the DC is classified as marginally useful, while FFMC falls in the not useful category.

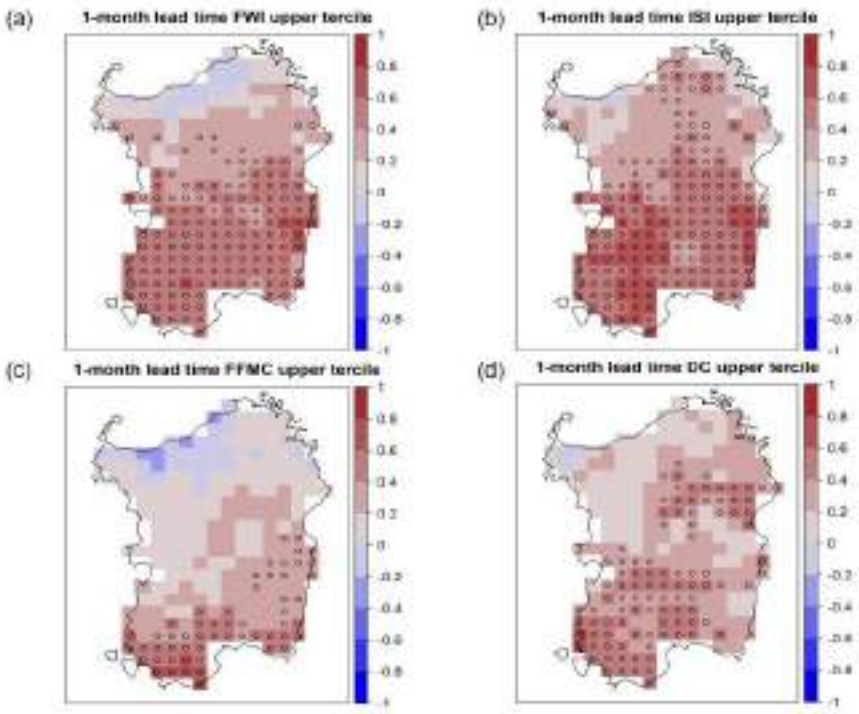

Figure 27: Same as Fig.24 but for the LL of Sardinia.

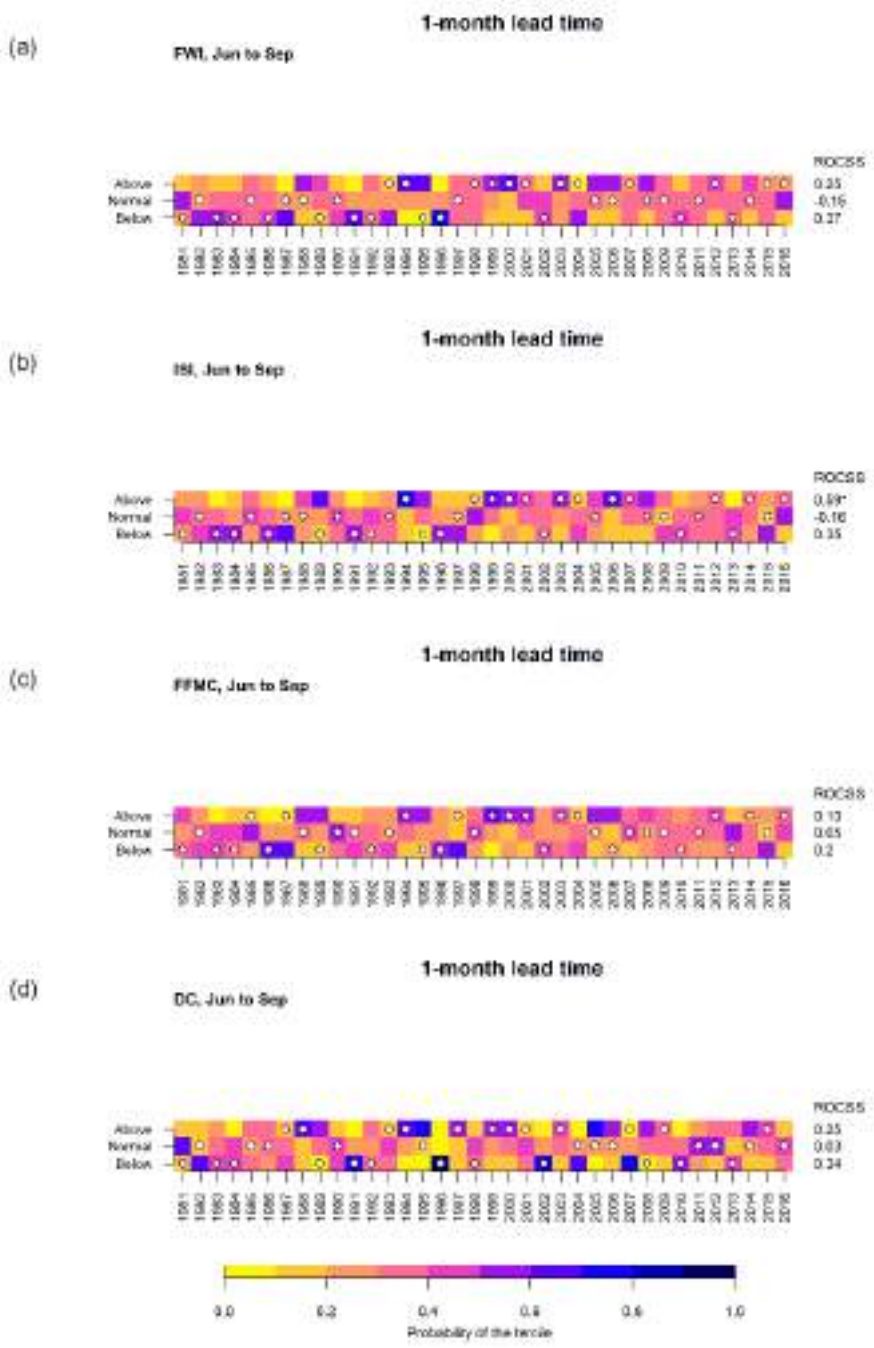

Figure 28: Same as Fig. 25 but for the LL of Sardinia.

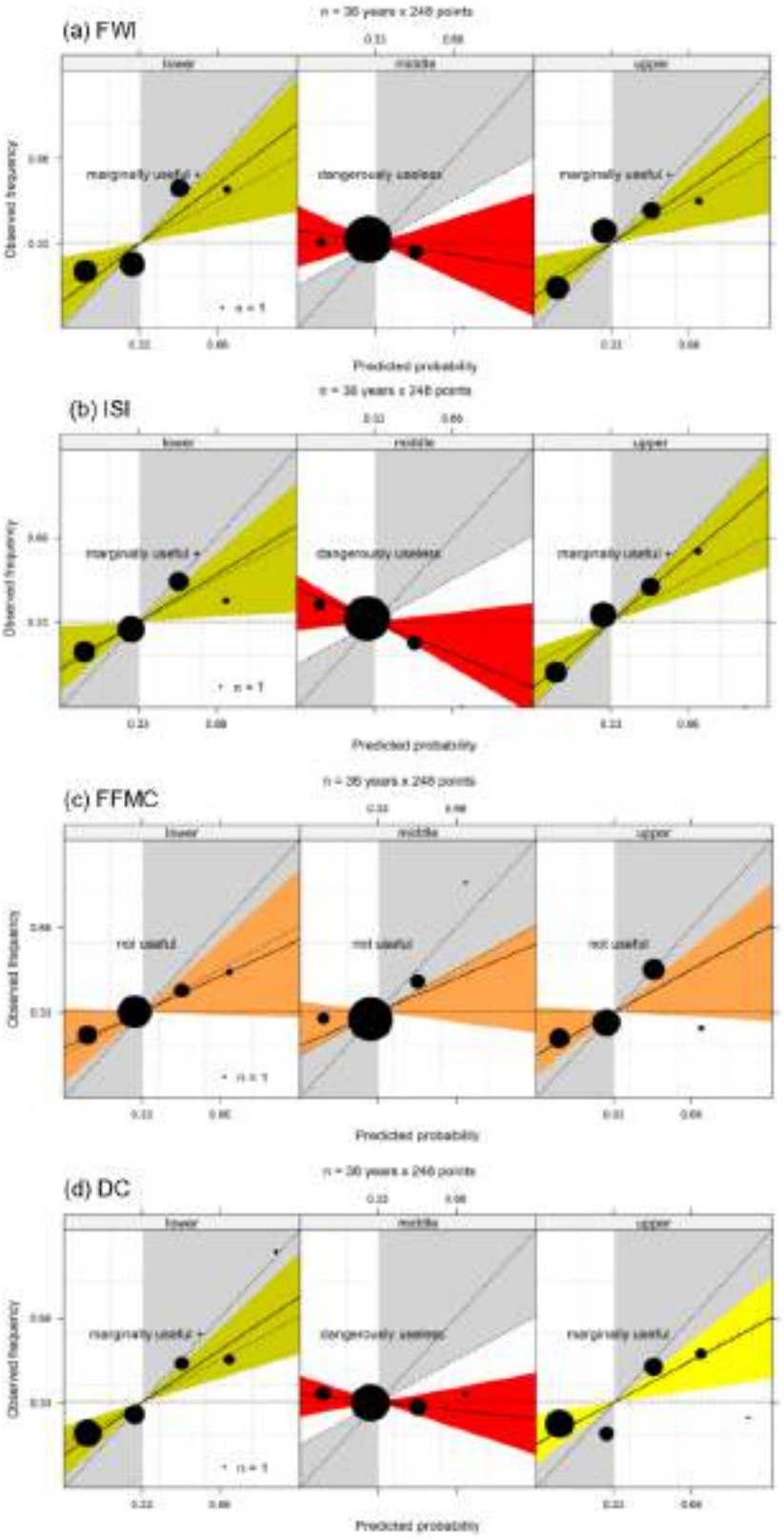

Figure 29: Same as Fig. 26 but for the LL of Sardinia.

6.2.3. Peloponnese

In Fig. 30 depicting the spatial distribution of ROCSSs in Peloponnese it is evident that ISI hindcasts outperform the remaining indices. ISI ROCSSs, in particular, range between 0.6-0.8 for a large part of Peloponnese. For FWI, statistically significant ROCSSs ranging between 0.4-0.6 are attained mainly in the eastern part of the domain, DC attains the same scores but in the western part and FFMC depicts no skill for the entire domain. In terms of year-to-year temporal performance, FWI, FFMC and DC hindcasts tend to underestimate the observed above normal years, as less than 40% of the above normal years are predicted by most of the ensemble members (by more than 60% of the members) (Fig. 31). Concerning ISI hindcasts, 60% of the observed above normal years were predicted by 50%-80% of the members. Finally, according to the reliability diagrams (Fig. 32), the FWI and ISI predictions are classified as marginally useful+, the DC is classified as marginally useful, while FFMC falls in the not useful category.

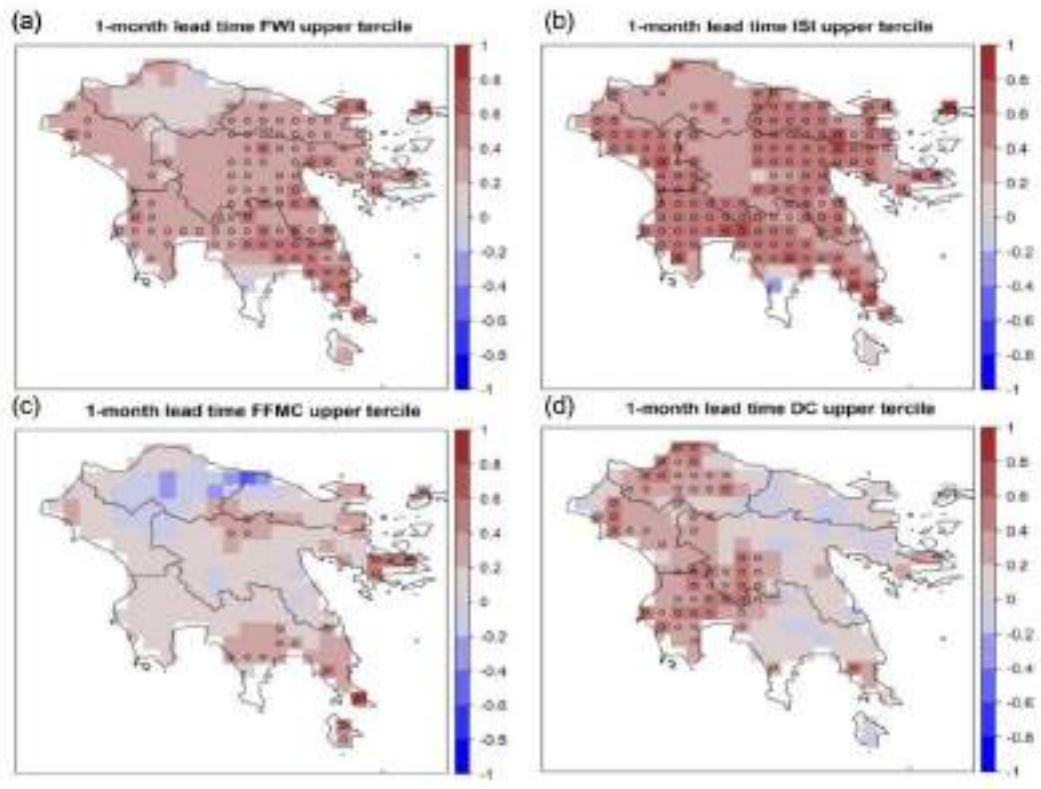

Figure. 30: Same as Fig. 24 but for the LL of Peloponnese.

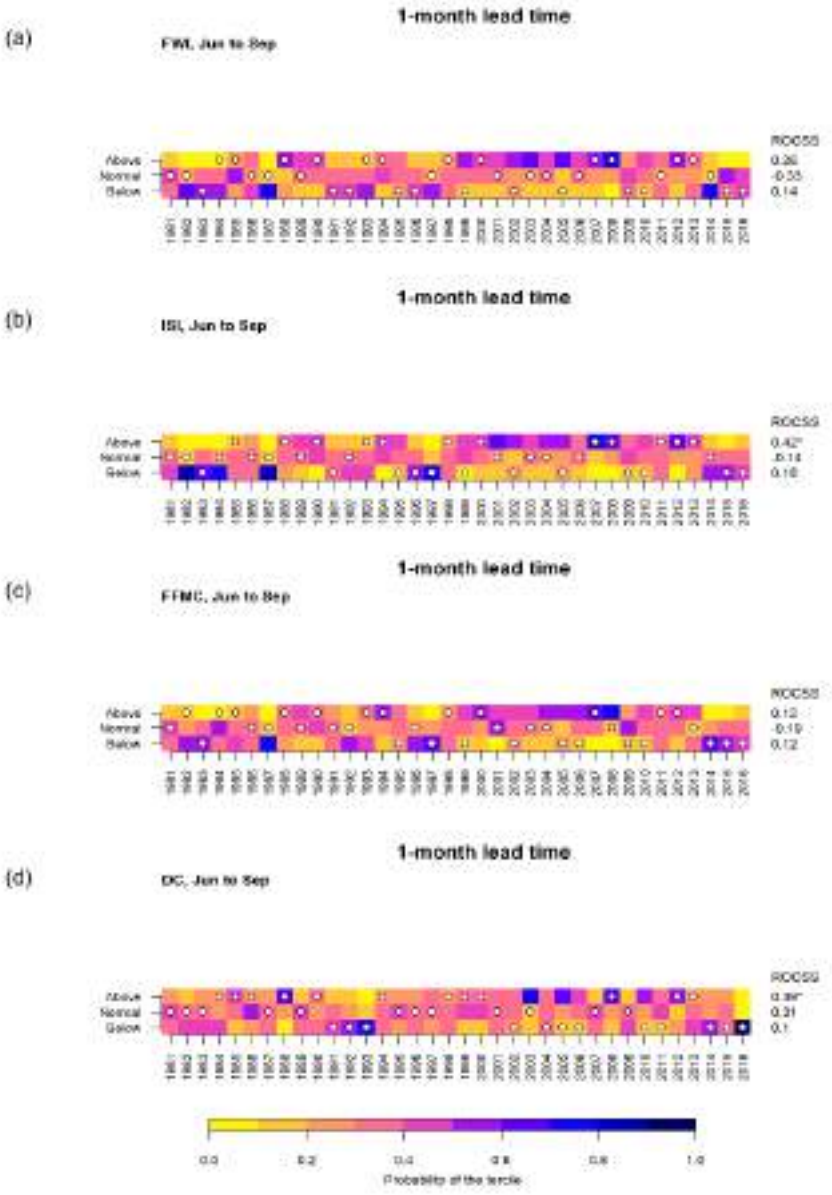

Figure 31: Same as Fig 25. but for the LL of Peloponnese

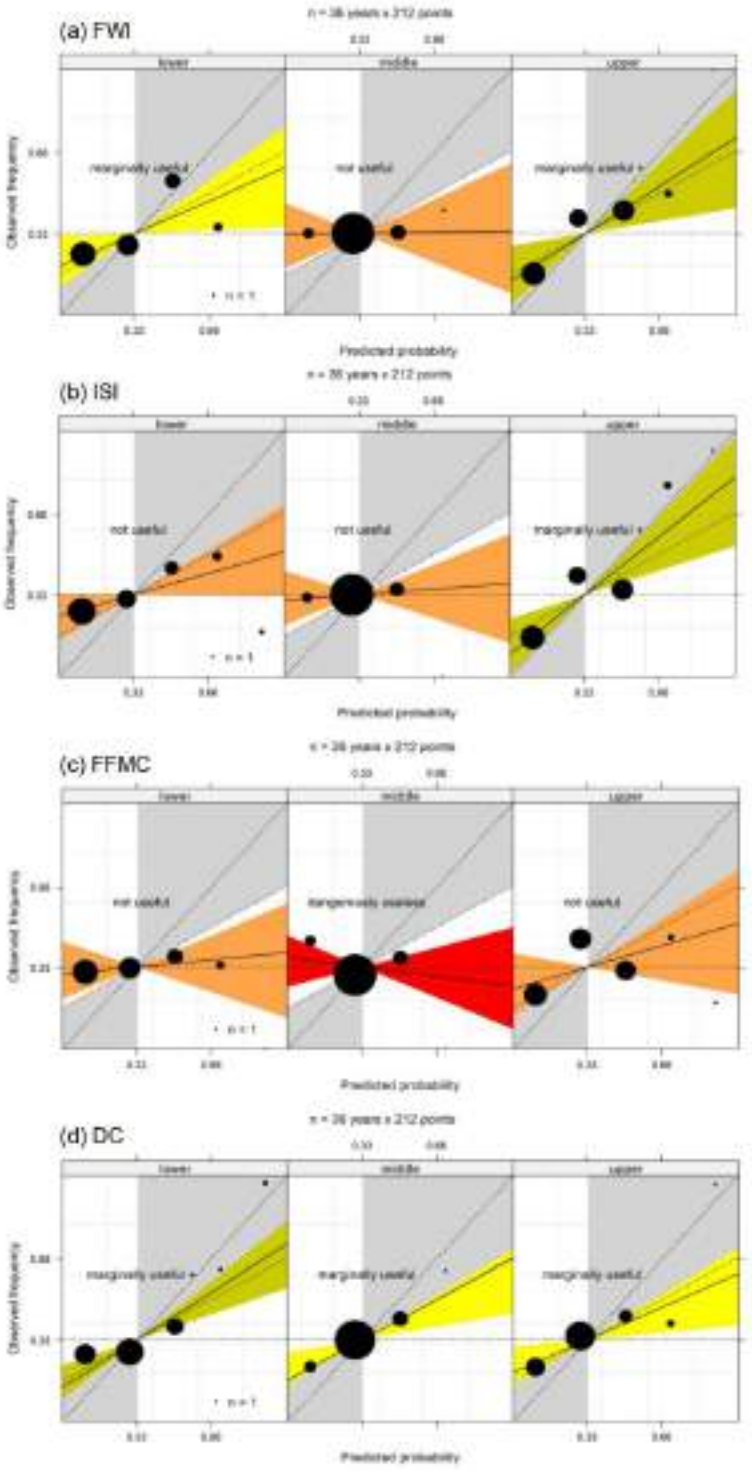

Figure 32: Same as Fig. 26 but for the LL of Peloponnese.

7. Summary and conclusions

- The evaluation of the Enhanced Fire Weather Index (FWIe) past trends (1995-2014) reveals high levels of extreme wildfire potential weather conditions in southern Europe, especially within the Mediterranean basin. In fact, some EWEs were registered in this period in many countries such as in Portugal (2003, 2005, 2013), Spain (2006, 2009, 2012), Italy (2007), and Greece (2007).
- The likely conditions of EWEs occurrence are projected to increase under climate change. FWIe showed higher values over the future periods (2041-2060 and 2081-2100) than the historical period. Indeed, the EWEs occurrence in Europe have become a common issue, with EWE strikes every season in recent years (e.g., Portugal (2016, 2017, 2018), Italy (2021) and Greece (2018, 2021)).
- The FWIe changes during the summer period results showed high increases (up to +27), especially in the southern regions such as Spain, Portugal, Greece Turkey, and some regions in the Balkans peninsula. The increases over the far future are expected to extend northward to reach central and northern European countries such as France and Austria and northwestern countries such as Belgium and Germany.
- Compared to the historical period, the suitable conditions for EWE to occur (FWIe ≥50) are expected to increase in the future in regions such as Portugal, Spain, Greece, and Turkey, especially during the summer period (JJA).
- The increase in the likely conditions leading to EWEs are the consequence of the increasing coincidence of high atmospheric instability (CHI) and near-surface fire risk (FWI), reflected in the increase of the enhanced FWI (FWIe)
- Regarding the Living Labs, the results indicate the highest JJA temperatures increases under SSP5-8.5, the lowest increases under SPP1-2.6 while intermediate increases are found under SSP2-4.5.
- In contrast to temperature results, the changes in JJA precipitation are less robust in most LLs and for the period 2041-2060 under all scenarios. The Peloponnese LL shows no statistically significant increases in summer precipitation due to a lack of agreement across models. The rest of LLs show similar behavior, except for

Portugal, where significant declines are projected. Precipitation decreases for the 2081-2100 time period are robust for all LLs under the SPP5-8.5. Robust FWI changes are projected for all LLs under SSP5-8.5 for both periods. Nevertheless, during the 2041-2060 period a class change in the FWI danger is projected only for Catalonia (compared to reference period) while by the end of the century in the majority of the LLs and FWI class change to worsening conditions is projected.

- Concerning fire danger seasonal forecasts, ISI performs better than FWI and the remaining subcomponents in all the examined LLs. According to the reliability diagrams, ISI validation falls in the marginally useful+ category. This means that a partial positive relationship between the Sys5 forecast probability and the observed frequency of occurrence of the above normal conditions is found, and therefore the index could potentially be useful in decision making as far as fuel management and resources allocation are concerned.

8.Data availability

Table 5 shows the portfolio of climate projections for variables linked to extreme wildfire events. The spatial data projections with their corresponding metadata will be available together with the deliverable 1.5 at month 24 of the project. The data and metadata will be available at the FIRE-RES Zenodo repository for the whole FIRE-RES consortium. Nonetheless, the data will be open for the general public after the publication of results in scientific journals.

Table 5. Portfolio of the climate projections included in the present deliverable.

Scale	Region	Variables	Scenarios	Models	Temporal periods	Spatial resolution	Temporal resolution	File type	Output type
European	EU countries	**C-Haines**	SSP1-2.6 SSP2-4.5 SSP5-8.5	CNRM-ESM2 AWI-CM-1-1-MR CMCC-ESM2 EC-Earth3-Veg-LR	1995-2014 2041-2060 2081-2100	0.5x0.5 degrees	Monthly	netcdf	Raw data Mean of models
European	EU countries	**Enhanced FWI**	SSP1-2.6 SSP2-4.5 SSP5-8.5	CNRM-ESM2 AWI-CM-1-1-MR CMCC-ESM2 EC-Earth3-Veg-LR	1995-2014 2041-2060 2081-2100	0.5x0.5 degrees	Monthly	netcdf	Raw data Mean of models
European	EU countries	**FWI, TX, TN, RR**	SSP1-2.6 SSP2-4.5 SSP5-8.5	CNRM-ESM2 AWI-CM-1-1-MR CMCC-ESM2 EC-Earth3-Veg-LR	1995-2014 2041-2060 2081-2100	0.5x0.5 degrees	Daily	netcdf	Raw data Mean of models
Living Lab	Catalonia Peloponnese Aquitaine Portugal Lower Saxony/North Rhine Westphalia, Netherlands	**FWI, TX TN, RR, Drought Code**	SSP1-2.6 SSP2-4.5 SSP5-8.5	EC-Earth3-Veg MIROC6 MPI-ESM1-2-HR NORESM2-MM CNRM-ESM2 CNRM-CM6-1-HR CMCC-ESM2 EC-Earth3-Veg-LR	1995-2014 2041-2060 2081-2100	0.1x0.1 degrees	Daily	netcdf	Raw data Mean of models
Living lab	Catalonia Peloponnese Sardinia	**Seasonal FWI (and subcomponents)**	-	ECMWF SEAS5 (v5.1)	1981-2016	0.1x0.1 degrees	June-September	tiff	Verification metrics (plots/maps)

9.References

Abatzoglou JT, Williams AP (2016) Impact of anthropogenic climate change on wildfire across western US forests. Proc Natl Acad Sci U S A 113:11770–11775. https://doi.org/10.1073/pnas.1607171113

Bedia J, Golding N, Casanueva A, Iturbide M, Buontempo C, Gutiérrez JM (2018) Seasonal predictions of Fire Weather Index: Paving the way for their operational applicability in Mediterranean Europe. Climate Services 9:101–110. https://doi.org/10.1016/j.cliser.2017.04.001

Castellnou M, Bachfischer M, Miralles M, et al (2022) Pyroconvection Classification Based on Atmospheric Vertical Profiling Correlation With Extreme Fire Spread Observations. J Geophys Res Atmos 127:. https://doi.org/10.1029/2022JD036920

Collins M, Minobe S, Barreiro M, et al (2018) Challenges and opportunities for improved understanding of regional climate dynamics. Nat Clim Chang 8:101–108. https://doi.org/10.1038/s41558-017-0059-8

Dacamara CC, Calado TJ, Ermida SL, et al (2014) Calibration of the Fire Weather Index over Mediterranean Europe based on fire activity retrieved from MSG satellite imagery. Int J Wildl Fire 23:945–958. https://doi.org/10.1071/WF13157

Di Virgilio G, Evans JP, Blake SAP, et al (2019) Climate Change Increases the Potential for Extreme Wildfires. Geophys Res Lett 46:8517–8526. https://doi.org/10.1029/2019GL083699

Doblas-Reyes FJ, García-Serrano J, Lienert F, et al (2013) Seasonal climate predictability and forecasting: Status and prospects. Wiley Interdiscip Rev Clim Chang 4:245–268. https://doi.org/10.1002/wcc.217

Duane A, Castellnou M, Brotons L (2021) Towards a comprehensive look at global drivers of novel extreme wildfire events. Clim Change 165:1–21. https://doi.org/10.1007/s10584-021-03066-4

Easterling DR, Meehl GA, Parmesan C, et al (2000) Climate extremes: Observations, modeling, and impacts. Science (80-) 289:2068–2074. https://doi.org/10.1126/science.289.5487.2068

Frich P, Alexander L V., Della-Marta P, et al (2002) Observed coherent changes in climatic extremes during the second half of the twentieth century. Clim Res 19:193–212. https://doi.org/10.3354/cr019193

Herrera S, Bedia J, Gutiérrez JM, Fernández J, Moreno JM (2013) On the projection of future fire danger conditions with various instantaneous/mean-daily data sources. Climatic Change 118:827–840. https://doi.org/10.1007/s10584-012-0667-2

Jolliffe IT, Stephenson DB (2003) Forecast Verification: A Practitioner's Guide in Atmospheric Science. John Wiley & Son, 126 pp.

Jolly WM, Cochrane MA, Freeborn PH, et al (2015) Climate-induced variations in global wildfire danger from 1979 to 2013. Nat Commun 6:1–11. https://doi.org/10.1038/ncomms8537

Karali A, Varotsos KV, Giannakopoulos C, Nastos PP, Hatzaki M (2023) Seasonal fire danger forecasts for supporting fire prevention management in an eastern Mediterranean environment: the case of Attica, Greece. Natural Hazards and Earth System Sciences 23:429–445. https://doi.org/10.5194/nhess-23-429-2023

Klein Tank AMG, Wijngaard JB, Können GP, et al (2002) Daily dataset of 20th-century surface air temperature and precipitation series for the European Climate Assessment. Int J Climatol 22:1441–1453. https://doi.org/10.1002/joc.773

Leone V, Elia M, Lovreglio R, et al (2023) The 2017 Extreme Wildfires Events in Portugal through the Perceptions of Volunteer and Professional Firefighters. Fire 6:1–22. https://doi.org/10.3390/fire6040133

Luo JJ, Behera SK, Masumoto Y, Yamagata T (2011) Impact of global ocean surface warming on seasonal-to-interannual climate prediction. J Clim 24:1626–1646. https://doi.org/10.1175/2010JCLI3645.1

Manzanas R, Lucero A, Weisheimer A, Gutiérrez JM (2018) Can bias correction and statistical downscaling methods improve the skill of seasonal precipitation forecasts? Clim Dyn 50:1161–1176. https://doi.org/10.1007/s00382-017-3668-z

Meier S, Strobl E, Elliott RJR, Kettridge N (2023) Cross-country risk quantification of extreme wildfires in Mediterranean Europe. Risk Anal 1745–1762. https://doi.org/10.1111/risa.14075

Ndalila MN, J. Williamson G, Fox-Hughes P, et al (2020) Evolution of a pyrocumulonimbus event associated with an extreme wildfire in Tasmania, Australia. Nat Hazards Earth Syst Sci 20:1497–1511. https://doi.org/10.5194/nhess-20-1497-2020

Nicholls N, Murray W (1999) Workshop on Indices and Indicators for Climate Extremes, Asheville, NC, USA, 3-6 June 1997 - Breakout Group A: Storms. Clim. Change 42:9–21

O'Neill BC, Kriegler E, Ebi KL, et al (2015) The roads ahead: Narratives for shared socioeconomic pathways describing world futures in the 21st century. Glob Environ Chang 42:169–180. https://doi.org/10.1016/j.gloenvcha.2015.01.004

Palmer TE, Mcsweeney CF, Booth BBB, et al (2023) Performance-based sub-selection of CMIP6 models for impact assessments in Europe. Earth Syst Dyn 14:457–483. https://doi.org/10.5194/esd-14-457-2023

Pinto MM, Dacamara CC, Hurduc A, et al (2020) Enhancing the fire weather index with atmospheric instability information. Environ Res Lett 15:. https://doi.org/10.1088/1748-9326/ab9e22

Pinto MM, DaCamara CC, Trigo IF, et al (2018) Fire danger rating over Mediterranean

Europe based on fire radiative power derived from Meteosat. Nat Hazards Earth Syst Sci 18:515–529. https://doi.org/10.5194/nhess-18-515-2018

San-Miguel-Ayanz J, Schulte E, Schmuck G, et al (2012) Comprehensive Monitoring of Wildfires in Europe: The European Forest Fire Information System (EFFIS). In: Approaches to Managing Disaster- Assessing Hazards, Emergencies and Disaster Impacts, Prof. John Tiefenbacher (Ed.)

Turco M, Marcos-Matamoros R, Castro X, et al (2019) Seasonal prediction of climate-driven fire risk for decision-making and operational applications in a Mediterranean region. Sci Total Environ 676:577–583. https://doi.org/10.1016/j.scitotenv.2019.04.296

Van Wagner CE (1987) Development and structure of the Canadian forest fire weather index system

Varotsos KV, Dandou A, Papangelis G, Roukounakis N, Kitsara G, Tombrou M, Giannakopoulos C (2023) Using a new local high resolution daily gridded dataset for Attica to statistically downscale climate projections. Clim Dyn. 60: 2931-2956. https://doi.org/10.1007/s00382-022-06482-z

Wagner CE Van, Forest P, Station E (1974) Structure of the Canadian. Can For Serv Publ

Weisheimer A, Palmer TN (2014) On the reliability of seasonal climate forecasts. Journal of The Royal Society Interface 11:20131162. https://doi.org/10.1098/rsif.2013.1162

Wotton BM (2009) Interpreting and using outputs from the Canadian Forest Fire Danger Rating System in research applications. Environ Ecol Stat 16:107–131. https://doi.org/10.1007/s10651-007-0084-2

10. Supplementary information

The Continuous Haines Index

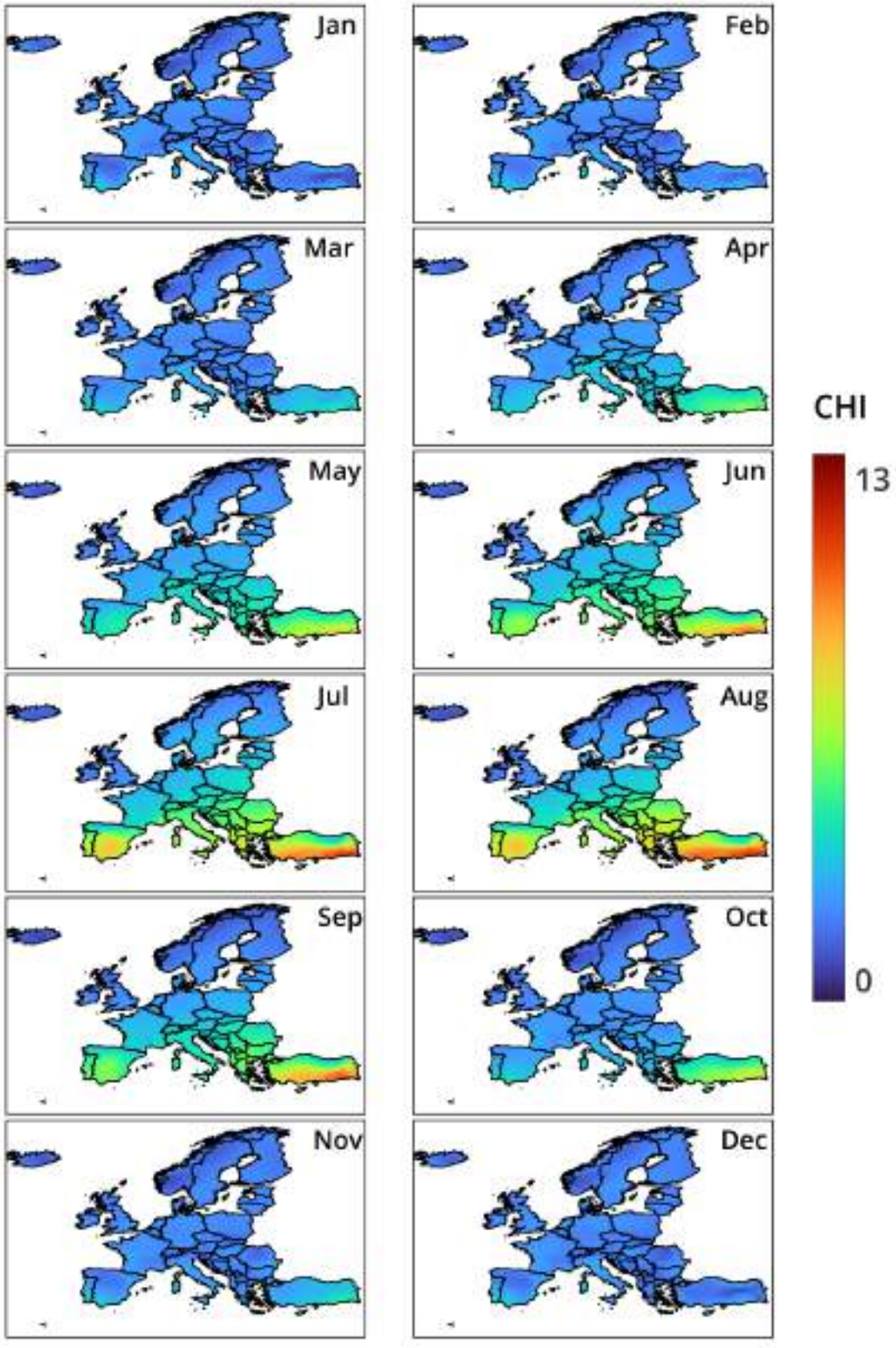

Figure S1. Monthly means of the C-Haines index over the historical period (1995-2014).

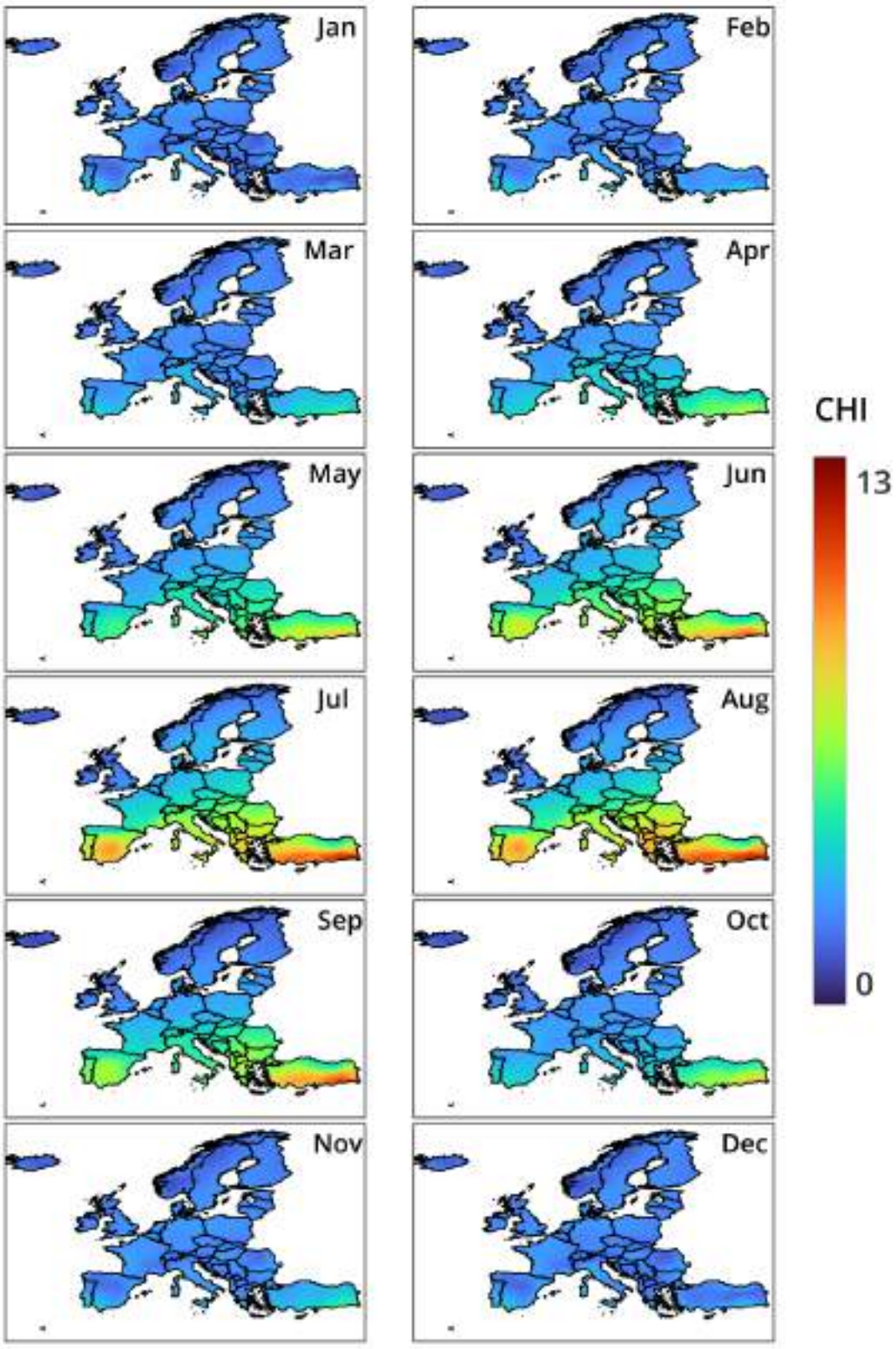

Figure S2. Monthly means of the C-Haines index over the near future period (2041-2060) under the SSP1-2.6 climate scenario.

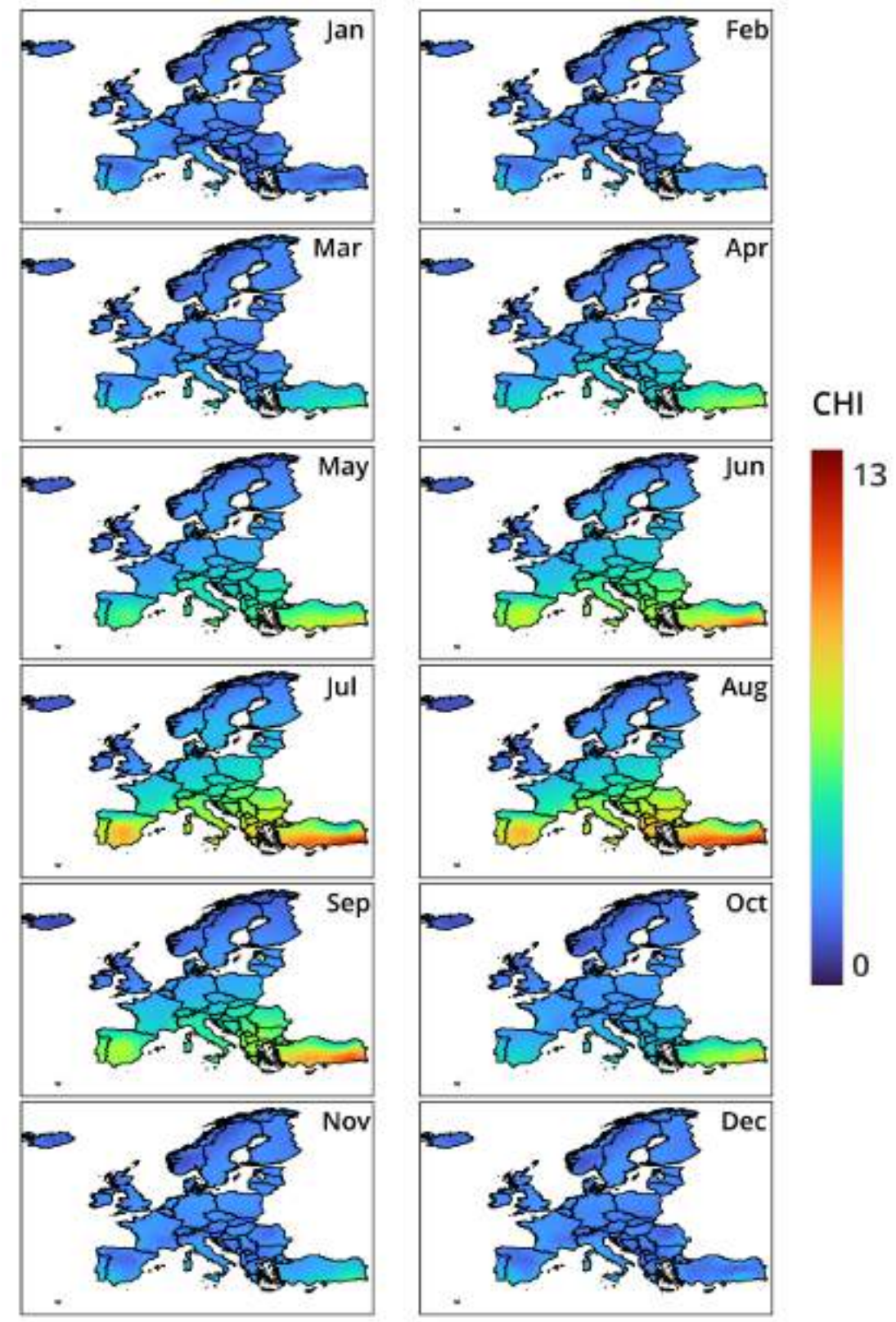

Figure S3. Monthly means of the C-Haines index over the near future period (2041-2060) under the SSP2-4.5 climate scenario

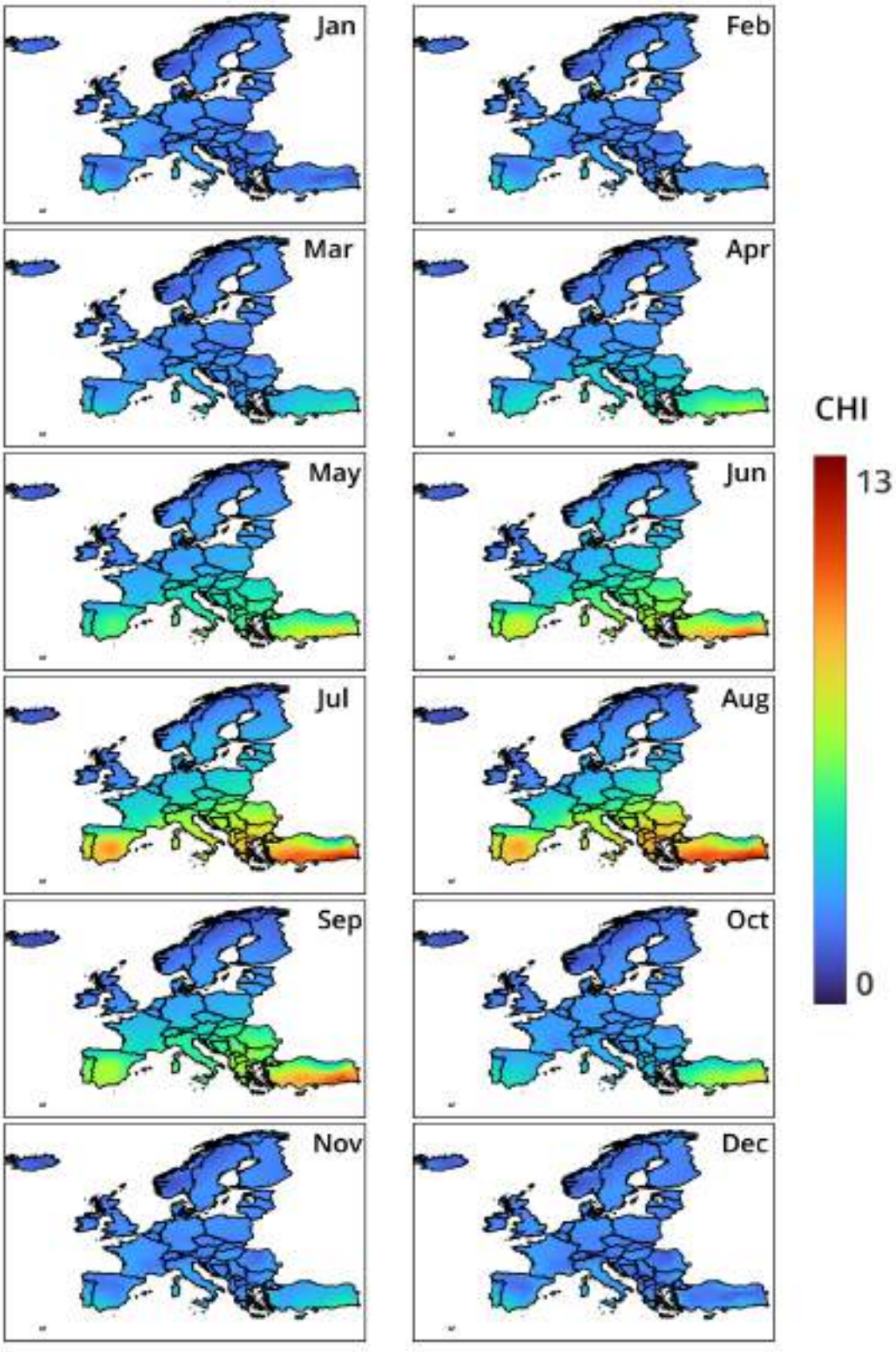

Figure S4. Monthly means of the C-Haines index over the near future period (2041-2060) under the SSP5-8.5 climate scenario.

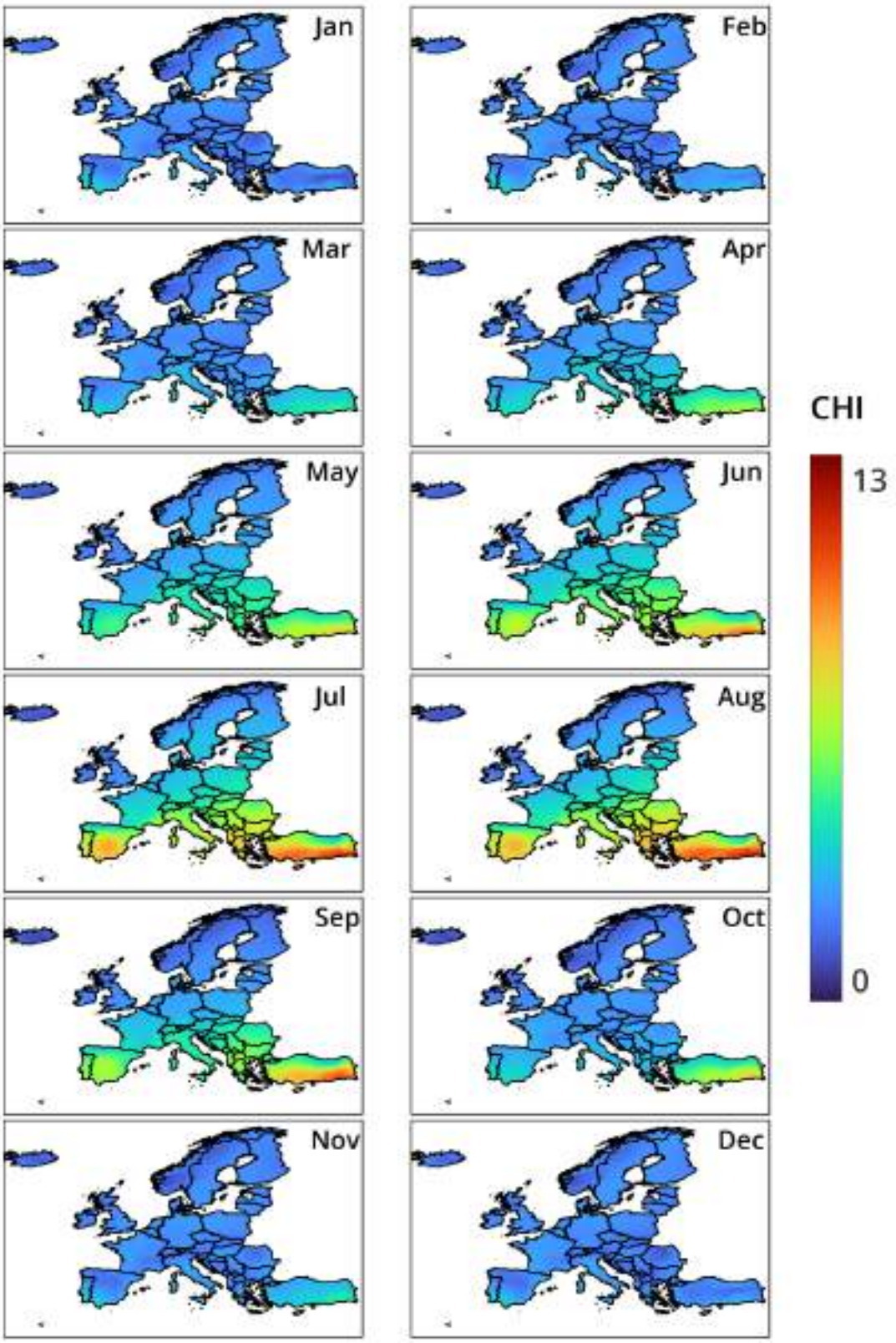

Figure S5. Monthly means of the C-Haines index over the far future period (2081-2100) under the SSP1-2.6 climate scenario.

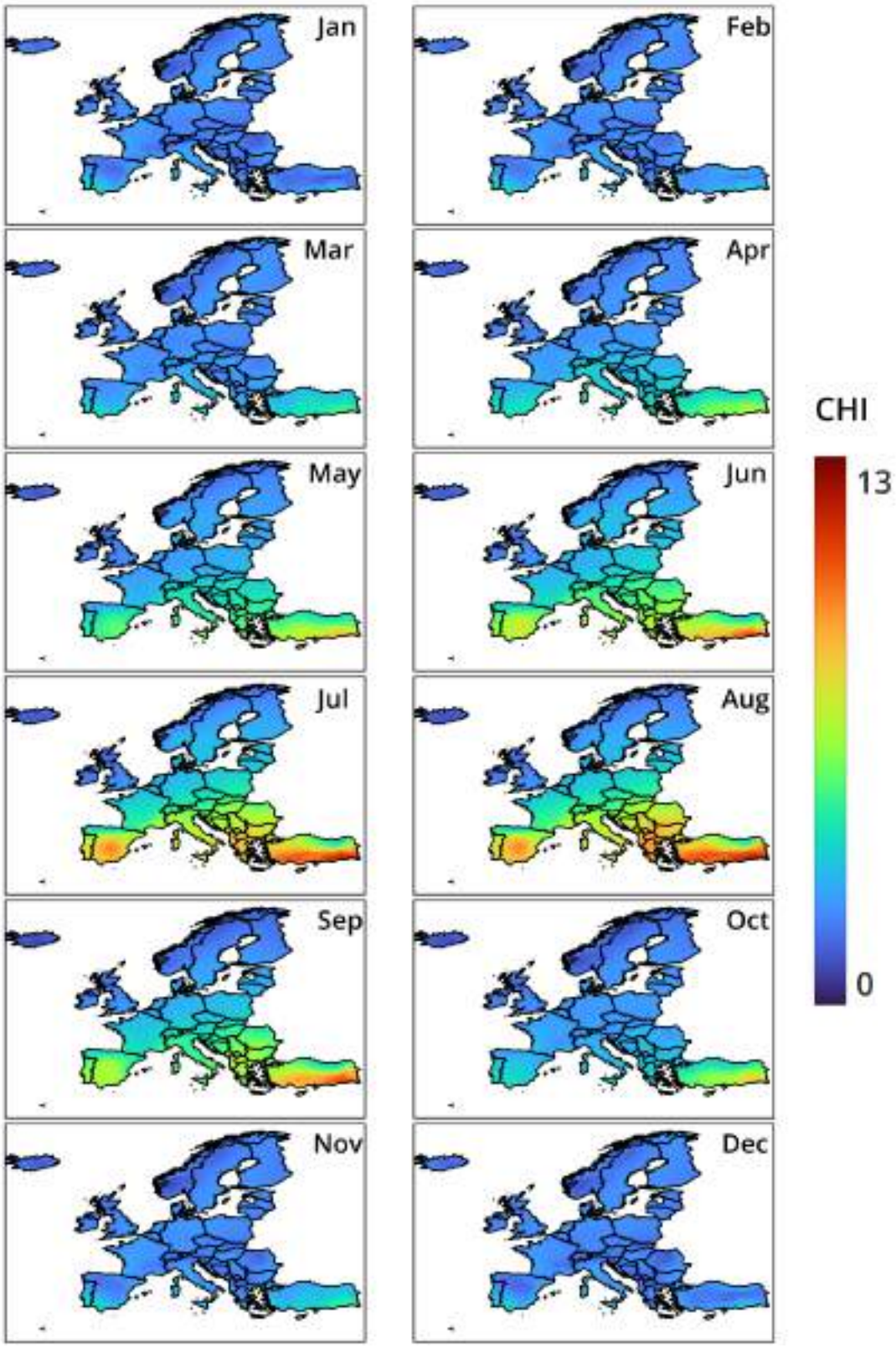

Figure S6. Monthly means of the C-Haines index over the far future period (2081-2100) under the SSP2-4.5 climate scenario.

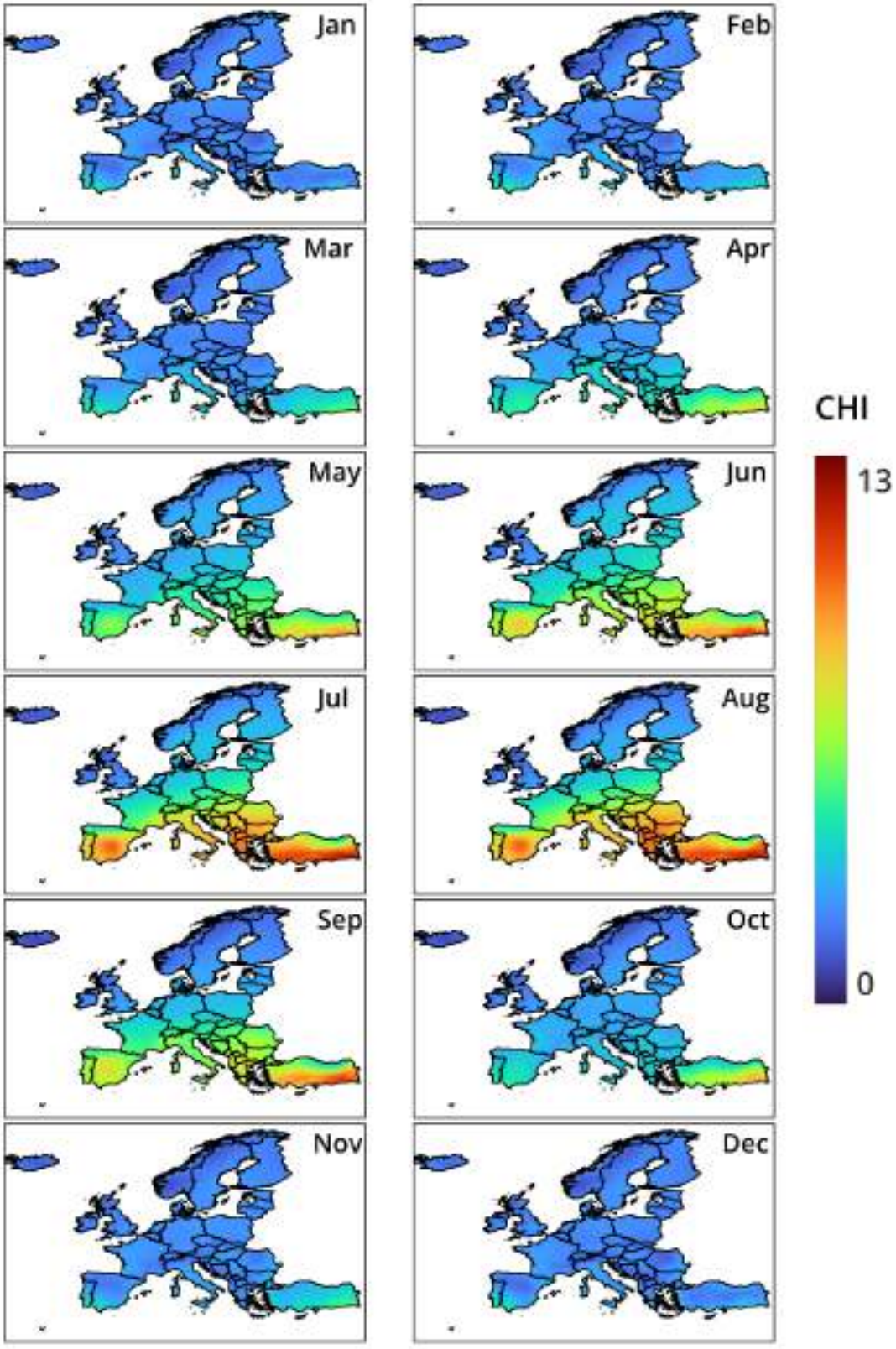

Figure S7. Monthly means of the C-Haines index over the far future period (2081-2100) under the SSP5-8.5 climate scenario.

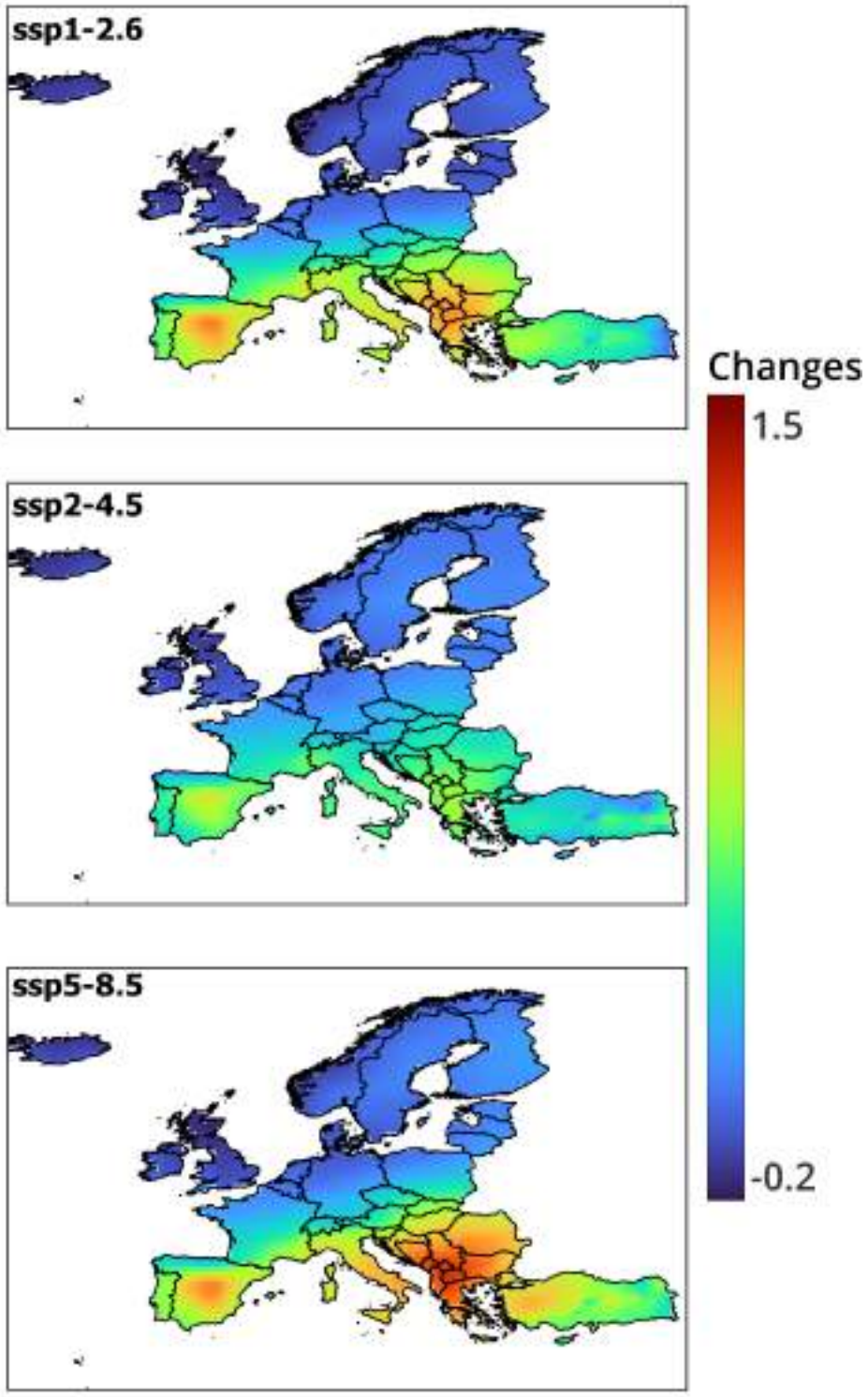

Figure S8. Changes in the mean summer C-Haines index (Jun-July-August) between the near future (2020-2041) and the historical period (1995-2014) under the SSP1-2.6, SSP2-4.5 and SSP5-8.5 respectively.

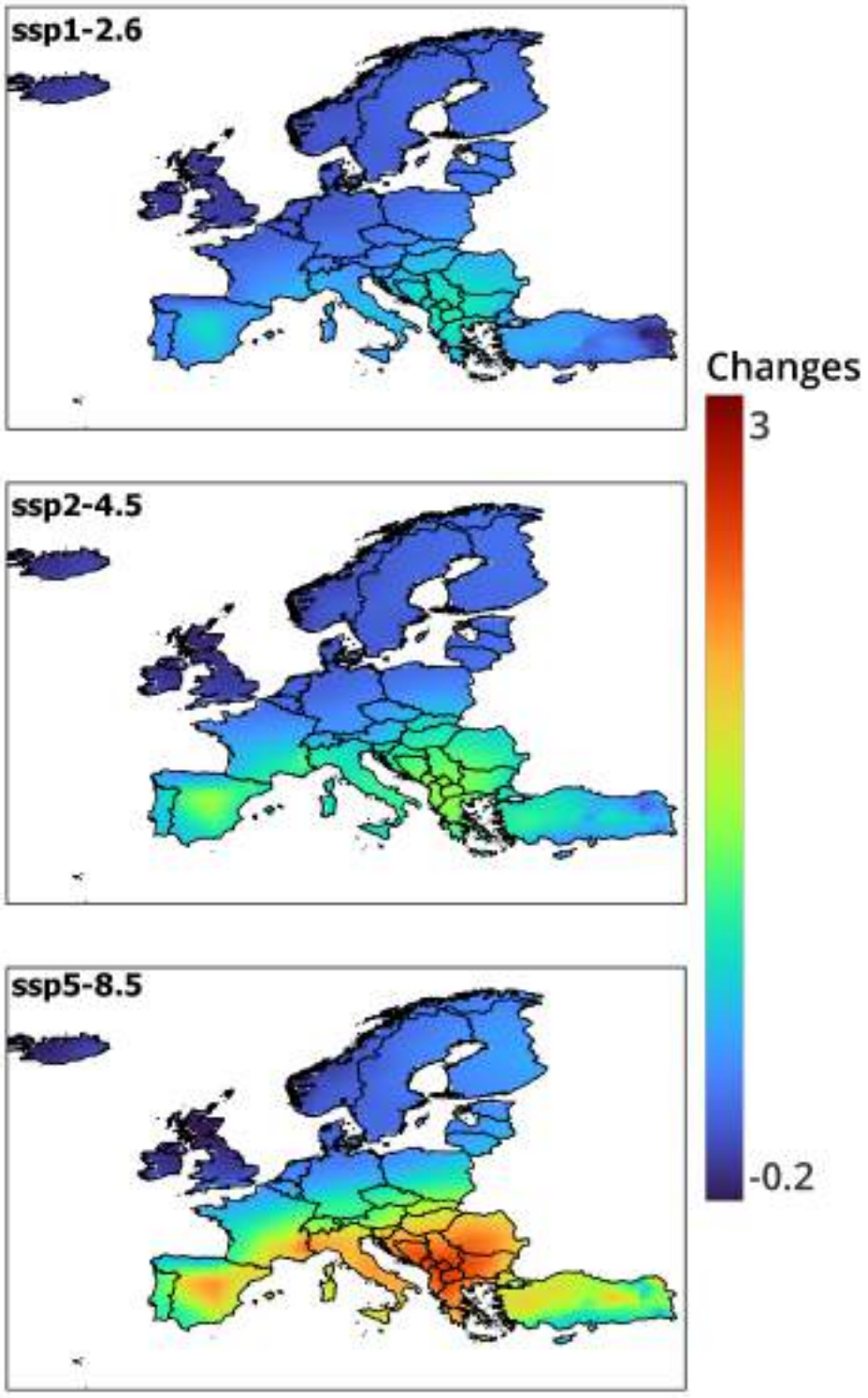

Figure S9. Changes in the mean summer C-Haines index (Jun-July-August) between the far future (2081-2100) and the historical period (1995-2014) under the SSP1-2.6, SSP2-4.5 and SSP5-8.5 respectively

The enhanced Fire Weather Index

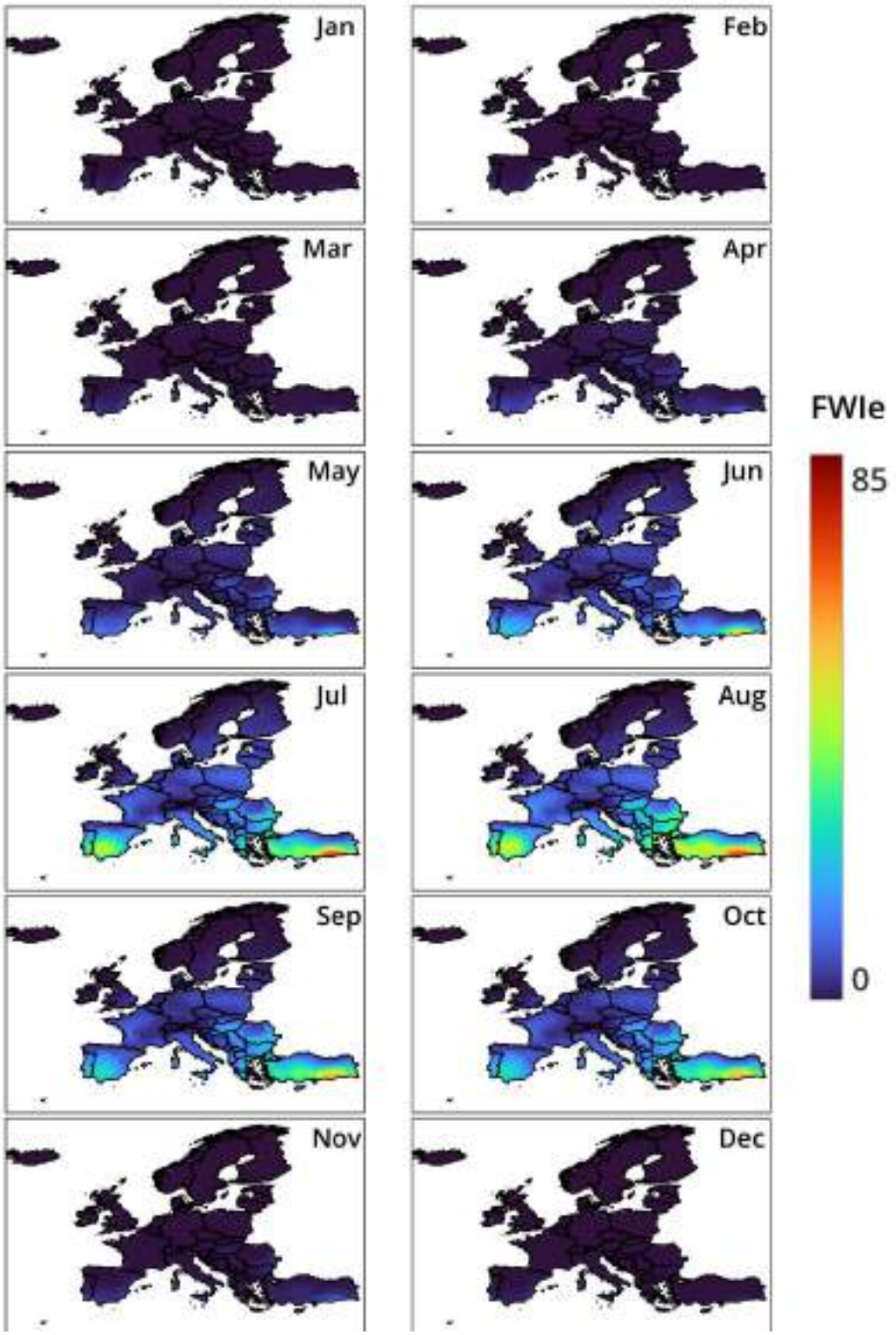

Figure S10. Monthly means of the enhanced fire weather index over the historical period (1995-2014).

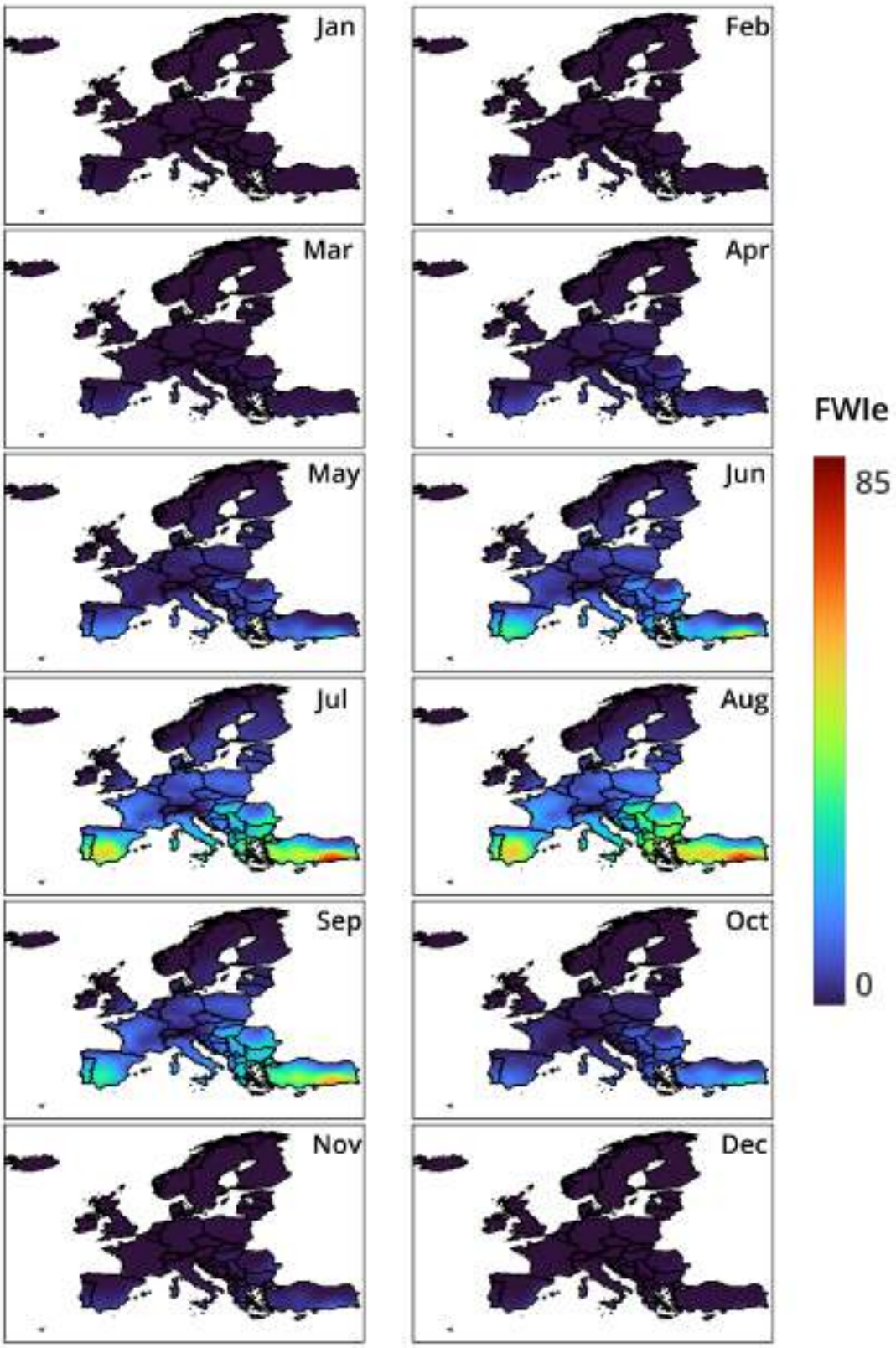

Figure S11. Monthly means of the enhanced fire weather index over the near future period (2041-2060) under the SSP1-2.6 climate scenario.

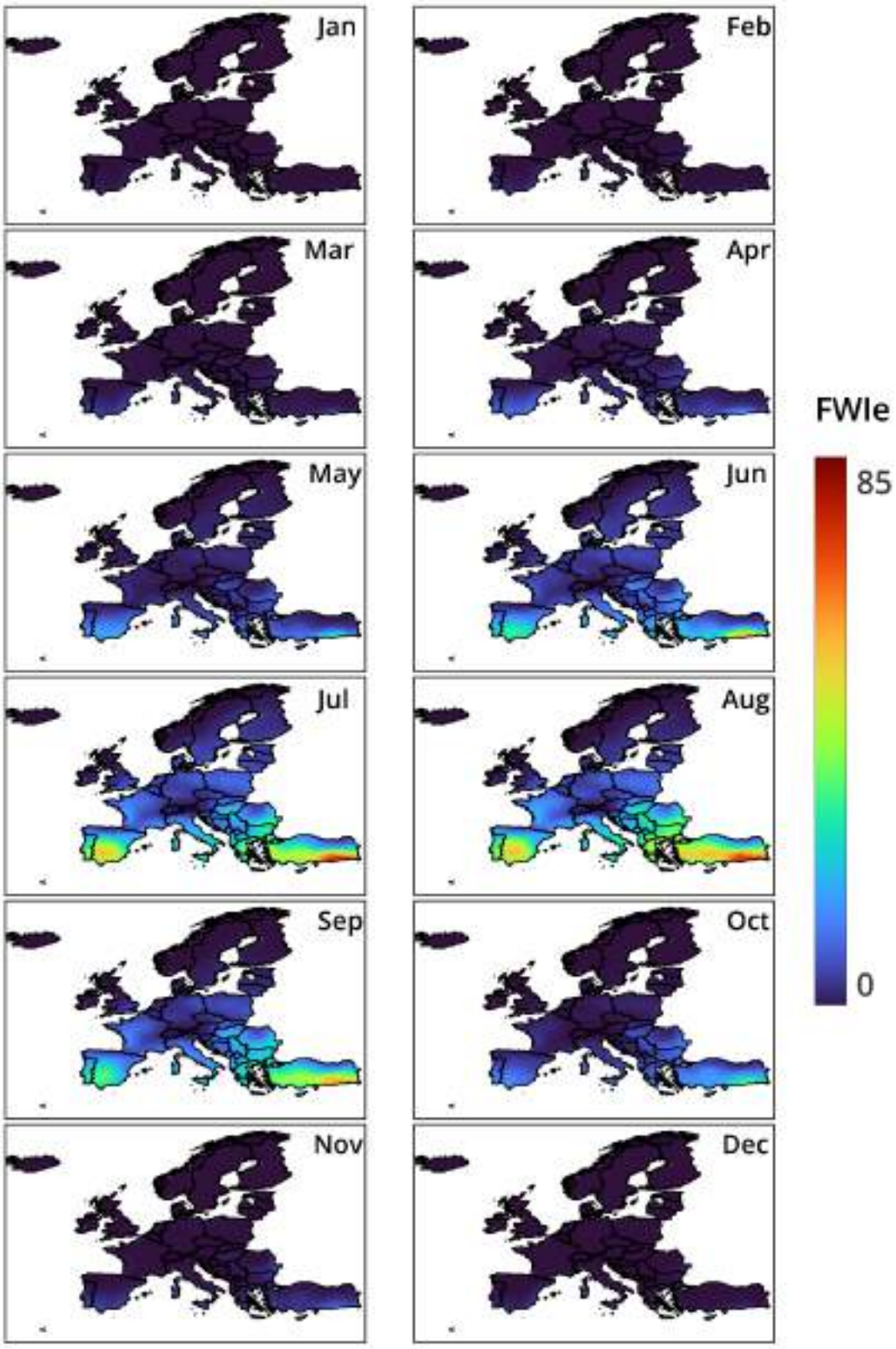

Figure S12. Monthly means of the enhanced fire weather index over the near future period (2041-2060) under the SSP2-4.5 climate scenario.

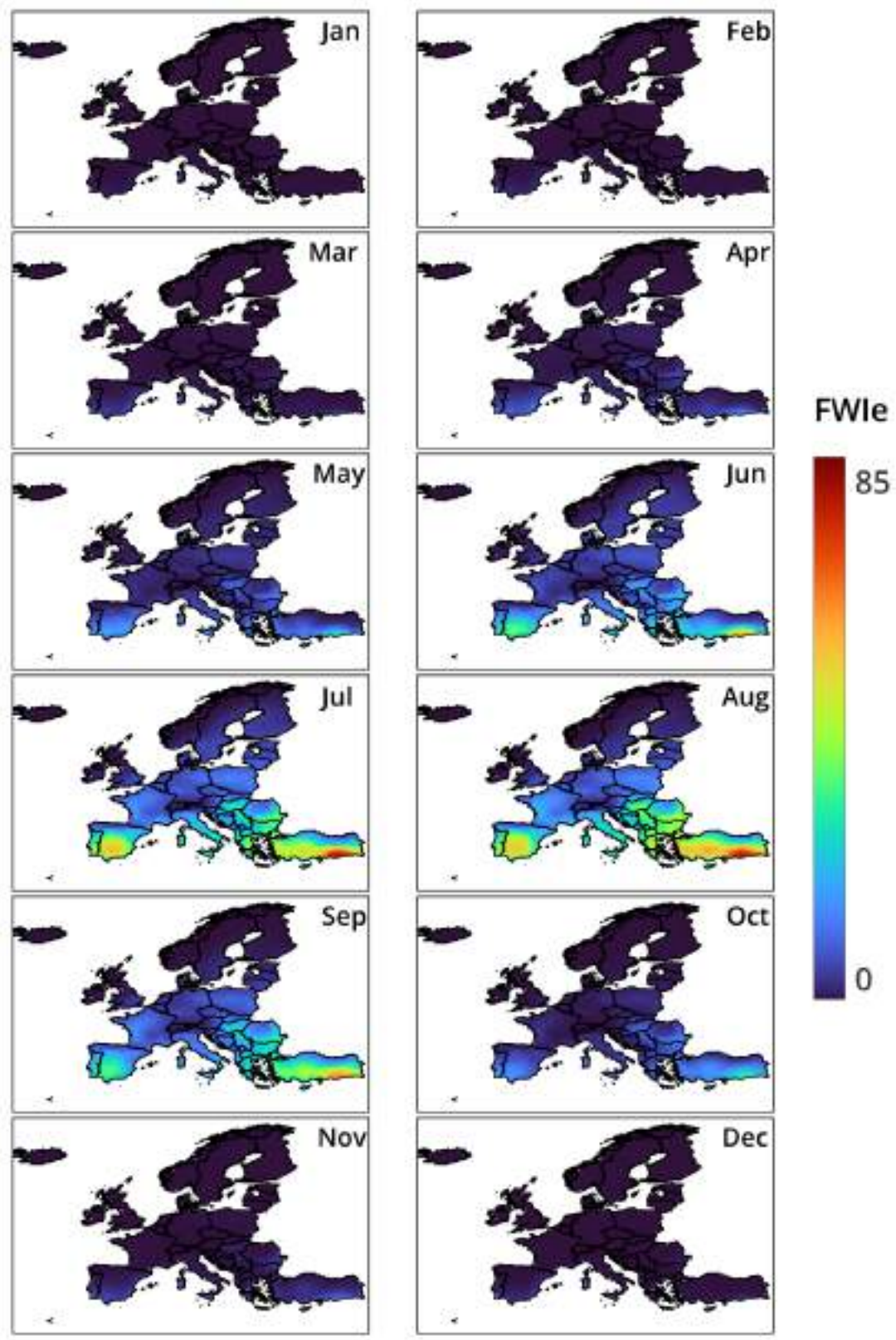

Figure S13. Monthly means of the enhanced fire weather index over the near future period (2041-2060) under the SSP5-8.5 climate scenario.

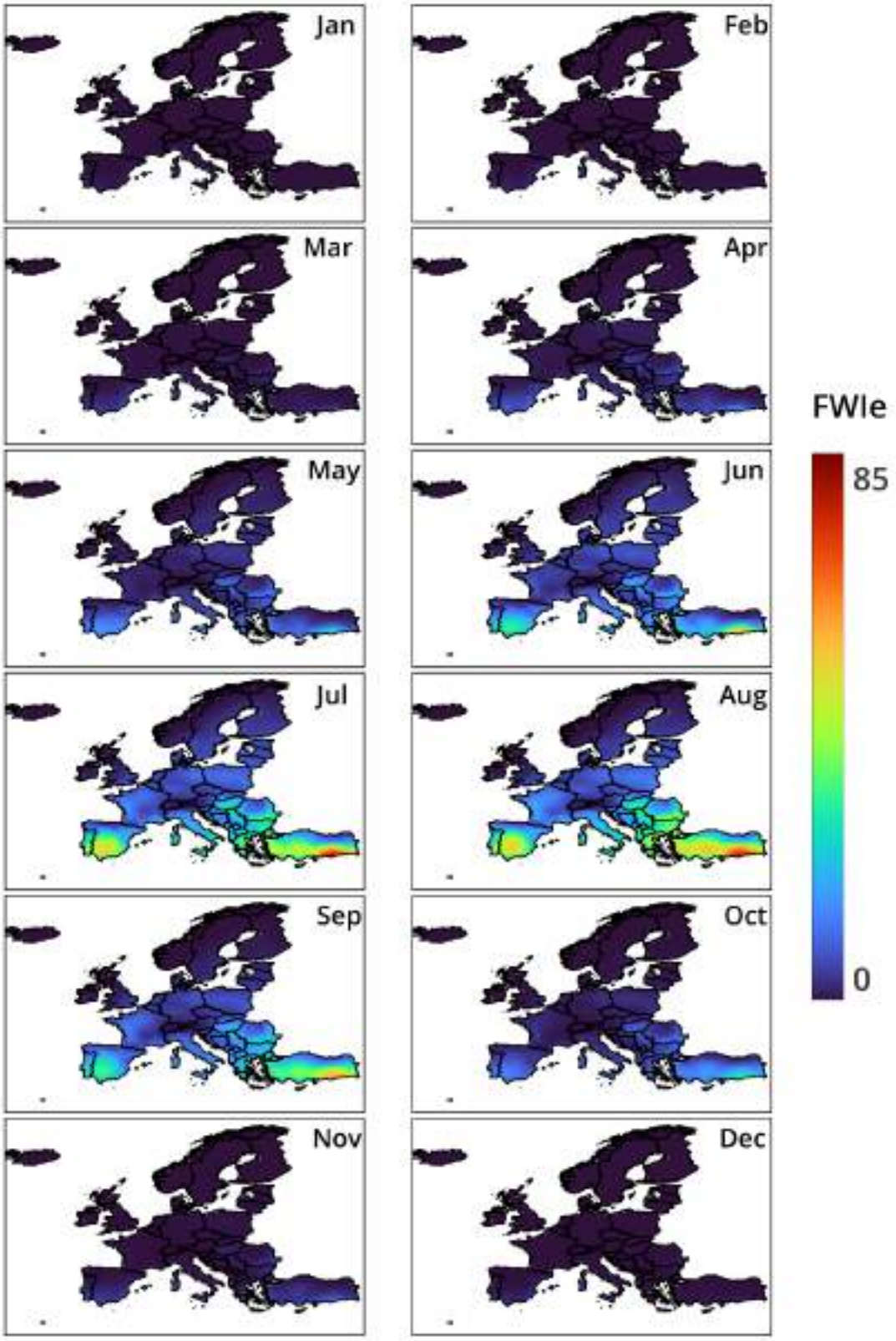

Figure S14. Monthly means of the enhanced fire weather index over the far future period (2081-2100) under the SSP1-2.6 climate scenario.

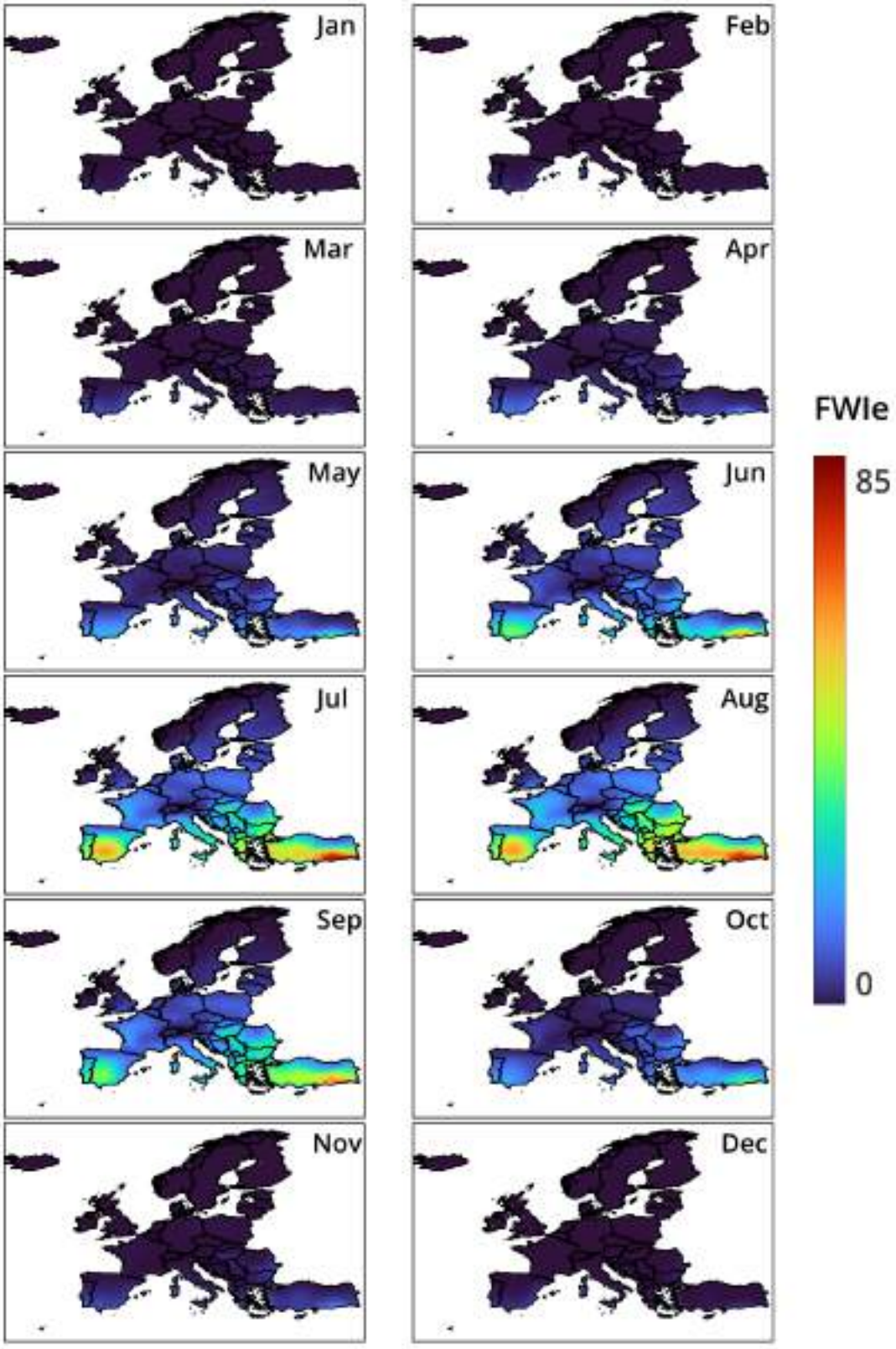

Figure S15. Monthly means of the enhanced fire weather index over the far future period (2081-2100) under the SSP2-4.5 climate scenario.

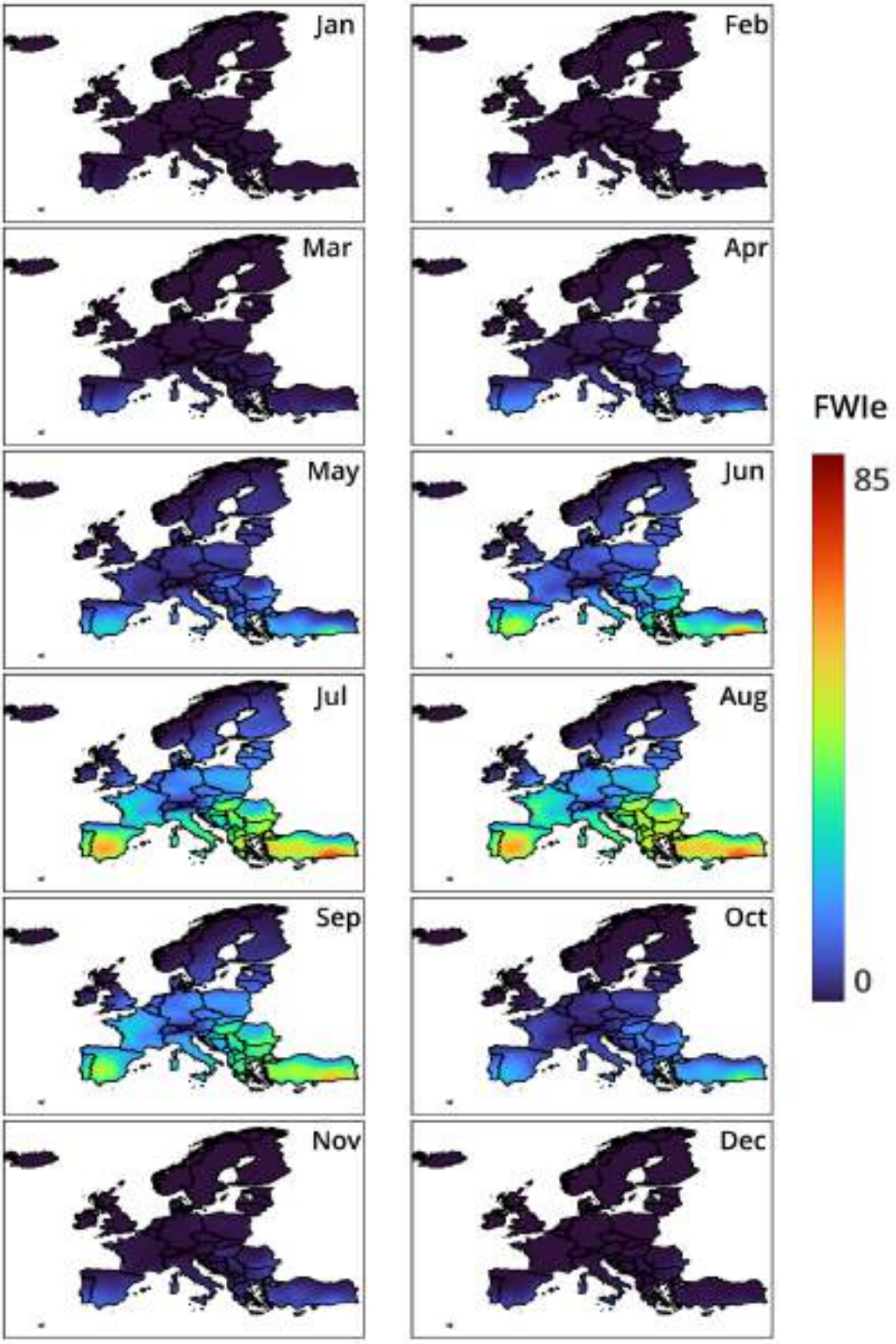

Figure S16. Monthly means of the enhanced fire weather index over the far future period (2081-2100) under the SSP5-8.5 climate scenario.

FIRE-RES